Circularly Polarised Luminescence Spectroscopy of Chiral Europium(III) Complexes

By Stefan Lopinski

A Thesis Submitted to the University of Glasgow Physical Sciences Department

for the degree of Doctor of Philosophy.

University of Glasgow Department of Chemistry

March 2003

Declaration

I, Stefan Lopinski, declare that the results presented in the following pages are a true representation of the work I have done throughout my Ph.D. studentship. Any results presented, not produced by myself, have been noted as such.

,

Abstract

Circularly Polarised Luminescence Spectroscopy of Europium(III) Complexes

Circularly Polarised Luminescence (CPL) spectroscopy detects the differential emission of left and right circularly polarised light from luminescent chiral species, and so can be thought of as the emission analogue of circular dichroism spectroscopy[1]. The circularly polarised emission of chiral europium complexes derived from the 12-ane-4 macrocycle cyclen, (examples of which are shown below) have been recorded using this technique.

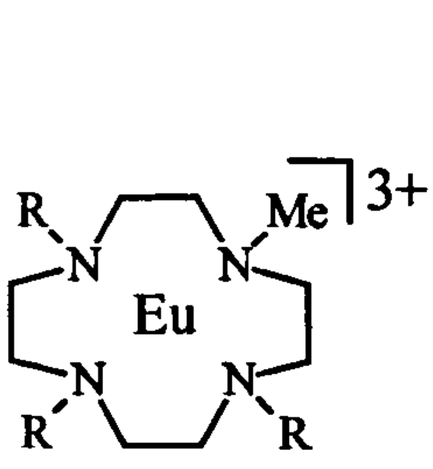

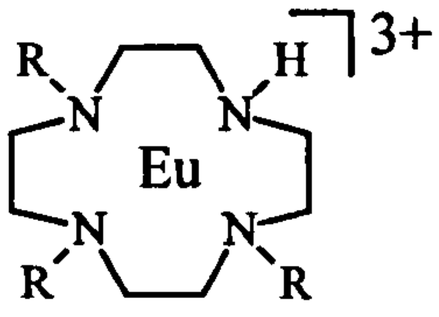

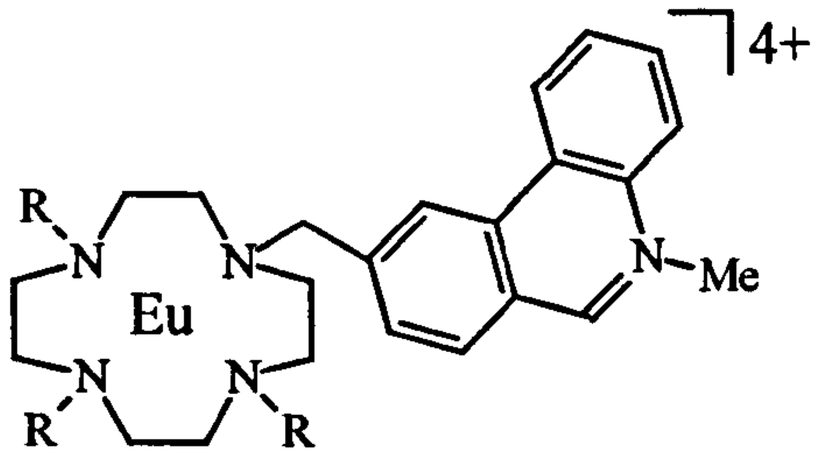

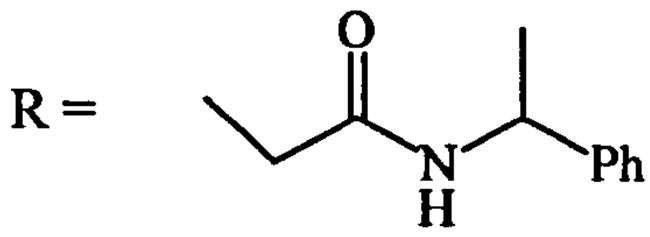

These and similar complexes have shown an ability to bind to biologically important anions such as carbonate and phosphate in aqueous media and are able to report this event by a change in luminescence[2]. These interactions have been investigated by monitoring the emitted circularly polarised light using the technique described and the binding of the substrate is clearly signalled. Typical CPL spectra of the europium complexes will be presented as will the binding study results and a detailed account of how the spectra is obtained.

[1] F.S.Richardson and J.P. Riehl *Chem. Rev.* 1986, **86**, 1
[2] R.S. Dickins, T. Gunnlaugsson, D. Parker and R.D.Peacock, *Chem. Comm.* 1998, 1643

Acknowledgements

I would like to thank Dr R.D. Peacock for all his time, help and patience. I would also like to thank Drs Benniston and Bruce as well as Professor Parker.

Finally, I would like to thank Mum, Dad, Emma and all my family and friends for their kind support.

Contents

List of Figures

List of Tables

Chapter1.

1. Introduction

Molecular recognition is a vast and ever expanding field encompassing many aspects of both the physical and the life sciences, making it a truly interdisciplinary subject area. The domestic carbon monoxide detector, the use of pulse oximetry in modern medicine, the home pregnancy kit, are all examples from everyday life of the need for workable and commercially viable molecular detection systems.

Within this wider field, the recognition of anions in aqueous media represents an important element of both supramolecular and biological chemistry[1] . A large number of metalloenzymes have been reported to bind to specific anions in a competitive anionic background. A great deal of study has been carried out in this field [2-7] to establish the *modus operandi* of enzymes such as carbonic anhydrase and alkaline phosphatase.

Although an aqueous environment is the natural medium for recognition of anions by naturally occurring receptors (proteins, antibodies), most synthetic receptors have been limited to use in nonaqueous solvents [8]. . This is not hard to understand when we consider the considerable demands placed on the receptor molecule by the very nature of anions in water. Many target anions are pH sensitive (carbonate, phosphate); there exists a wide range of anionic geometries (trigonal planar, tetrahedral, octahedral); high energies of hydration ΔG_{hyd} (HCO_3^-, -335kJ mol^{-1}; $H_2PO_4^-$ and F^-, -465 kJ mol^{-1}; SO_4^{2-}, -1080 kJ mol^{-1} ; CO_3^{2-} , -1315 kJ mol^{-1}) make the design of a receptor for a particular anion a non-trivial task.

The aim of this research project was to use the inherent luminescent properties of synthetic europium(III) complexes to signal the binding of biologically important anions. This was intended to be achieved in a physiological background with a view to a viable system operable *in vivo*. In addition to the demands placed on a water based anionic receptor as discussed above, the design of any metal complex intended for use in such an environment is subject to further constraints. Obviously the complex must be water soluble and thereafter must be both kinetically and thermodynamically stable with respect to europium ion dissociation.

1.1 Complex Stability

For any system that is planned for used in a biological environment, this factor cannot be taken lightly - whereas a metal complex may pose no threat an organism, the metal ion itself is highly toxic. Although this is a problem for metal complexes in such an environment generally, the kinetically labile nature of lanthanide(III) ions is a further problem in the design of a europium(III) complex. It is also imperative that the metal complex is stable over a wide pH range since local environments in the body have a much lower pH than the pH 7 of the circulatory system[9]. There have been systems developed, however, which are stable with respect to metal ion dissociation and which can provide a template for a stable metal complex. The ligands shown (**Figures 1.1,1.2,1.3** and **1.4**) have high association constants with specific metals, are stable to metal ion dissociation and have all been used in a biological environment.

Both cryptand **(Figure 1.1)** and DPTA **(Figure 1.2)** form stable complexes with Ln(III) ions and have been used in luminescence experiments to probe ligand-receptor binding[10] and in DNA recognition[11] respectively. Although these ligands form relatively stable metal complexes, it is the complexes based on 1,4,7,10 – tetraazacyclododecane - 1,4,7,10 - tetraacetate or DOTA (**Figure 1.3**) which is of particular importance in this discussion.

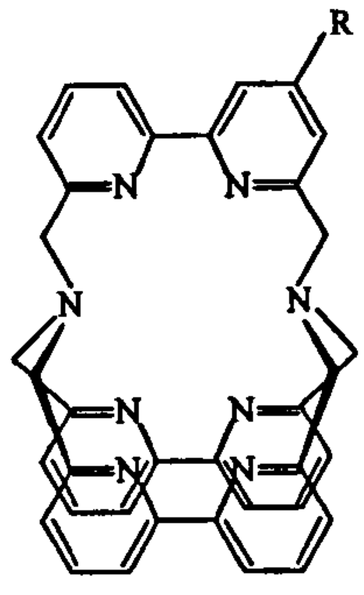

Figure 1.1

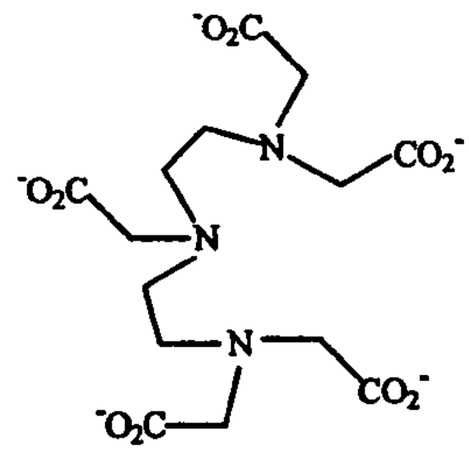

Figure 1.2

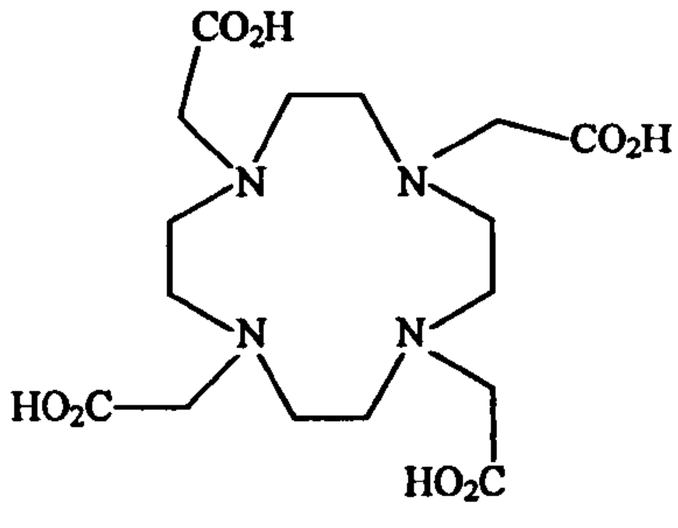

Figure 1.3

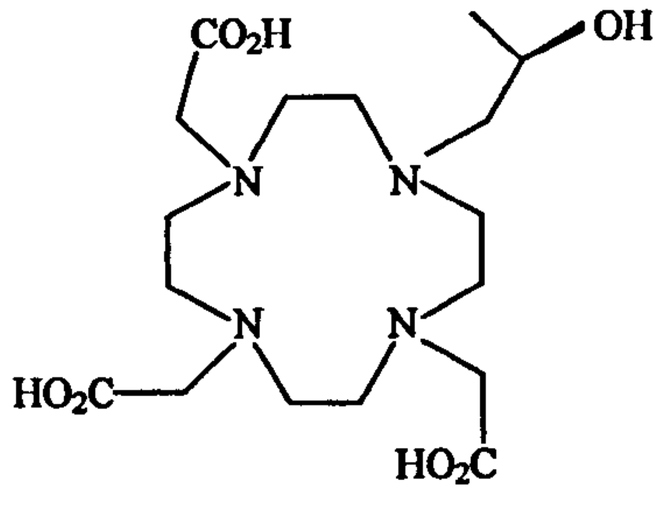

Figure 1.4

The DOTA ligand and its many derivatives have been used extensively and successfully in many metal complexes. DOTA incorporates a cyclen macrocyclic backbone with four carboxylate pendant arms

and is very stable with respect to metal ion dissociation [12,13] . Owing to the robust nature of the ligand in this respect, DOTA has played an integral role in the complexation of metal ions used in therapeutic and diagnostic medicine.

In radiotherapy, cancerous tumors may be selectively targeted using a suitable vehicle, usually an engineered human antibody [14]. A radioisotope able to emit enough radiation to cause cell death can be attached to such a targeting vehicle meaning that the radioactive dose is delivered directly to the tumor, minimising the risk to healthy cells. **Figure 1.5** shows one such example of the DOTA moiety being used to such effect, in this case complexed to the β emitter ^{90}Y.

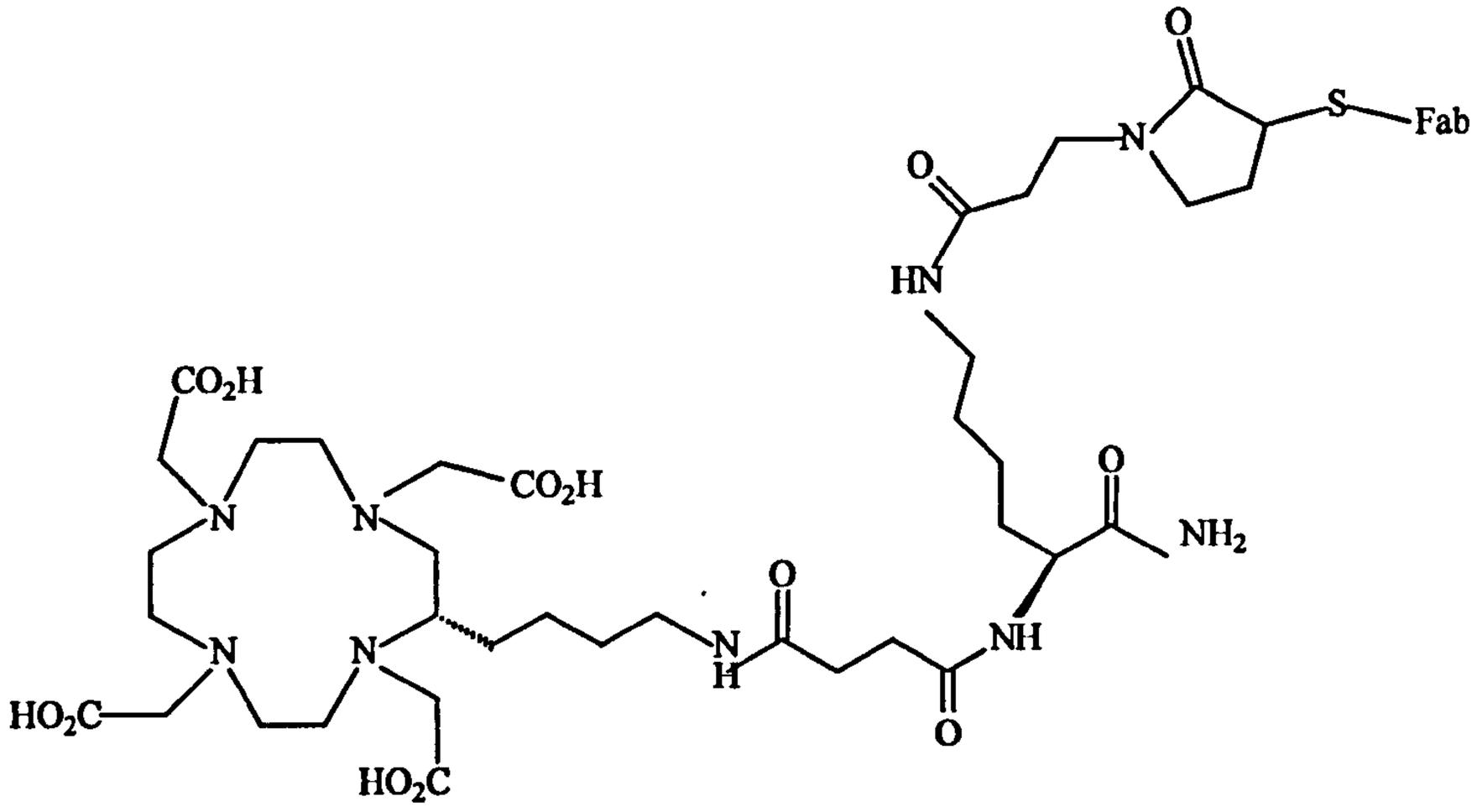

Figure 1.5. In this example of a *tumor targeting* system, the radioisotope ^{90}Y is complexed to the DOTA moiety which is attached via a linking unit to a targeting vehicle (FAB fragment).

The most significant use of the DOTA ligand in a medicinal context, however, has been as a Gadolinium(III) complex used as a contrast agent for magnetic resonance imaging (MRI). Indeed DOTA and the the chiral derivative (**Figure 1.4**) when complexed to Gd^{3+} are now commercially available contrast agents, marketed as Dotarem and Prohance respectively[15]. MRI is an technique which uses the proton resonances of water molecules *in vivo* to build a three-dimensional image of the local environment inside the body.

It is the ability of well defined contrast agents such as $[Gd(DOTA)]^-$ to bind one or two labile water molecules that prompted interest in these systems as a model for an anion receptor by Parker et al. It was hoped that the loss of the bound water molecules would provide a binding site for small anions.

1.2 Reporting of an Event

Although a receptor may successfully recognise a target molecule, the exercise is rendered pointless unless the event is reported or signalled in some manner. There has been a wide range of techniques employed for this purpose in the field of molecular recognition including radioisotopic and electrochemicacal investigations.

Ultrasensitive immunological bioassays were originally dominated by the use of radioisotopic labelling systems which utilised the high energy or particle emission of isotopes such as I^{125} H^3 and P^{32} [14] . The

detection of metal ions by potentiomeric and electrochemical means is well known [16-20] . Given the difficulties that have to be overcome by an anionic detector in aqueous media (differing anionic geometries, pH dependence etc), it is not surprising that fewer examples of electrochemical based anionic receptors have been reported.[1,21-23] .

More relevant to this discussion, however, is the use of metal based luminescent reporters. Lanthanide based probes are now widely used in immunological studies [24-26] and preferential over radioisotopic methods. Of the non-lanthanide luminescent species, ruthenium tris(diimine) complexes have been studied extensively. [27-28] These complexes have been used to report the sensing of target molecules [30] One such target molecule has been DNA and has been successfully sensed by the $[Ru(bipy)_2DPPZ]^{2+}$ (**Figure 1.6**) [31] complex [32-34] . Characteristic ruthenium luminescence is observed for the complex in organic solvents but in water the luminescence is quenched. It is thought that this is a result of the interaction of the nitrogens of the phenazine with closely diffusing solvent water molecules. Ruthenium luminescence is once again observed, however, in the presence of DNA in aqueous solution. It is proposed that the DPPZ moiety acts as an intercalating unit, slipping between adjacent base pairs of DNA. This inhibits the deactivating effect of solvent molecules and the molecule emits.

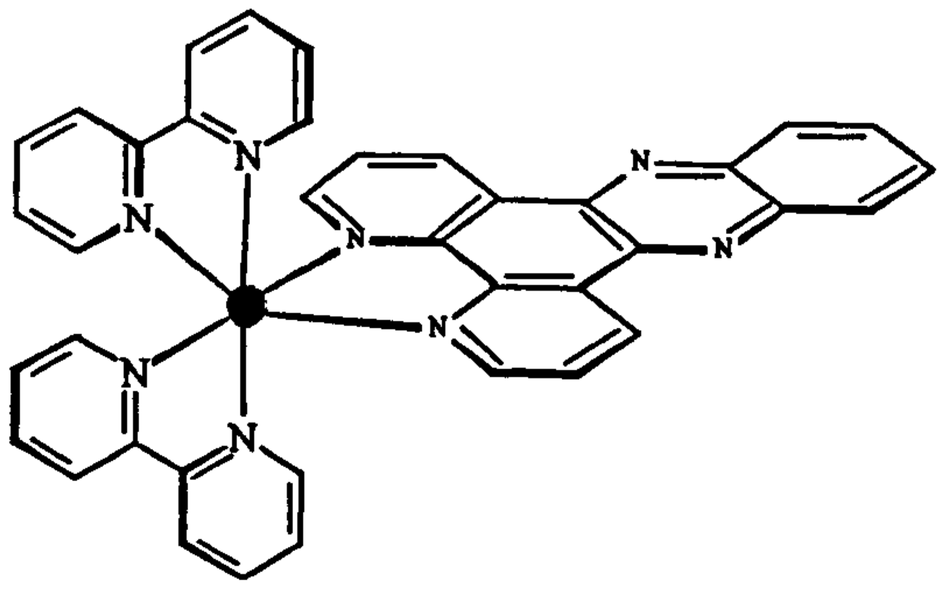

Figure 1.6 Representation of the $[Ru(bipy)_2DPPZ]^{2+}$ System

1.3 Lanthanide Luminescence

It is the characteristic long lived luminescence of lanthanide(III) systems, however, which has been of growing interest in recent years. The lanthanides contain filled or partially filled f orbitals[35]. These f orbitals are found well within the electronic shell of the atom and so are well shielded from the perturbing effects of any ligand field. This means that unlike transition metals where distinct spectroscopic energy levels of the metal ion are determined by the coordination geometry of the surrounding ligands, the phenomenon of *spin-orbit coupling* has a more pronounced effect in lanthanide systems. Both electrons and orbitals have intrinsic angular momentum. These momenta interact ie couple to give a resultant angular momentum. This is known as spin-orbit coupling[36]. This phenomenon means that the (2S+1) fold degeneracy of a spectroscopically distinct energy levels is split (where S is the spin multiplicity). Each new distinct level is characterised by a value of J, the

resultant angular momentum. **Figure 1.7** shows the lowest lying energy levels of the Eu^{3+} and Tb^{3+} ions and the splitting of the ^7F_J and ^5D_J levels by spin-orbit coupling.

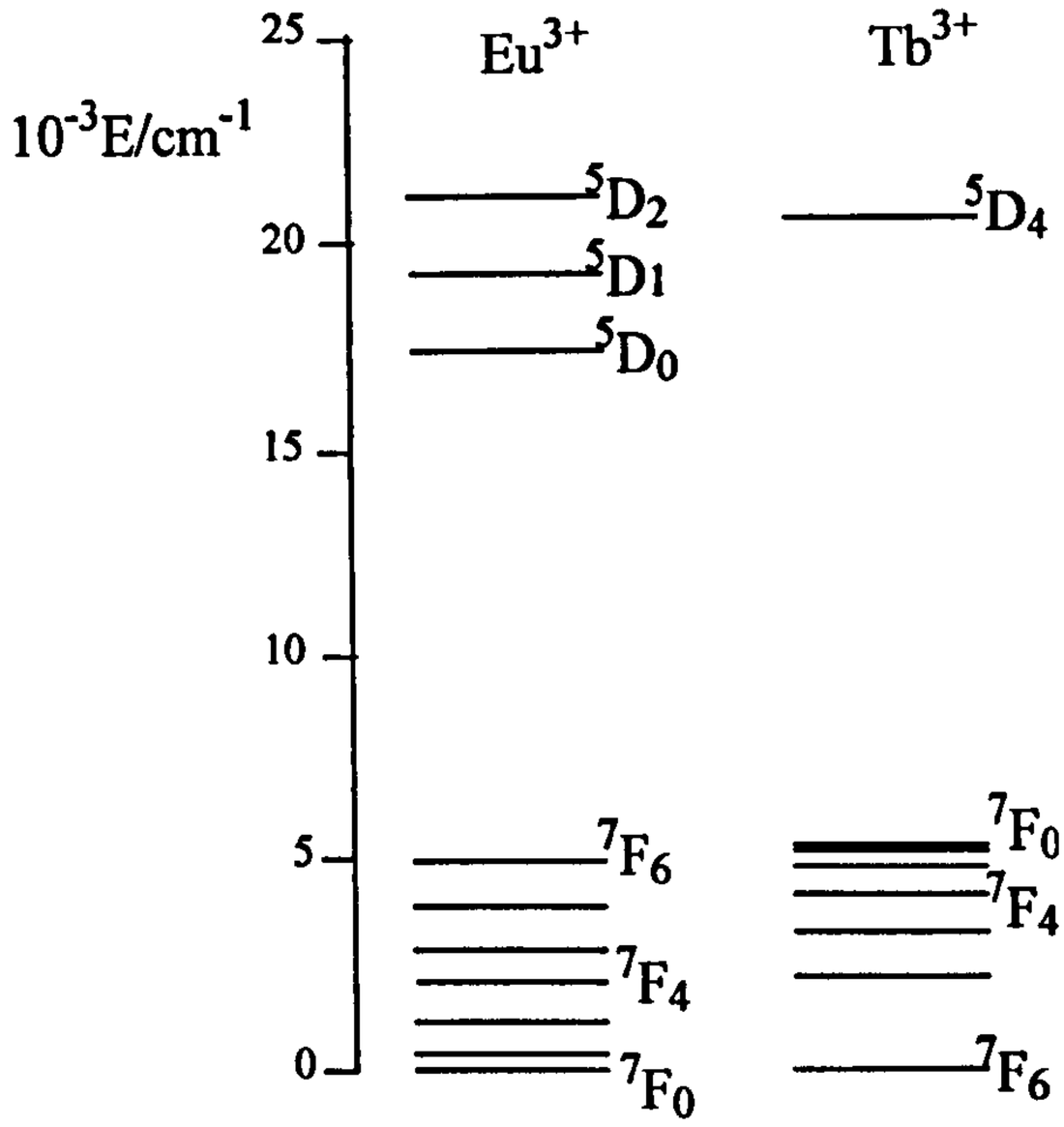

Figure 1.7. Lowest lying energy levels of Eu^{3+} and Tb^{3+}

In general for metal based luminescence, the transitions that give rise to the emission are those from the lowest lying excited level (and any other level in thermal equilibrium with it) to the electronic ground state[37]. For Eu^{3+} the emissive state is the $^5D_0$ level and the luminescence occurs as a result of transitions from this level to the seven ^7F_J levels. Similarly, Tb^{3+} luminescence occurs from the $^5D_4 \rightarrow {}^7F_J$ transitions.

1.4 Lanthanide Emission Spectra

The emission spectra associated with these localised 4*f*-4*f* transitions are characterised by well defined, sharp, emission bands [38] have been the subject of much study. These characteristic emission bands are evident in the luminescence spectrum of the previously reported[39] europium(III) complex of the ligand L^{tet} as shown (**Figure 1.8**).

The transitions labelled a, b, c, d and e represent the $^5D_0 \rightarrow {}^7F_0$, $^5D_0 \rightarrow {}^7F_1$, $^5D_0 \rightarrow {}^7F_2$ and $^5D_0 \rightarrow {}^7F_3$ and $^5D_0 \rightarrow {}^7F_4$ transitions respectively using conventional notation. These transitions can also be described in terms of the change in the angular momentum quantum number, J, from the excited state ^5D_J (J=0) manifold to the degenerate ^7F_J states (J=0,1,2,3,4,5 and 6). Thus the transition $^5D_0 \rightarrow {}^7F_0$ may be noted as a $\Delta J = 0$ transition, the transition $^5D_0 \rightarrow {}^7F_1$ a $\Delta J = 1$ transition, $^5D_0 \rightarrow {}^7F_2$ a $\Delta J = 2$ transition and so forth. A pictorial representation of these transitions of the $^5D_0$ manifold to the electric ground state is shown by **Figure 1.9.**

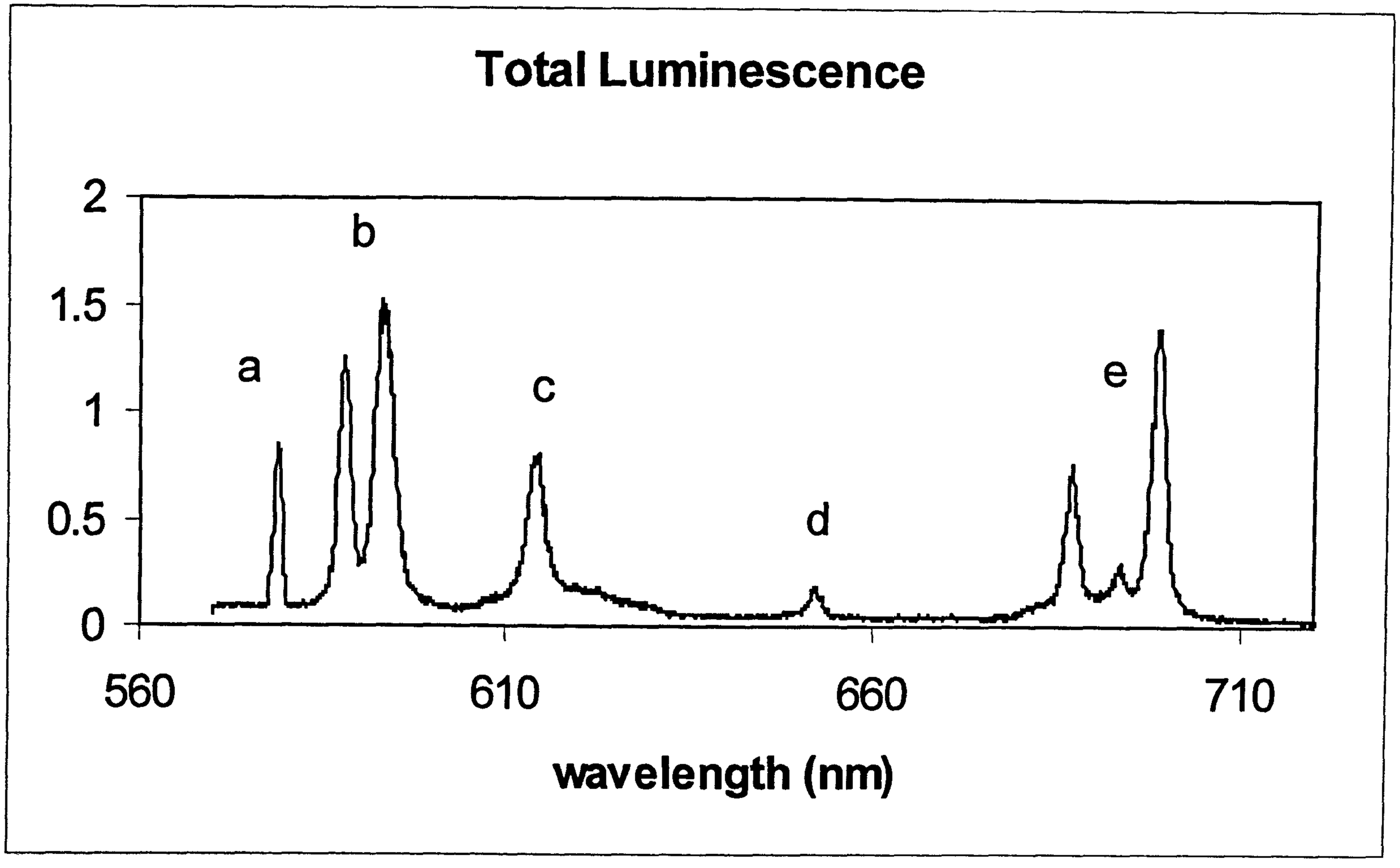

Figure 1.8. Conventional luminesence spectrum of the $[EuL^{tet}]^{3+}$ complex

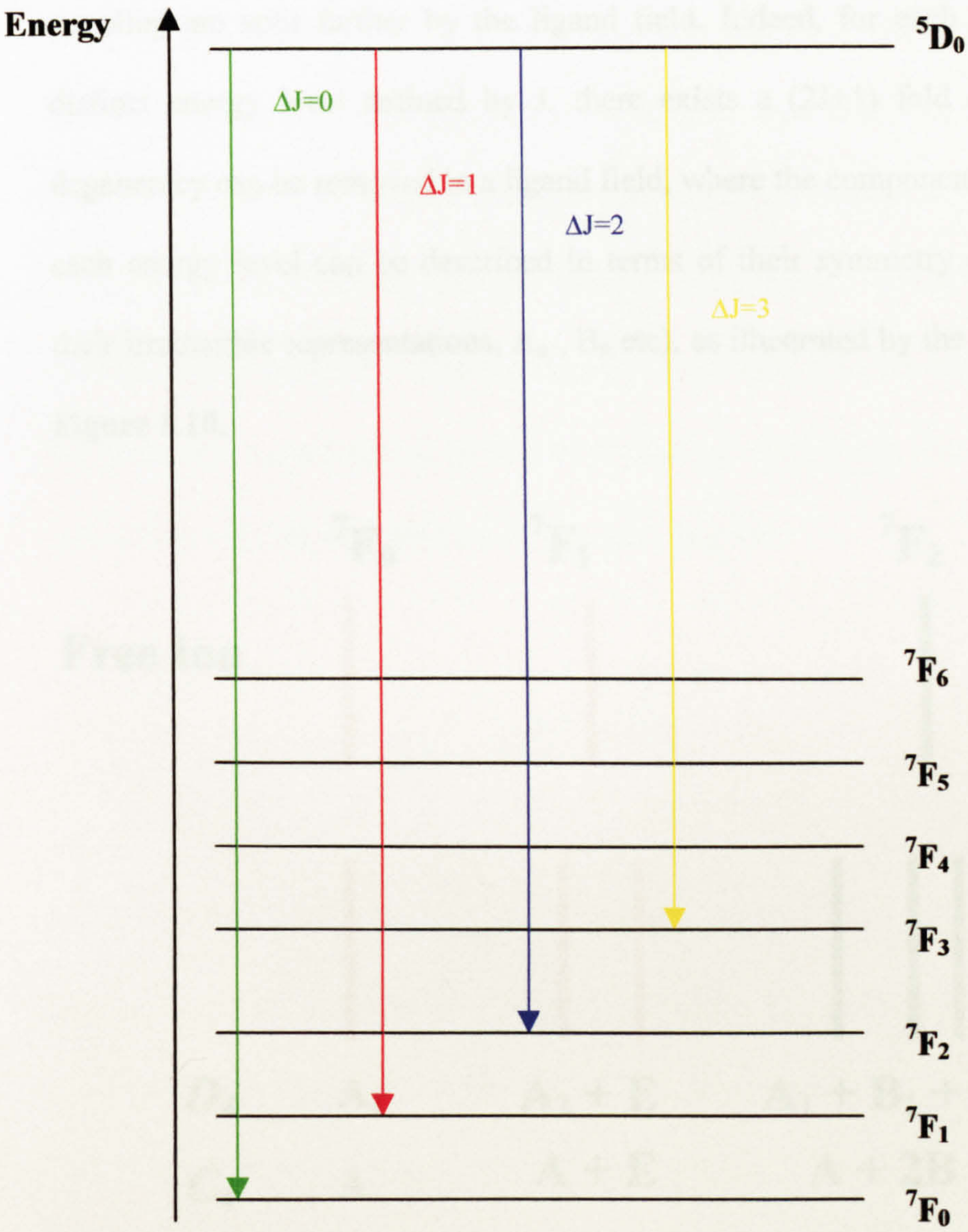

Figure 1.9 Pictorial representation of ΔJ=0, 1, 2 and 3 transitions of the $^5D_0$ manifold of Europium(III)

1.5 Ligand Field Effects

Even although the f electrons are well shielded, the ligand field does indeed perturb the electronic make-up of lanthanide(III) ions. The energy levels split by spin-orbit coupling are split further by the ligand field. Indeed, for each spectroscopically distinct energy level defined by J, there exists a (2J+1) fold degeneracy. This degeneracy can be removed in a ligand field, where the components associated with each energy level can be described in terms of their symmetry characteristics (ie their irreducible representations, A_n , B_n etc), as illustrated by the schematic below.

Figure 1.10.

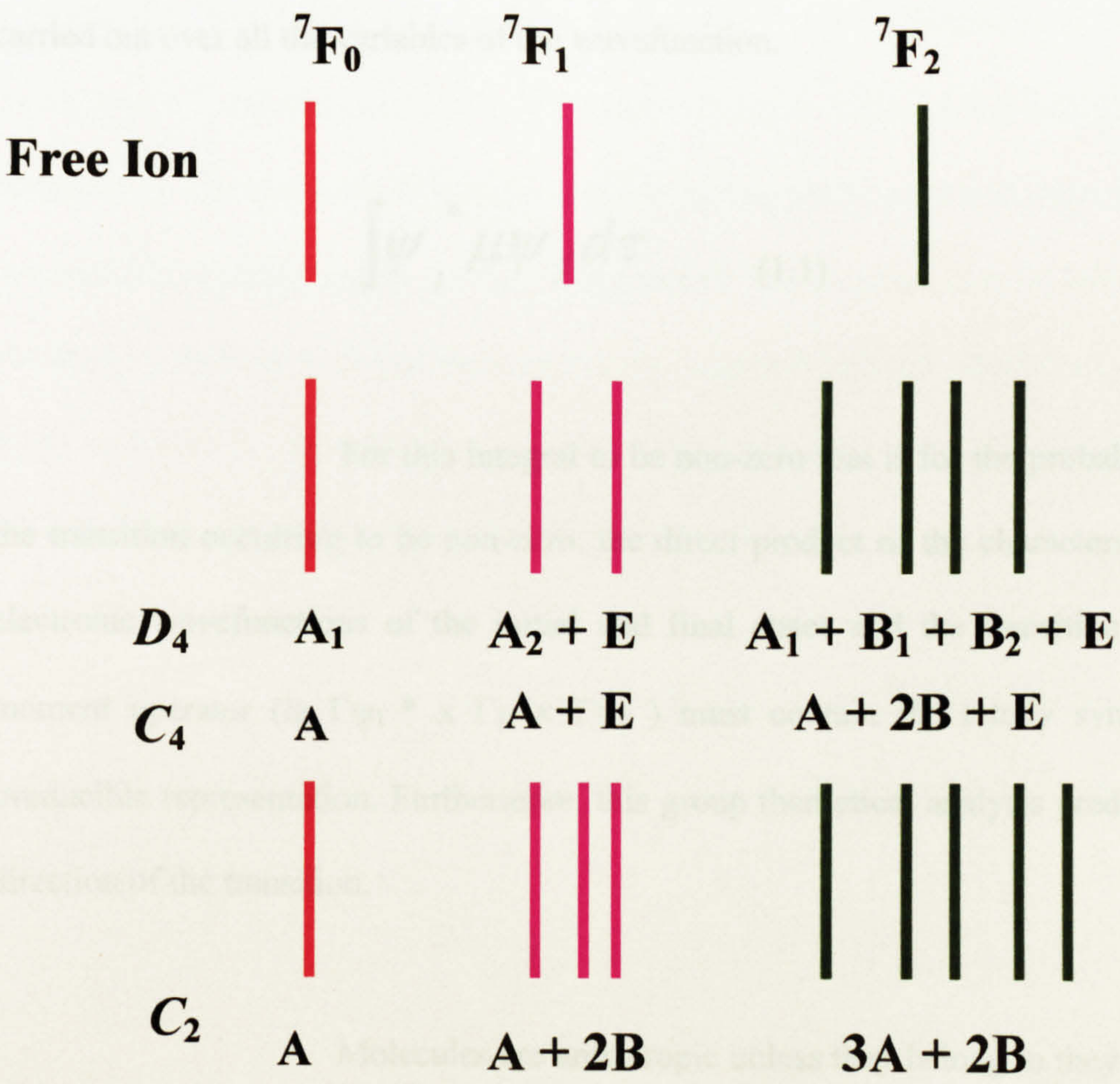

Figure 1.10. The effect of a ligand field on the splitting of Eu^{3+} energy levels

1.6 Group Theory

In order to determine whether an electronic transition within a molecule will occur; that is whether the transition is electric or magnetic dipole allowed, the symmetry of the molecule and therefore the transition must be investigated. An electronic transition between an initial electronic state *i* and a final state *f* involves an interaction with the electronic dipole moment μ. The probability of this transition occurring is proportional to the integral outlined below where ψ_i * is the complex conjugate of the electronic wavefunction of the initial state and ψ_f is the electronic wavefunction of the final state and $d\tau$ implies that the integration is carried out over all the variables of the wavefunction.

$$\int \psi_i^* \mu \psi_f d\tau \qquad (1.1)$$

For this integral to be non-zero that is for the probability of the transition occurring to be non-zero, the direct product of the characters of the electronic wavefunctions of the initial and final states and the transition dipole moment operator (ie $\Gamma\psi_I$ * x $\Gamma\mu$ x $\Gamma\psi_f$) must contain the totally symmetric irreducible representation. Furthermore, this group theoretical analysis predicts the direction of the transition.

Molecules are anisotropic unless they belong to they belong to the cubic or icosahedral point groups: that is their molecular axes transform as either two or three irreducible representations. During the course of an electronic

transition a transient charge distribution is set up such that the transition is polarised along a molecular axis or plane. The irreducible representation(s) of the direct product indicate the direction of this transient charge distribution. When the irreducible representation transforms as x, y, or z there exists a *translation* of charge: the transition is therefore *electric dipole moment* allowed along the corresponding axis (x, y, or z). Similarly when the irreducible representation transforms as R_x , R_y or R_z there exists a *rotation* of charge and the transition is *magnetic dipole moment* allowed.

When a transition is both electric and magnetic dipole moment allowed the resultant transient charge distribution is helical in nature: that is, the scalar product of an electric and magnetic dipole moment is a helical charge distribution. The emission is therefore said to be circularly polarised. Since a helix is inherently chiral in nature (left or right handed) the emission may be left or right circularly polarised. Left and right circularly polarised light are illustrated (**Figure 1.11**) and can be thought of as arising from two orthogonal beams of plane polarised light which are out of phase by a quarter of a wavelength.

A further constraint is placed on the 'allowedness' of a given transition. The Laporte selection rule forbids transitions between electronic states of similar parity ($\Delta l \neq 0$).

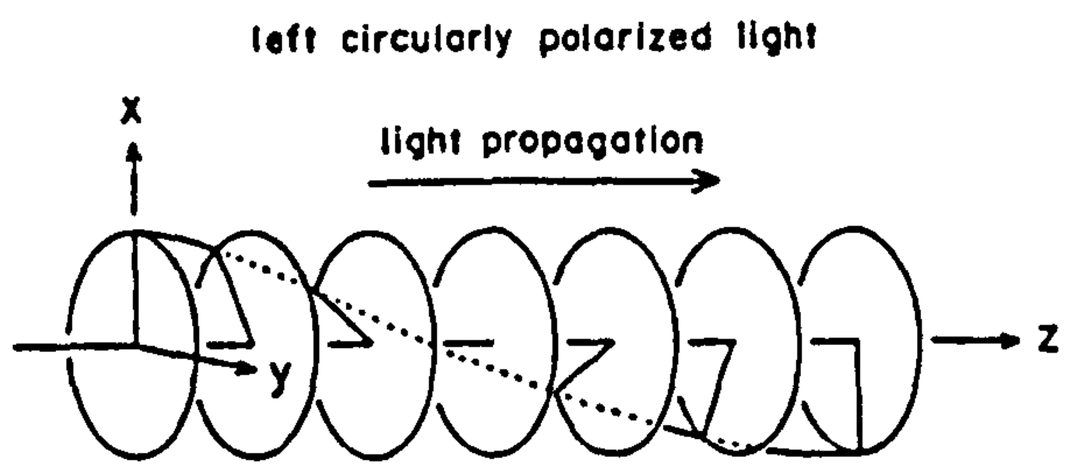

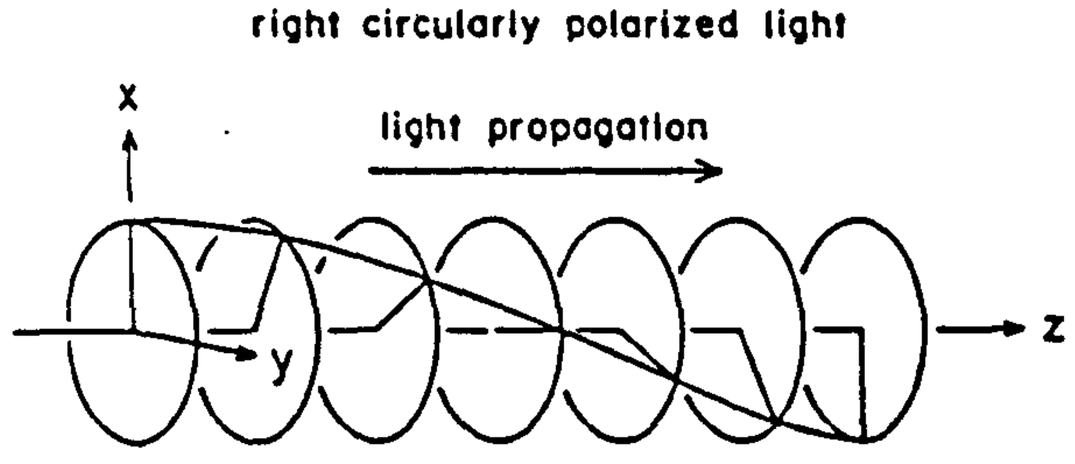

Figure 1.11 Pictorial representation of the helical nature of left and right circularly polarised light.

1.7 4f – 4f Emission Intensities

Whereas the localised 4f-4f transitions are all parity allowed in magnetic dipole radiation, they are parity forbidden in electric dipole radiation [40] . Although the observed intensity of the $^5D_0 \rightarrow {}^7F_1$ transition may be explained in terms of a magnetic dipole mechanism [41,42] this mechanism does not account for the remaining transitions. Work conducted primarily by Judd [43] and Ofelt [44] produced the theoretical formalism of the two independent mechanisms by which the states of the $4f^N$ configurational manifold may incorporate the odd parity states required for the 4f-4f transitions to gain their intensity [44,45] .

In the *static coupling* [40,43,44,47] (or forced electric dipole) mechanism, odd parity states of the spectroscopic basis set are taken from the lanthanide $4f^{N-1}$ 5d and $4f^{N-1}$ ng configurations as a result of multipole (lanthanide)-point chage (ligand interactions. The *dynamic coupling* [40,47,48,49] (or ligand polarisation) mechanism proposes that odd parity states are included in the spectroscopic basis set as a result of lanthanide-ligand interactions where the interaction may be described as multipole (lanthanide) – dipole (ligand) couplings. It should be noted that the transitions that are particularly effected by the polarisability of the ligand and have thus been classed as *hypersensitive* transitions [39] .

Of the first five transitions of the europium(III) $^5D_0$ manifold to the electric ground state (the $\Delta J = 0$, 1, 2, 3 and 4 transitions) we

can now postulate which mechanism is responsible for the observed luminescence intensity. The $\Delta J = 0$ transition is both electric and magnetic dipole forbidden. The observed intensity of this transition has been attributed to d (or g) orbital mixing via the linear A_{1p} term in the crystal field expansion of the C_{nv}, C_n and C_s point groups. The $\Delta J = 1$ transition is magnetic dipole allowed, electric dipole forbidden. As stated previously the intensity of this transition is gained via a magnetic dipole mechanism. The $\Delta J = 2$ and 4 transitions are electric dipole allowed by considering the Judd-Ofelt mechanisms. Finally the $\Delta J = 3$ transition is both electric and magnetic dipole forbidden. The intensity of this transition is believed to derive via J mixing with the allowed transitions.

J mixing is the transfer of excitation between fine-structure sub levels. J is a 'good' quantum number, thus J can be mixed with J' by the even part of the crystal field. As an example, the intensity of the $^7F_2$ transition may the a result of the mixing of this transition with the allowed $^7F_2$ transition as described by:

$$\left|{}^7F_3\right\rangle = \left|{}^7F_3\right\rangle + \lambda\left|{}^7F_1\right\rangle \qquad (1.2)$$

The mechanisms outlined above provide a theoretical basis to explain the observed intensities for lanthanide *f-f* transitions. As stated, however, for the resultant transient charge distribution set up during these transitions to be helical in nature, that is for the emission of circularly polarised light, the transitions must be both electric and magnetic dipole moment allowed. This can only be achieved via J mixing.

On inspection of Character tables it is clear that translations of charge and the corresponding rotations of charge transform as the same irreducible representations only for chiral point groups. Thus circularly polarised luminescence spectroscopy is a technique applicable only to chiral molecules.

1.8 Circularly Polarised Luminescence

Systems which emit and absorb circularly polarised light differentially are those which have a chromophore that experiences a chiral force field[50]. Systems that are naturally optically active, such as those described above, have an inherent chiral force field. Electronic transitions which give rise to luminescence, can, in such an environment, emit left and right circularly polarised radiation differentially. Circularly polarised luminescence (CPL) spectroscopy involves the detection of this differential emission and can be thought of as the emission analogue of circular dichroism (CD) spectroscopy[45,46,50-53].

Whereas the electronic ground state of a system is investigated by CD, it is the electronic excited state which is probed in a CPL experiment. The primary observables in CPL spectroscopy are the **circular emission intensity differential**

$$\Delta I(\lambda) = I_L(\lambda) - I_R(\lambda) \qquad (1.3)$$

and the **emission dissymmetry factor, g_{em}**, a measure of the degree of chirality experienced by an electronic transition.

$$g_{em}(\lambda) = 2\Delta(\lambda) / I(\lambda) \qquad (1.4)$$

where I_R and I_L denote respectively the intensities of the right and left circularly polarised components of the emitted radiation and $I(\lambda) = I_R(\lambda) + I_L(\lambda)$ gives the total intensity of the emission at wavelength λ. These terms can be related directly to the observables in CD spectroscopy namely the circular absorption intensity differential

$$\Delta\varepsilon(\lambda) = \varepsilon_L(\lambda) - \varepsilon_R(\lambda) \qquad (1.5)$$

and the absorption dissymmetry factor

$$g_{abs}(\lambda) = \Delta\varepsilon(\lambda) / \varepsilon(\lambda) \qquad (1.6)$$

where ε_L and ε_R denote respectively the absorption coefficients of the right and left circularly polarised components of the incident radiation and $\varepsilon(\lambda) = [\varepsilon_L(\lambda) + \varepsilon_R(\lambda)] /2$ gives the total absorption.

It is from the extensive work on optical rotation and circular dichroism that the theoretical development of CPL has its basis [50-53]. From an analysis of optically active ketones [54], Emesis and Oosterhof were the

first to show that in the limit that the orientational distribution of the emitting molecules is isotropic, there is a direct analogy between the theoretical expressions of CD and CPL. For a given transition (a ↔ b) in this limit, both $\Delta\varepsilon$ and ΔI may be expressed in terms of a single electronic parameter, the *rotary strength*.[45,46,50,53] The rotary strength can be described by

$$R_{ab} = \mid P_{ab} \mid \mid M_{ba} \mid \cos\tau_{ab} \qquad (1.7)$$

Where $|P_{ab}|$ is the electric dipole transition moment vectors and $|M_{ba}|$ the magnetic dipole transition moment vector with τ_{ab} the angle between these vectors. The emission dissymmetry factor, g_{em}, of a given transition (a ↔ b) at wavelength, λ, as described by equation 1.8 is given by

$$g_{em}(\lambda) = \frac{2\Delta(\lambda)}{I(\lambda)} = \frac{2(I_L - I_R)}{(I_L + I_R)} \qquad (1.8)$$

This value can also be described in terms of the rotary strength R_{ab} and the electric dipole strength D_{ab} as shown by **Equation 1.9.**

$$g_{em} = \frac{4R_{ab}}{|D_{ab}|} \qquad (1.9)$$

given that $D_{ab} \approx \sqrt{|P_{ab}|}$, [45] then the dissymmetry factor may also be expressed as:

$$g_{em} = \frac{4|M_{ba}|}{|P_{ab}|}\cos\tau_{ab} \qquad (1.10)$$

The largest dissymmetry factor would then be shown by magnetic dipole allowed, electric dipole forbidden transitions. The most intense CPL transitions, however, will be both magnetic and electric dipole allowed [46]. Furthermore, **Equation 1.10** implies that the dissymmetry factor and therefore the CPL signal would vanish when the magnetic and electric dipole moment vectors are at right angles to one another.

1.9 Spectra – Structure Correlations

Although CD and CPL are fundamentally related, CPL has several advantages over CD. For systems which show very little absorption, making CD spectra very difficult or impossible to obtain, it is often the case that CPL data can be obtained by population of the emissive state by indirect means (as is the case for lanthanide(III) ions). It is also found that for a luminescent species, it is usually only one emissive state that yields the characteristic luminescence. This is unlike an absorption study where several absorption bands may be observed and often overlap to 'hide' some transitions.

However, whereas there has been much work in the development of formal theories to determine the stereochemistry of related compounds using CD spectroscopy, there have been few attempts made at

developing CPL spectra-structure relationships. This is not entirely surprising considering the difficulties that have to be over come to achieve such a relationship. As stated a CPL experiment is the direct probe of the excited state of a molecule; whereas the ground state geometry may be well defined, the geometry of the emitting state, an essential piece of information for any theoretical formalism is a quantity that is rarely well defined. For systems where the emitting species is largely independent of ground and excited state conformational changes (such as the $n \leftrightarrow \pi^*$ transitions in β, γ - enones), and in conjunction with CD data, some CPL spectra-structure relationships have been made [55,56].

Although there have been studies made on the rotational strengths of the 4f-4f transitions of the lanthanide ions, these calculations are non-trivial and cannot be used to determine the absolute configuration of the emitting species from CPL data. The inherent problem lies in the poorly understood mechanism by which optical activity is induced in systems of this type; more specifically it is the effect of *J-mixing* that is not well defined. As defined by equation 1.7, the origins and magnitude of the observed optical activity of these transitions is described by the rotary strength. The rotary strength can also be expressed in such a way as to define the effect of the mixing of J states. For example the mixing of $^7F_1$ and $^7F_2$ states

$$R \approx \mathrm{Im}\langle {}^5D_0|\mu|{}^7F_2\rangle\langle {}^7F_2|V|{}^7F_1\rangle\langle {}^7F_1|m|{}^5D_0\rangle \qquad (1.11)$$

The differing symmetry characteristics of components of the transitions (*eg* A and E) can be assessed independently from one another.

$$R(E) \approx \mathrm{Im}\langle {}^5D_0|\mu|{}^7F_2(E)\rangle\langle {}^7F_2(E)|V|{}^7F_1(E)\rangle\langle {}^7F_1(E)|m|{}^5D_0\rangle \quad (1.12)$$

$$R(A) \approx \mathrm{Im}\langle {}^5D_0|\mu|{}^7F_2(A)\rangle\langle {}^7F_2(A)|V|{}^7F_1(A)\rangle\langle {}^7F_1(A)|m|{}^5D_0\rangle \quad (1.13)$$

Despite valiant efforts (notably by Richardson [56]), no methodology has been developed to fully account for the action of the operator V and thus explain comprehensively the role that J-mixing plays in f-f systems. It is for this reason that no spectra-structure relationship has yet been developed for CPL spectroscopy.

1.10 Luminescence Lifetimes and Quantum Yield

As noted, the resultant luminescence from these localised f-f transitions are characteristically long-lived. Although the term long-lived may appear to be an arbitrary description of a photon emitter, the *lifetime* of a luminescent species is an experimentally obtained quantity.

In an investigation into the luminescent properties of a given entity, if a single luminescent species is present we would expect monoexponential decay of this luminescence [57] . That is, the emission intensity at a time t after an excitation pulse will be given by:

$$I_t = I_0 \exp(-k_{obs} t) \qquad (1.14)$$

where I_0 is the emission intensity at t = 0 and k_{obs} is the observed rate constant for the monoexponential decay and is equal to the sum of the radiative rate constant k^0 and the first order rate constants for competing non-radiative processes, k^{nr}.

$$k_{obs} = k^0 + \sum k_i^{nr} \qquad (1.15)$$

The observed lifetime of the emission, τ_{obs}, is simply the reciprocal of k_{obs}. Another useful quantity is the quantum yield of emission, φ_{em}, which is defined as the ratio of the number of photons emitted to the number of photons absorbed.

$$\varphi_{em} = \frac{k^0}{k^0 + \sum k_i^{nr}} \qquad (1.16)$$

1.11 Sensitised Emission

Although the advantages to be gained from using Ln(III) ions are very attractive there are several obstacles that have to be overcome before this becomes a viable technique. These problems are mainly the low molar absorptivities of the Ln(III) ions and the deactivation of the emissive state by non-radiative processes.

As discussed in 1.4, as a consequence of the forbidden nature of the 4f-4f transitions in electric dipole radiation, low molar absorptivities of the lanthanide(III) ions are observed. To overcome this problem the emissive state is populated by *sensitised* rather than direct excitation[57]. A photosensitiser (usually called an antenna or chromophore) is a species which can act as an electron and/or energy donor to a electron/energy acceptor without being chemically changed. The photosensitising unit is often attached to the electron/energy acceptor via a spacer to ensure maximum efficiency of energy/electron transfer. The concept of sensitised emission is shown schematically **Figure 1.12.**

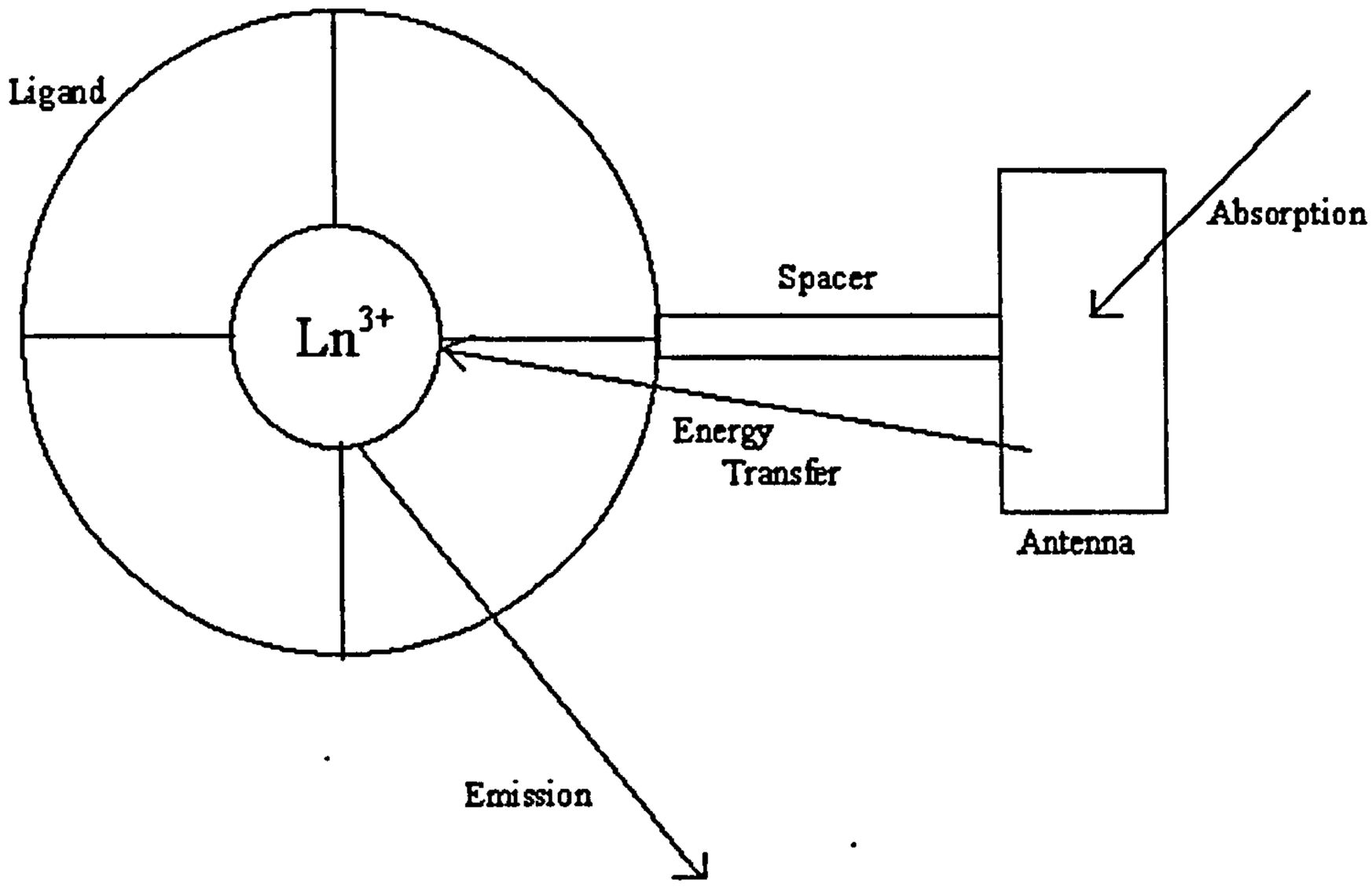

Figure 1.12 Schematic representation of the concept of sensitised emission of a Ln(III) ion

1.12 Competitive Deactivation Modes

In general, once the excited state has been populated, there are several ways in which decay to the ground state can be achieved. The system may emit radiation, it may decay thermally through vibrations and rotations or it may also be deactivated (or quenched) by an external component. In the 1960s the deactivating or quenching effect of water molecules was observed by Kropp and Windsor[58]. It was shown that both the intensity and lifetime of emission from Eu^{3+} and Tb^{3+} in D_2O was greater than in H_2O. Further study showed that the quenching of aquated Ln^{3+} was a result of energy transfer from the emissive state to the O-H stretching vibrations. Similarly, D_2O quenching occurs via energy transfer to O-D oscillators. Water is a better quenching agent than D_2O since the O-H vibrationally excited state

wavefunctions are more closely matched to the wavefunctions the Ln^{3+} excited state than the O-D wavefunctions (Franck – Condon).

1.13 Estimation of Hydration State [57,58-60]

It was also found that in general, the rate of quenching by an A-B oscillator was proportional to the number of A-B oscillators. Further work showed that the quenching by O-H oscillators could be considered separately from other deactivating processes, as defined by the equation below.

$$k_{\text{obs}}^{H_2O} = k^0 + \sum k_i^{nr} + k_{OH} \qquad (1.17)$$

Where $k_{obs}^{H_2O}$ is the observed luminescence decay constant in water

k_{OH} is the rate of energy transfer to O-H vibrational levels and

$\sum k_i^{nr}$ the sum of all other rate constants for non-radiative deactivation of the excited state.

However in D_2O the expression for the observed rate constant is

$$k_{obs}^{D_2O} = k^0 + \sum k_i^{nr} \qquad (1.18)$$

Heller and Stein[61] showed that

$$\Delta k_{obs} = k_{obs}^{H_2O} - k_{obs}^{D_2O} = k_{OH} \qquad (1.19)$$

Since k_{OH} is an independent factor in the quenching process, it follows that:

$$\Delta k_{obs} = k_{OH} = A'q \qquad (1.20)$$

Where q is the number of water molecules associated with the metal ion and A' is a proportionality constant. Rearranging equation X in terms of τ, the luminescence and defining A_{ln} as a proportionality constant for a given lanthanide ion,

$$q = A_{Ln}(\tau_{H_2O}^{-1} - \tau_{D_2O}^{-1}) \quad (1.21)$$

We now have a direct relation between the number of associated water molecules and the lifetime of the luminescence in H_2O and D_2O. The proportionality constants A_{ln} have been determined by plots of $\Delta\tau^{-1}$ vs q (determined by X-ray crystallography) for both Eu^{3+} (A_{eu}=1.05) and Tb^{3+} (A_{tb}=4.20). Thus a measurement of the lifetime of a lanthanide complex in H_2O and in D_2O can give an estimation of the hydration state, q, of the molecule.

1.14 Stereoisomerism of the DOTA System

Lanthanide(III) complexes of dota in solution can adopt a square antiprismatic and twisted square antiprismatic conformation. These conformations are chiral and so the complexes may adopt four distinct conformations. More specifically there exists two enantiomeric pairs of diastereomers which are all interconvertable via either pendant arm rotation or ring inversion[39] (**Figure 1.13**). The major pair of enantiomers (denoted M_1 and M_2 in the diagram) have the square antiprismatic form whereas the minor pair (m_1 and m_2) have the twisted square antiprismatic form [62] . The ratio of these (*ie* M:m) is 4:1. The major enantiomers are labelled Δ(λλλλ) and Λ(δδδδ) according to conventional classification[63] where Δ and Λ signify the helicity of the pendant arms (clockwise and anticlockwise respectively) and λλλλ and δδδδ signify the two enantiomeric conformations of the macrocyclic ring.

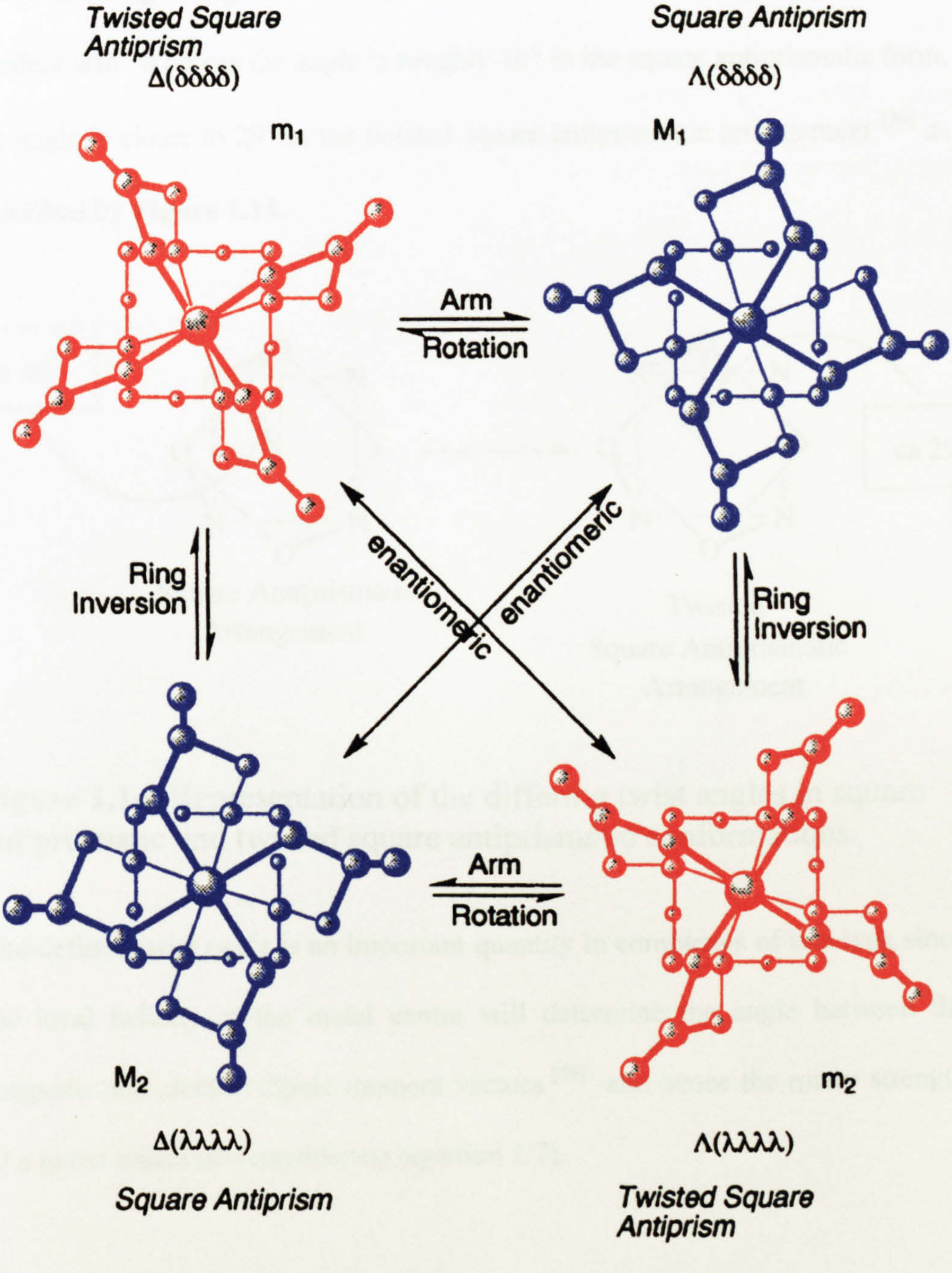

Figure 1.13 Representation of the isomers of complexes of dota showing possible exchange mechanisms

The square antiprismatic and twisted square antiprismatic forms can be defined in terms of the twist angle between the plane of the four ring nitrogens and the plane of the four coordinating oxygens of the pendant arm. Whereas the angle is roughly 40° in the square antiprismatic form, the angle is closer to 29° in the twisted square antiprismatic arrangement [39] as described by **Figure 1.14.**

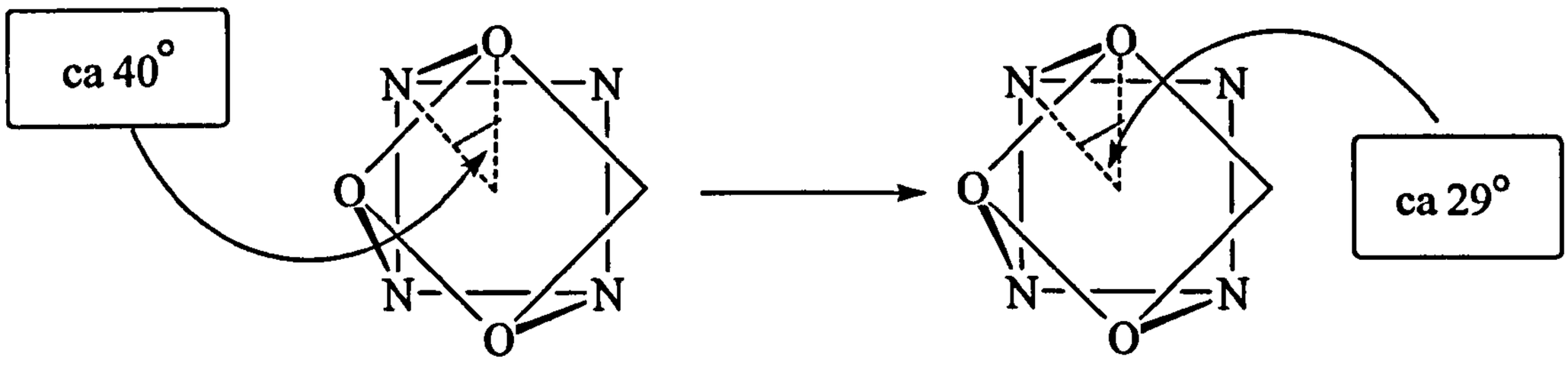

Figure 1.14. Representation of the differing twist angles in square antiprismatic and twisted square antiprismatic conformations.

The defined twist angle is an important quantity in complexes of this type since the local helicity at the metal centre will determine the angle between the magnetic and electric dipole moment vectors [46] and hence the rotary strength of a given transition (considering equation 1.7).

1.15 Predetermined Stereochemistry

From the extensive work carried out on macrocyclic complexes based on this DOTA system most notably by Parker *et al* it has been shown that structural rigidity may be induced in complexes of this kind. It is

found that the introduction of a remote chiral centre on the pendant arm δ to the ring nitrogen both locks the ring conformation and prevents arm rotation[39]. This then leads to the formation of an enantiopure complex that may be made selectively by altering the nature of the remote stereogenic centre. This is exemplified by the mirror image nature of the (previously reported [12]) crystal structures of (*SSSS*)- and (*RRRR*)-[EuL^{tet}]$^{3+}$ complex, shown overleaf (**Figure 1.15**).The nature of the chiral ligand L^{tet} and associated ligands L^{1a}, L^{1b} and L^{1c} are described by **Figure 1.16** below.

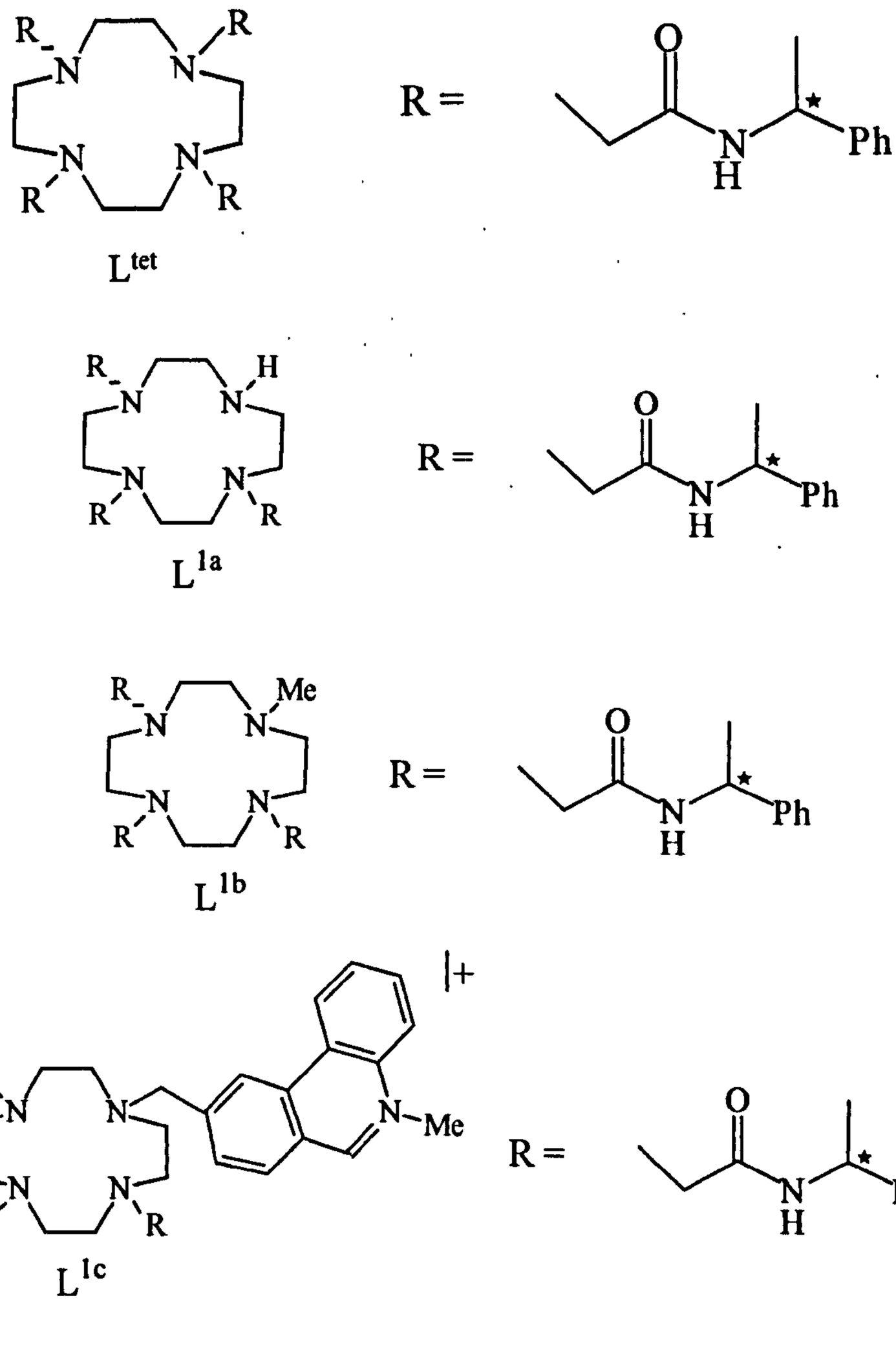

Figure 1.6 Chiral Ligands L^{tet} L^{1a}, L^{1b} and L^{1c}

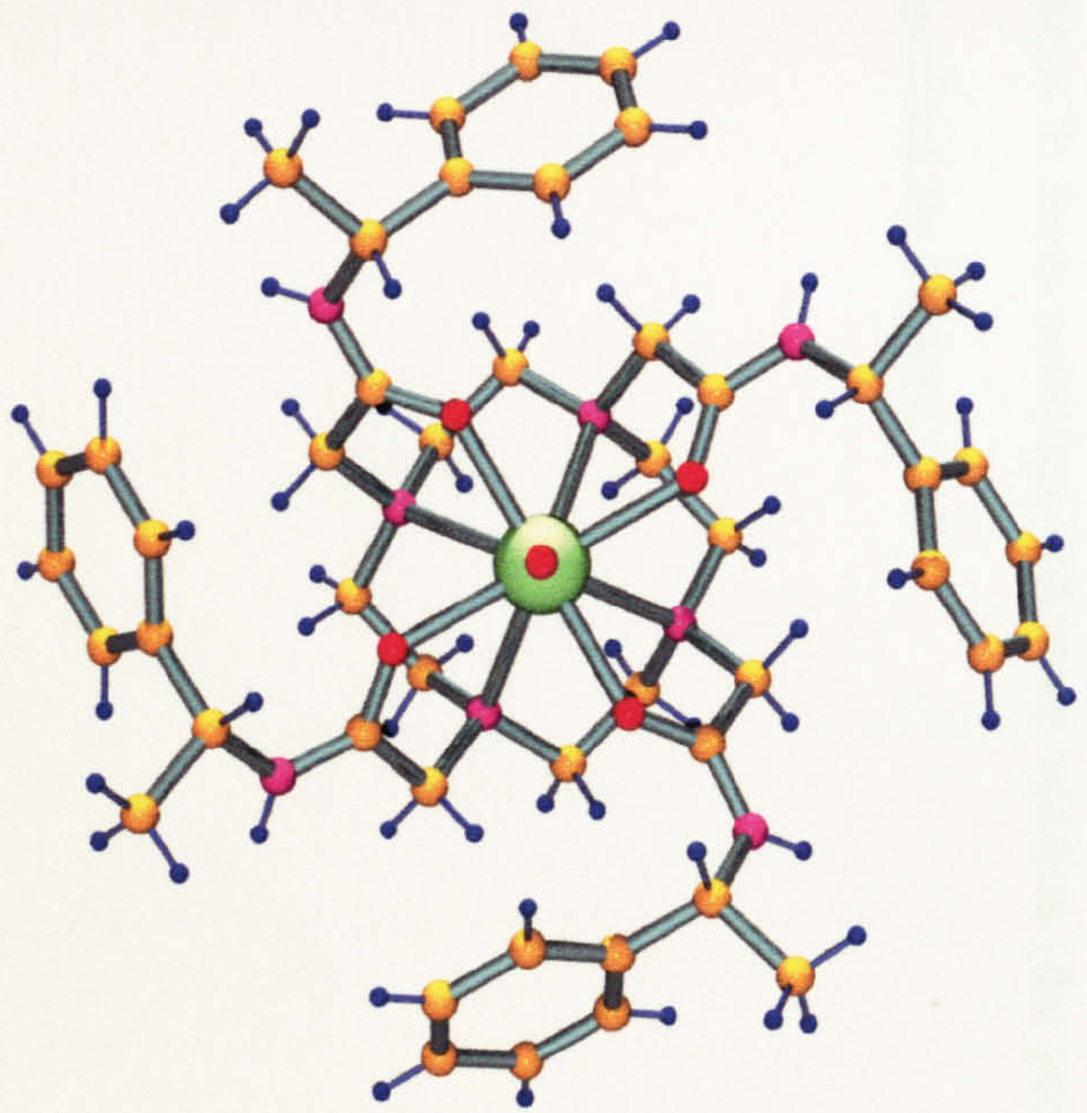

(*SSSS*)-[Eu(L^{tet})(H_2O)]$^{3+}$

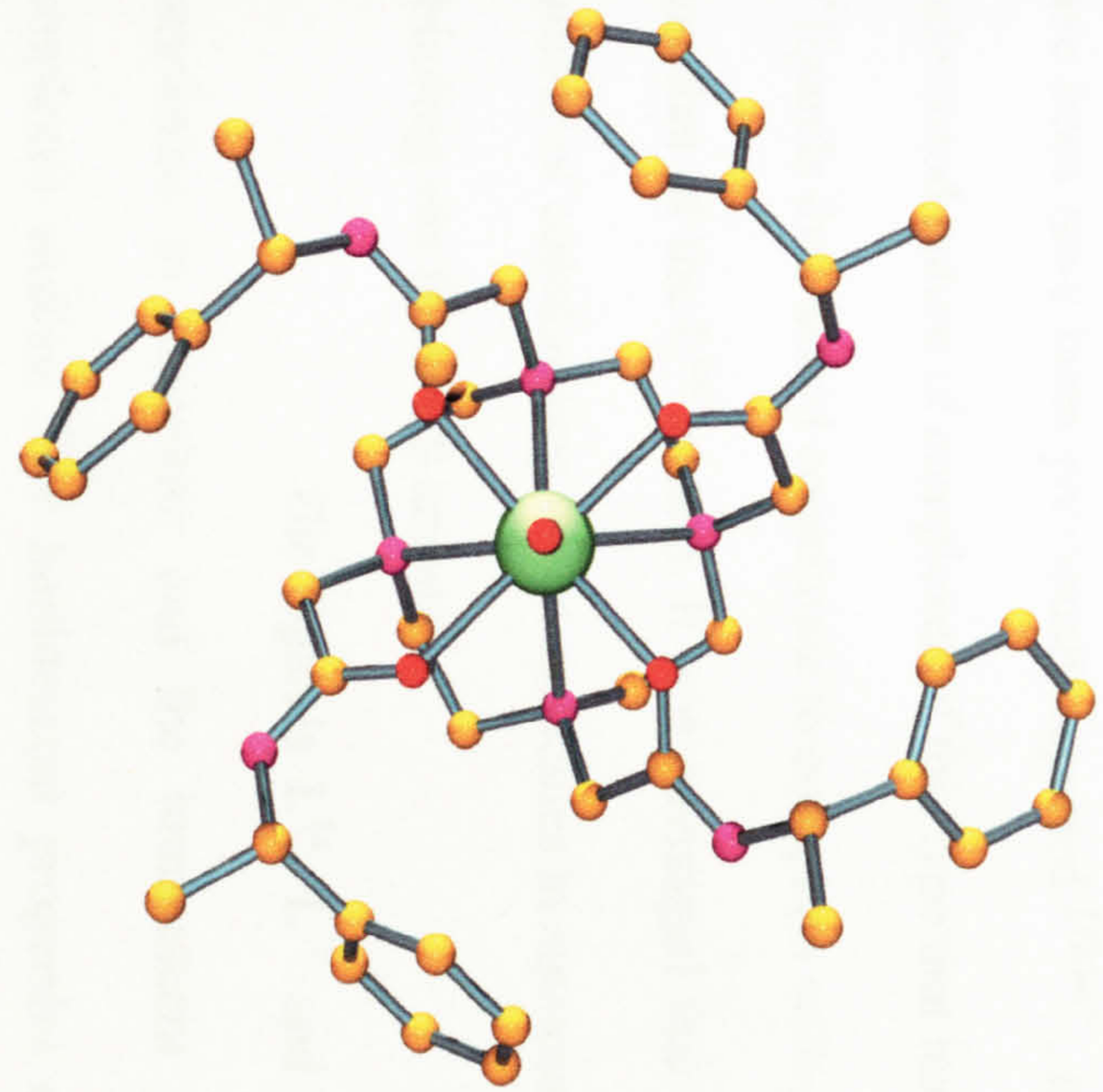

(*RRRR*)-[Eu(L^{tet})(H_2O)]$^{3+}$

Figure 1.15 Crystal Structures of the enantiomers of the [EuL^{tet}]$^{3+}$ System

1.16 Luminescence Studies

The luminescent properties of the $[EuL^{tet}]^{3+}$ complex have been have been previously reported [12,64] . It was as a result of the well understood nature of complexes of this type that lead to the design and synthesis of ligands that would coordinate to europium with a lower coordination number than that of the L^{tet} system. It was envisaged that this would then increase the number of coordinating water molecules in aqueous solution and in effect create a binding site for small anions.

The ligands L^{1a}, L^{1b} and L^{1c} were duly synthesised, complexed to europium and the luminescent properties of the resultant complexes studied. The luminescent properties of these systems were then investigated in the presence of a range of anions including carbonate, phosphate, fluoride, malonate citrate and lactate[8,12]. The results of these studies suggested that in some cases, the coordinating water molecules were displaced by these anions to form complex-substrate adducts (the proposed structures of which are described by **Figure 1.17**).

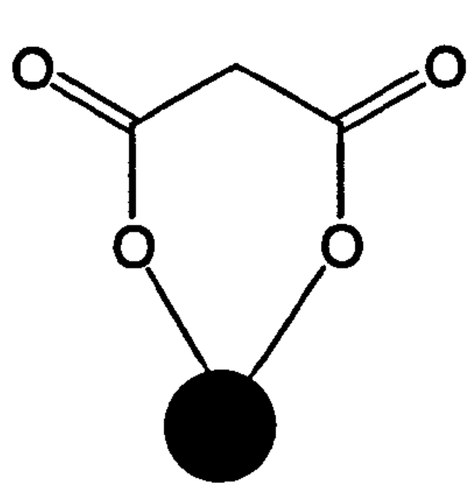

malonate

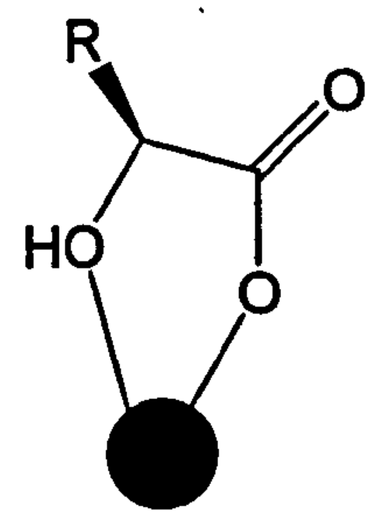

lactate/citrate

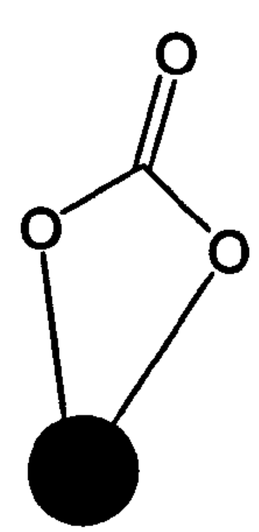

carbonate

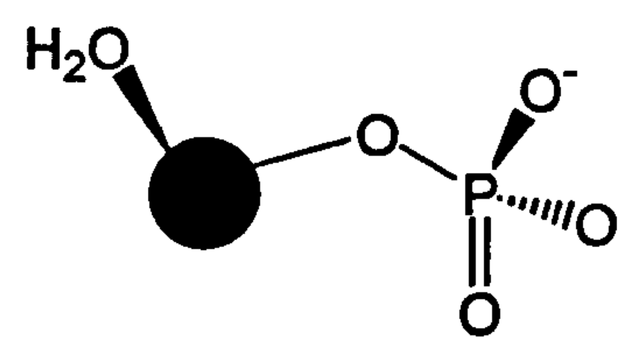

phosphate/phosphate ester

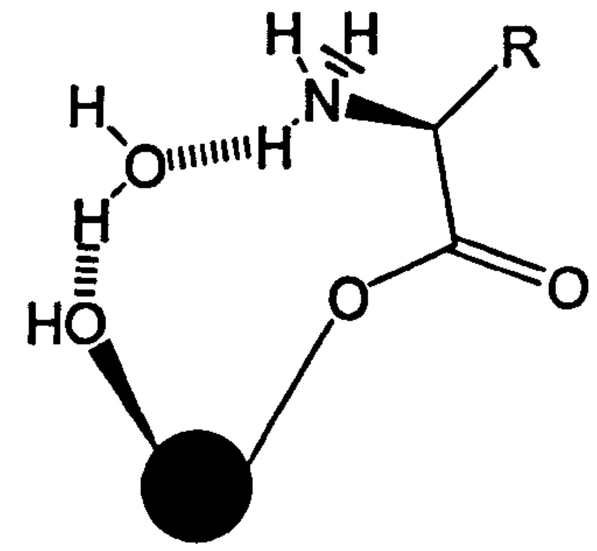

amino acid

Figure 1.17 Proposed structure of the complex-substrate adducts

It is the well defined *chiral* nature of these complexes that prompted the collaboration with Dr. Peacock at the University of Glasgow. Although the target substates are generally achiral in nature, it was hoped that the binding of anions to the synthetic receptor would be signalled by a *change* in the circularly polarised luminescence of the lanthanide ion.

Chapter 2. Experimental

2.1Experimental Set-up

CPL spectrometers are not commercially available. The CPL spectrometer at the University of Glasgow was constructed using a standard fluorimeter (Instrument SA Fluorolog 3-11) adapted to house a photoelastic modulator (Edinburgh Intruments), both of which were then connected to a lock in amplifier as outlined below.

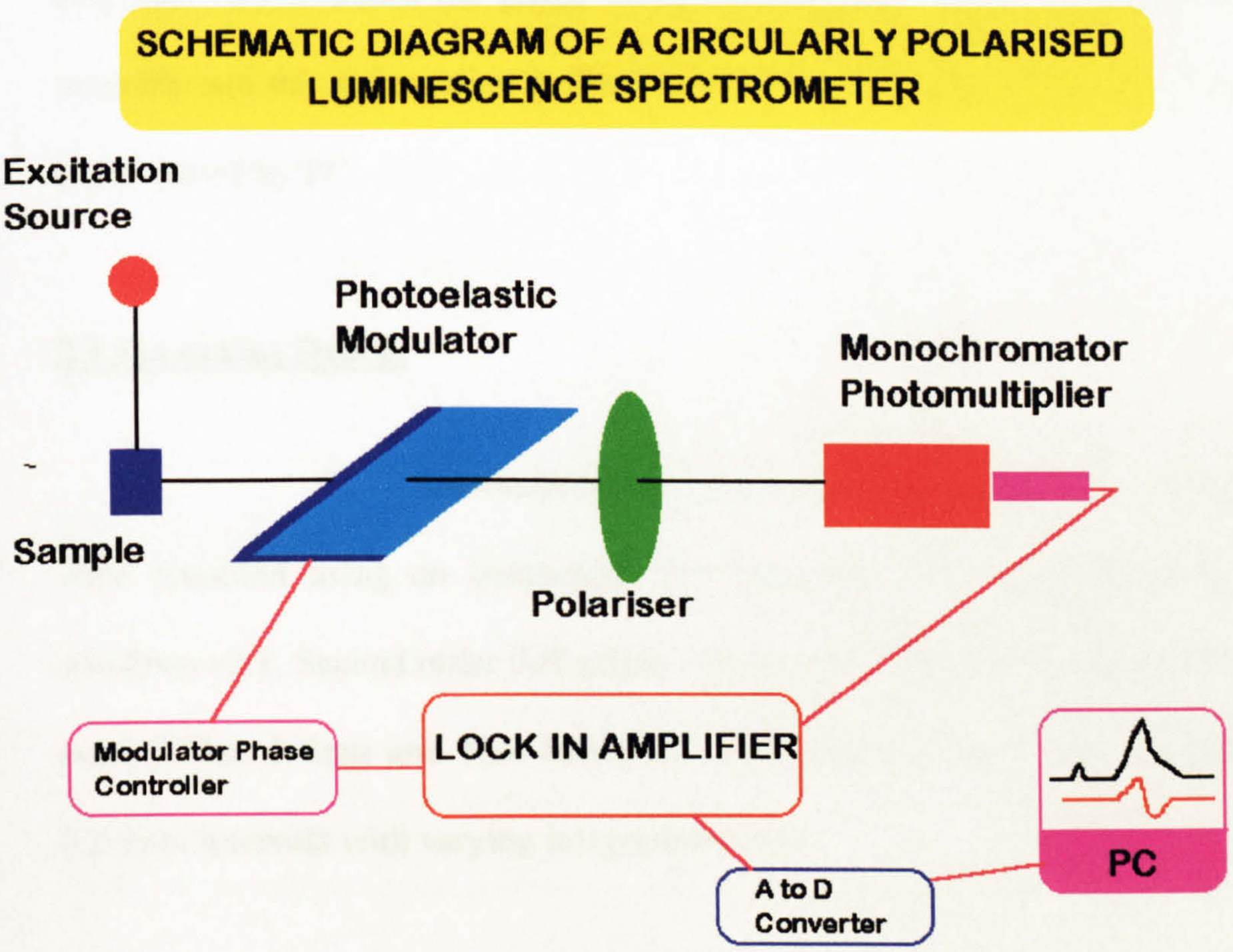

The basic design of the CPL spectrometer is outlined schematically above. The monochromatic excitation beam is usually orientated at 45 degrees to the direction of emission detection. The emitted circularly polarised radiation is initially passed through a photoelastic modulator (PEM)

which converts the circularly polarised radiation to the appropriate linear polarisation. The PEM achieves this by acting as an oscillating quarter wave plate; on alternate cycles of the modulator oscillation, the PEM acts as a quarter-wave retarding and quarter-wave enhancing device. The linearly polarised radiation is then passed through a polariser, aligned at 45 degrees to the modulator crystal axis, which allows only light oscillating in a particular direction through. The emitted radiation is then detected by the photomultiplier and its wavelength determined by the emission monochromator. The lock-in amplifier then matches the phase of the emitted light to the wavelength and intensity and this information is then converted to a digital form which can be manipulated by PC.

2.2 Recording Details

Luminescence measurements for europium complexes were recorded using an Instrument SA Fluorolog 3-11 using Datamax for windows v2.1. Second order diffraction effects were obviated by using a 375nm cut-off filter 2-5nm and 1nm bandpass, respectively. Points were recorded at 0.1-1nm intervals with varying integration times.

2.3 Excitation Wavelengths

Excitation of the lanthanide chromophore of the complexes bearing the ligands L^{tet} , L^{1a} and L^{1b} was achieved via direct excitation at 397nm. Population of the same chromophore was achieved via

excitation at 365nm for complexes bearing the ligand L^{1c} as is discussed in chapter 7.

2.4 Synthesis of Europium Complexes

All the ligands presented throughout (*ie* ligands L^{tet}, L^{1a}, L^{1b} and L^{1c}) and associated europium complexes were synthesised by Professor Parker and co-workers at the University of Durham using previously reported methods [8] . Similarly, purification, structural characterisation and an assessment of the optical purity of the studied complexes and substrates was also carried out by Professor Parker and co-workers at the University of Durham. [8]

2.5 Estimation of Hydration State

An estimation of the hydration state (the theory of which was outlined in the introductory section) of the europium complexes of the various ligands was again carried out solely by Professor Parker and co-workers at the University of Durham. The estimation was based a conventional Horrocks type analysis but was adapted to take into account the specific deactivating resonances occurring within the synthesised complexes as has previously been reported [65,8] .

2.6 Titration of bicarbonate with the Europium(III) Systems

The $[EuL^{1a}]^{3+}$ complex as its triflate salt was dissolved in a 0.1M 2,4,6-collidine/HCL buffer solution to give a 2.5mM solution of complex and adjusted to pH7.4. Sodium bicarbonate was then introduced to the complex solution by addition of 0.05 molar equivalents (10μL of a prepared sodium bicarbonate solution) until 1 molar equivalent had been added. Thereafter, 1 molar equivalents were added (10μL of a prepared sodium bicarbonate solution) until 10 equivalents had been added in total.

The titration of bicarbonate with the $[EuL^{1c}]^{4+}$ system was carried out in an analogous manner to the procedure as outlined above.

2.7 Crystallography

All crystal structures presented throughout were again solved by Professor Parker and co-workers at the University of Durham.

Chapter 3.

Emission Spectra of the Tetraamide System

3. Emission Spectra of the Europium Tetraamide Complex

The total and circularly polarised luminescence of the europium complex (*SSSS*)-$[EuL^{tet}]^{3+}$ was obtained using the experimental set-up as described, where the tetraamide ligand L^{tet} is shown below.

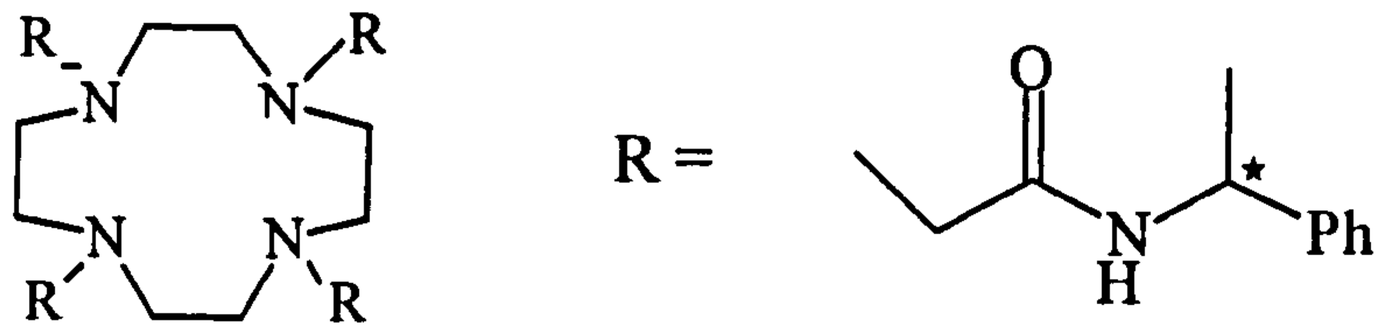

L^{tet}

The synthesis and CPL characteristics of the terbium(III) complex of the ligand L^{tet} have been previously reported [12] . Obtaining the emission spectra of the resulting europium(III) complex of the same ligand in water seemed a natural starting point for this project since the systems earmarked for investigation are all derived from this model. The CPL spectrum of the (*SSSS*)-$[EuL^{tet}]^{3+}$ complex in aqueous solution with the corresponding conventional luminescence spectrum is shown overleaf (**Figure 3.1**).

Although the splitting of transitions by the ligand field can be seen in a conventional luminescence experiment (as shown by the multi peak nature of the transitions in the luminescence spectrum), this is often poorly defined. For a chiral molecule, a CPL experiment can often show how transitions are resolved into their constituent components more clearly.

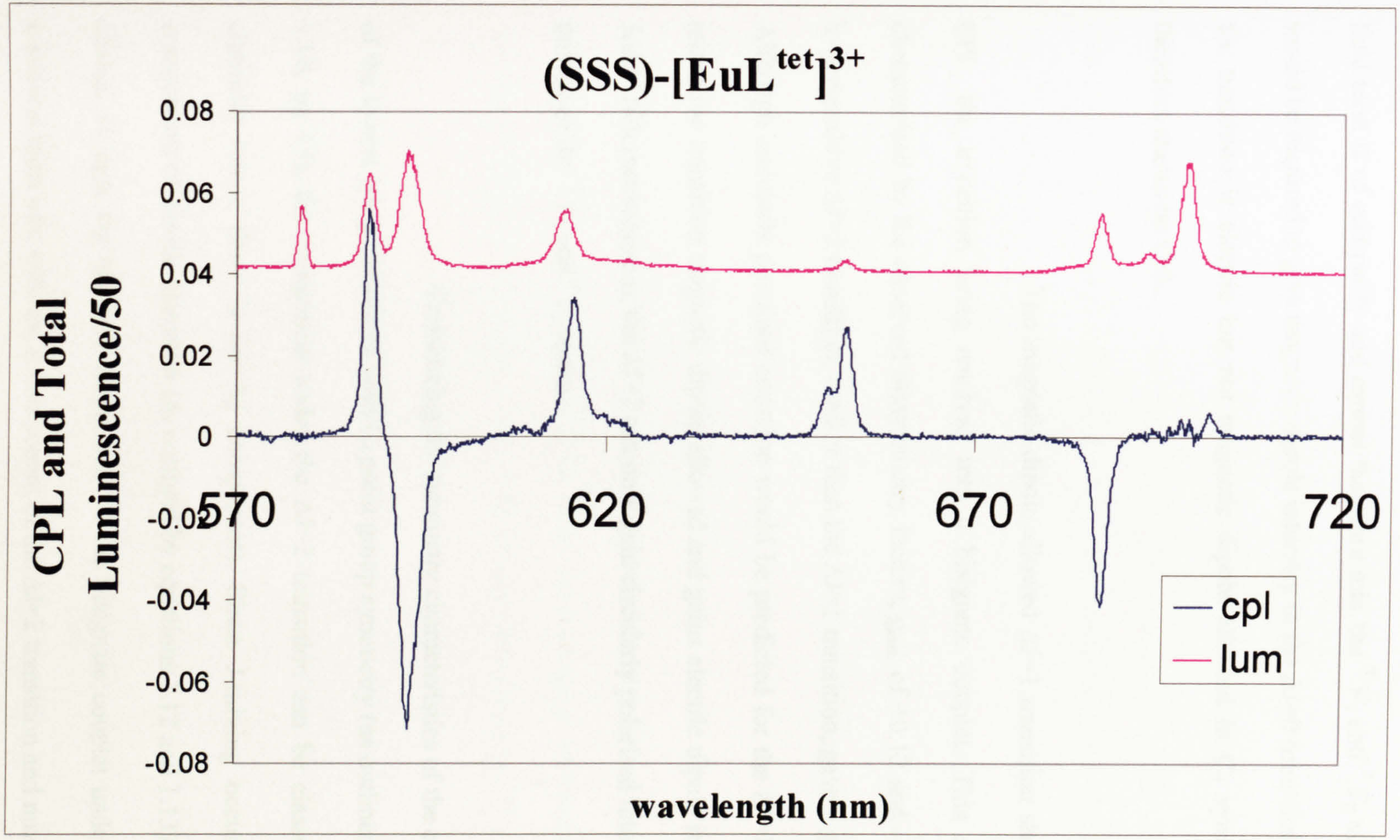

Figure 3.2. *Upper* Total emission of the ΔJ=1,2,3 and 4 transitions of the (SSSS)- $[EuL^{1tet}]^{3+}$ (H_2O solution of complex recorded at 295K. *Lower* Circularly polarised emission of the ΔJ=1,2,3 and 4 transitions of the (SSSS)-$[EuL^{1tet}]^{3+}$ complex under the same conditions.

As is shown the $\Delta J=0$ transition is relatively strong in the emission spectrum but carries no CPL. This is explained by the fact that the crystal field term is of *odd* parity and cannot therefore mix the $^7F_1$ and $^7F_0$ states which would be required to give magnetic dipole intensity to the $\Delta J=0$ transition [39] . Thus the transition is electric but not magnetic dipole allowed in C_4 symmetry and therefore shows no CPL.

The magnetic dipole allowed $\Delta J=1$ transition shows strong CPL, the transition being resolved into a bisignate couplet. This strength is characterised by the observed dissymmetry factors, g_{em}, of +0.12 and –0.18. The hypersensitive $\Delta J=2$ transition, weaker than the $\Delta J=1$ transition, gave a g_{em} of +0.1. Although circularly polarised emission would be predicted for the $\Delta J=1$ transition (since the transition magnetic dipole allowed and gains electric dipole intensity via Judd-Ofelt mechanisms), the $\Delta J=2$ can only gain circularly polarised intensity via J-mixing of the $^7F_1$ and $^7F_2$ states.

Considering the symmetry characteristics of the components of the lowest lying transitions with C_4 point group symmetry (as outlined by Figure 1.10, pg 13), the component under the $\Delta J=2$ transition can be classed as E in character (since there is no A_2 component). Since J-mixing occurs between components of similar character (as outlined by equations 1.12 and 1.13) and with a change in sign, the negative component of the bisignate couplet under the $\Delta J=1$ transition must mix with the E component of the $\Delta J=2$ transition and must also be E in character. Because there are only two components (A and E) that can be

resolved under the ΔJ=1 transition in C_4 symmetry, the remaining positive component of the bisignate couplet must be of symmetry type A.

The ΔJ=3 and 4 transitions gave weaker CPL, g_{em} of +0.3 and (–0.11 and 0), respectively. Again the observed circularly polarised intensity of the ΔJ=4 transition is explained by mixing of the $^7F_1$ and $^7F_4$ states; the negative component can therefore be assigned A in character and the positive component E. The circularly polarised intensity observed under the ΔJ=3 transition can again only be attributed to the mixing of J states. The $^7F_3$ state can mix with both the $^7F_1$ and $^7F_4$ states although it is thought that most of the intensity it derived from the magnetic dipole allowed ΔJ=1 transitions and thus the component peak has been labelled E in character.

The CPL emission observed for this complex is consistent with the emission spectrum obtained from an analogous tetraamide complex bearing a naphtyl chromophore which has previously been reported [39].

The structure of this complex is well defined, as noted in the introduction section. The complex adopts a square antiprismatic structure with a solvent water molecule capping along the principle axis. Both axial and equatorial (right angles to the principle axis) views of the solved crystal structure (obtained by Parker and co-workers at the University of Durham) [12] are shown below (**Figures 3.3** and **3.4** respectively).

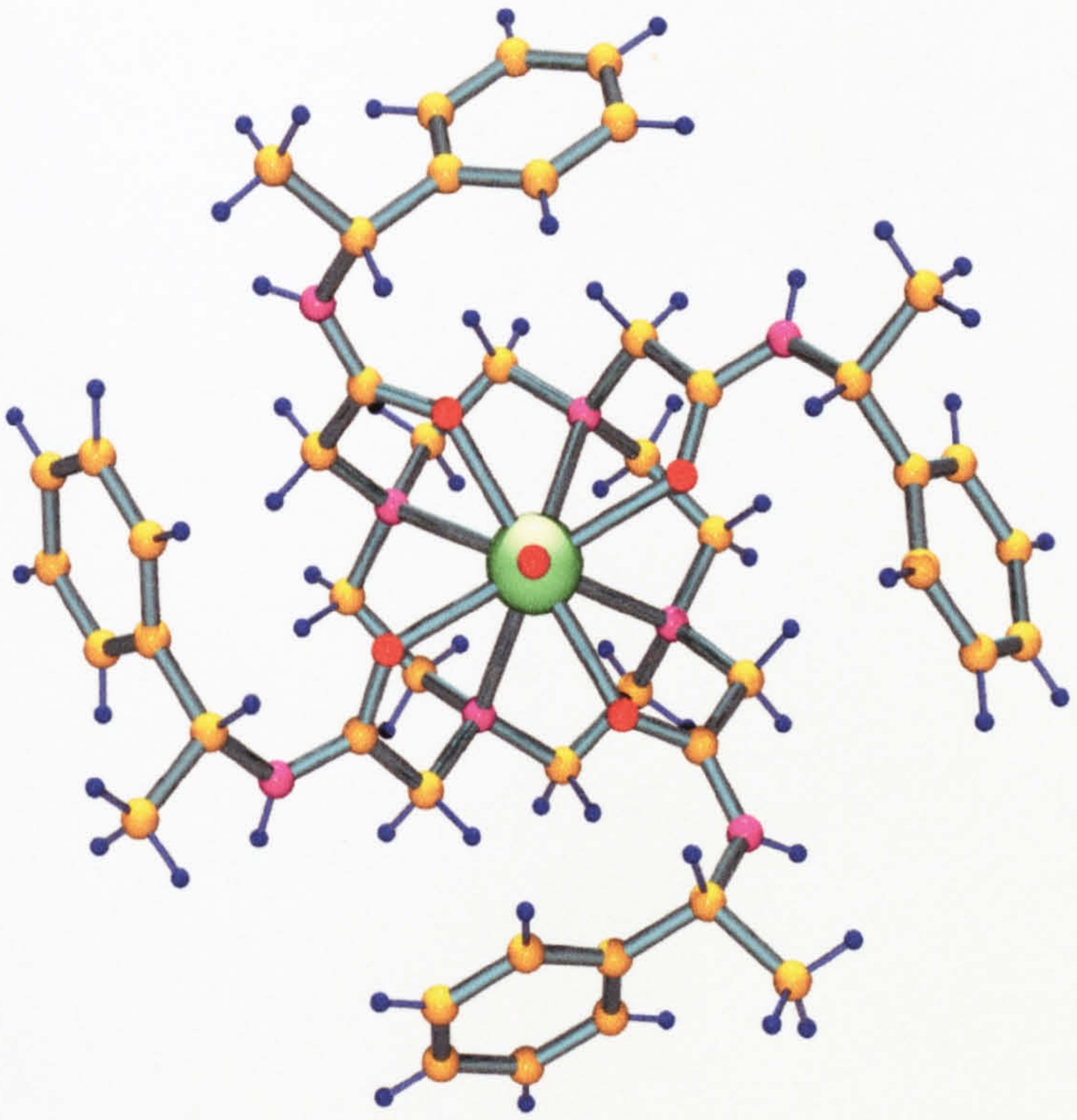

Figure 3.3. Axial view of the (SSSS)-$[EuL^{tet}]^{3+}$ complex

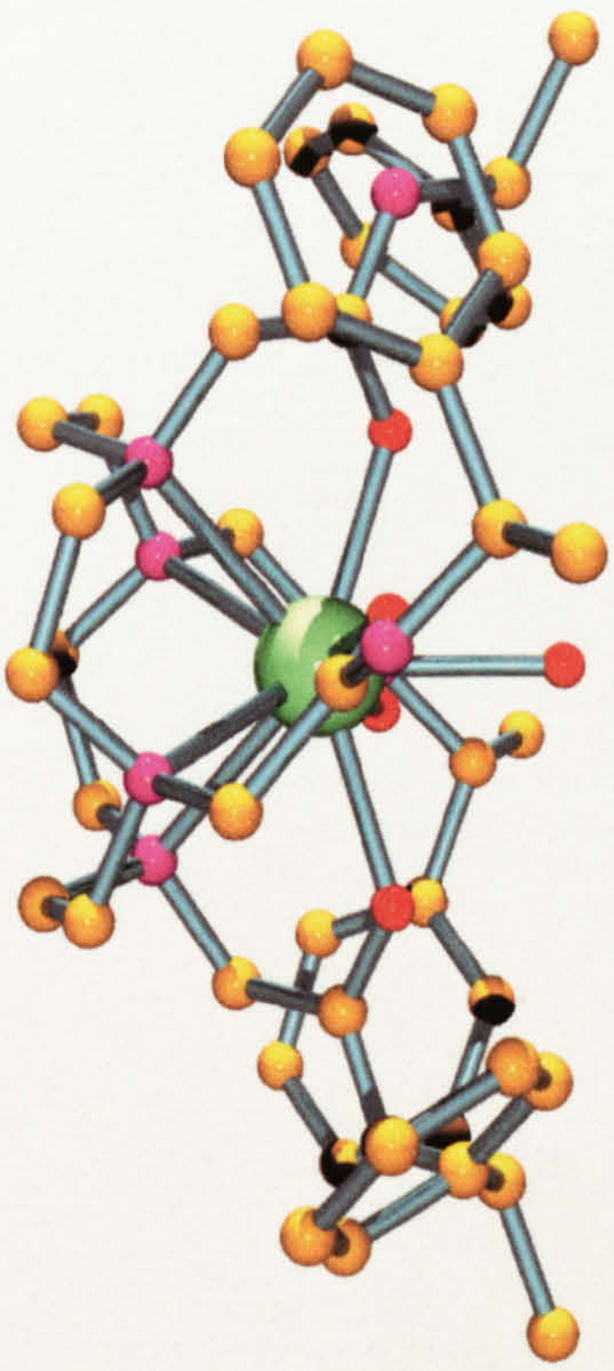

Figure 3.4. Equatorial view of the (SSSS)-$[EuL^{tet}]^{3+}$ complex

Chapter 4

4. Emission Spectra of Europium(III) Triaamide Complexes

Using the well defined model of the europium(III) tetraamide complex described in the previous chapter, the analogous triaamide ligands L^{1a}, L^{1b} and L^{1c} were synthesised, where the nature of the pendant arm, R, varied only in respect to the absolute configuration of the chiral centre δ to the ring nitrogen

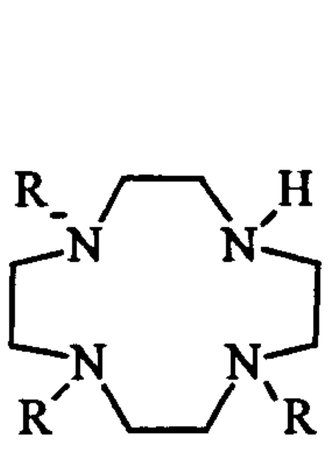

L^{1a}

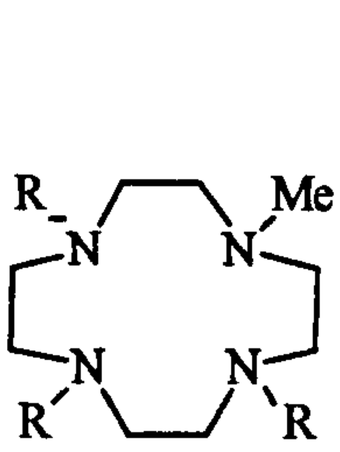

L^{1b}

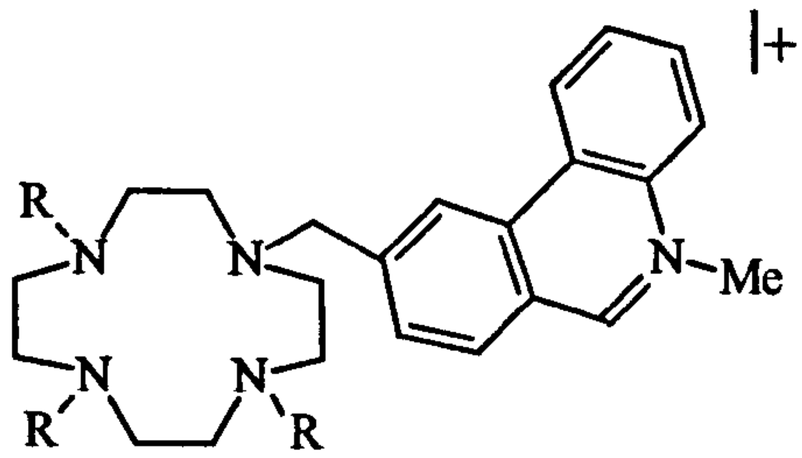

L^{1c}

R =

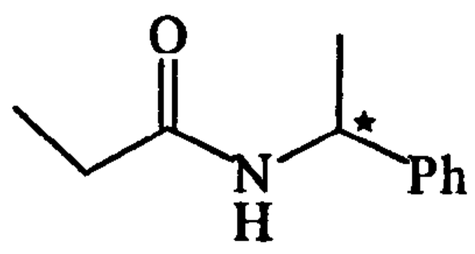

After complexation to europium(III), the total and circularly polarised emission spectra of the complexes were obtained.

4.1 Emission Spectra of the $[EuL^{1a}]^{3+}$ System

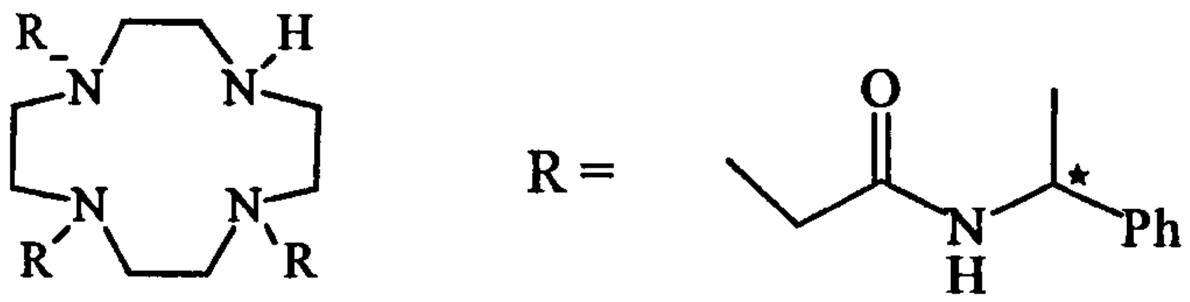

L^{1a}

Both enantiomers of the $[EuL^{1a}]^{3+}$ complex were dissolved in D_2O to give 2.87 mM solutions. The emission spectrum of the solutions was then recorded at 295K and at pD6. **Figure 4.1** and **Figure 4.2** show the CPL and total emission over the full spectral range (570 to 720nm) of the (*SSS*)- $[EuL^{1a}]^{3+}$and (*RRR*)- $[EuL^{1a}]^{3+}$complexes respectively.

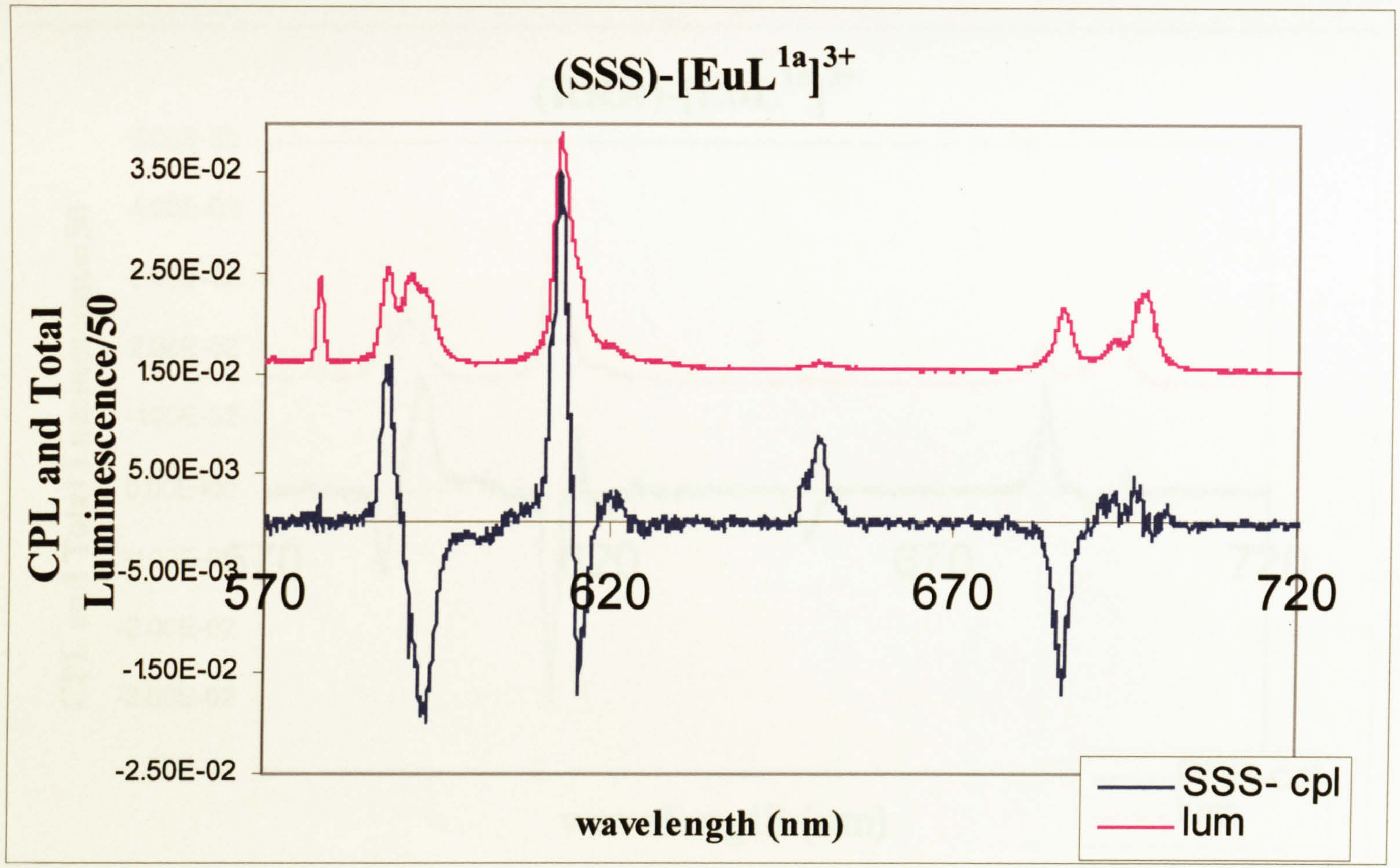

Figure 4.1 *Upper* Total emission of the ΔJ=1,2,3 and 4 transitions of the (SSS)- $[EuL^{1a}]^{3+}$ (2.87mM D_2O solution of complex recorded at 295K and at pD6)*Lower* Circularly polarised emission of the ΔJ=1,2,3 and 4 transitions of the (SSS)-$[EuL^{1a}]^{3+}$ complex under the same conditions.

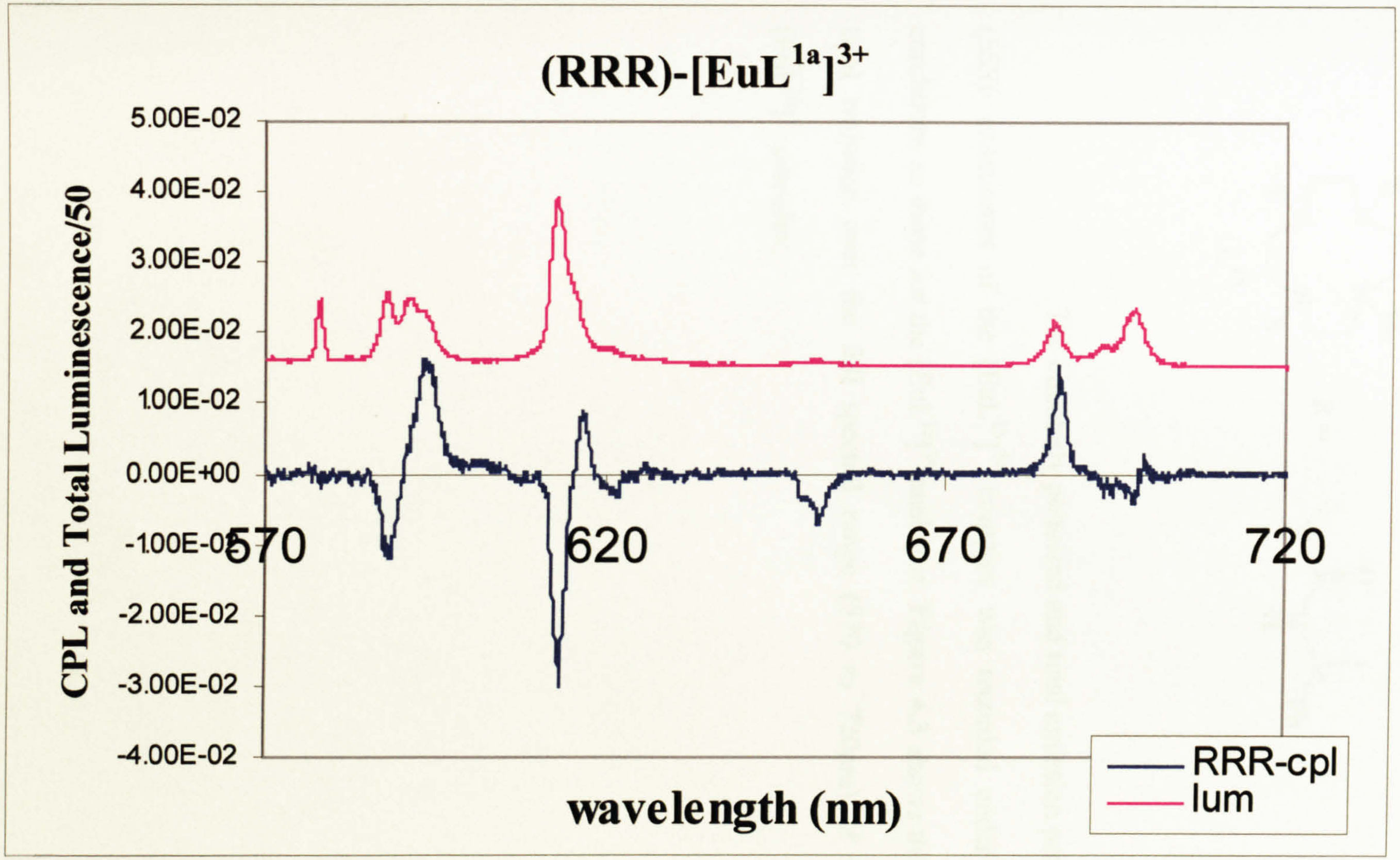

Figure 4.2 *Upper* Total emission of the ΔJ=1,2,3 and 4 transitions of the (RRR)- $[EuL^{1a}]^{3+}$ (2.87mM D_2O solution of complex recorded at 295K and at pD6). *Lower* Circularly polarised emission of the ΔJ=1,2,3 and 4 transitions of the (RRR)-$[EuL^{1a}]^{3+}$ complex under the same conditions.

4.2 Emission Spectra of the $[EuL^{1b}]^{3+}$ System

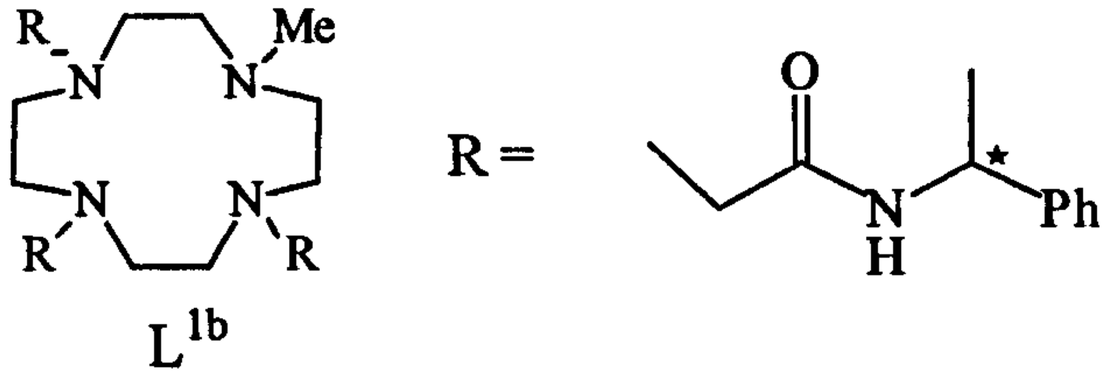

The circularly polarised and total emission profile of the (*SSS*)- enantiomer of the $[EuL^{1b}]^{3+}$ complex was recorded under the same conditions as those for the $[EuL^{1a}]^{3+}$ analogue. **Figure 4.3** shows the CPL and total emission over the full spectral range (570 to 720nm) of the (*SSS*)-$[EuL^{1b}]^{3+}$ complex.

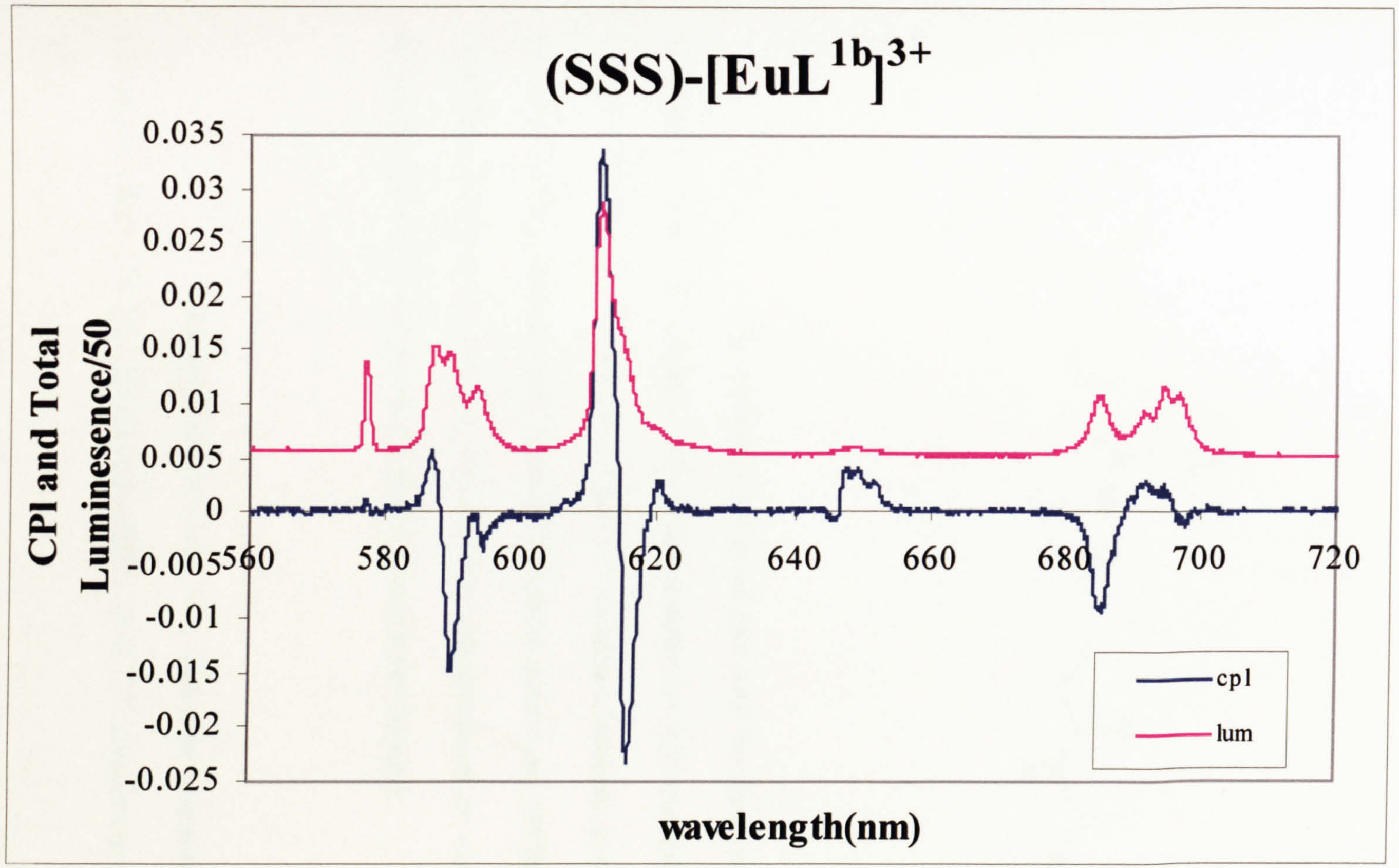

Figure 4.3 *Upper* Total emission of the ΔJ=1,2,3 and 4 transitions of the (SSS)- $[EuL^{1b}]^{3+}$ (2.87mM D_2O solution of complex recorded at 295K and at pD6). *Lower* Circularly polarised emission of the ΔJ=1,2,3 and 4 transitions of the (SSS)-$[EuL^{1b}]^{3+}$ complex under the same conditions.

4.3 Emission spectra of the $[EuL^{1c}]^{3+}$ System

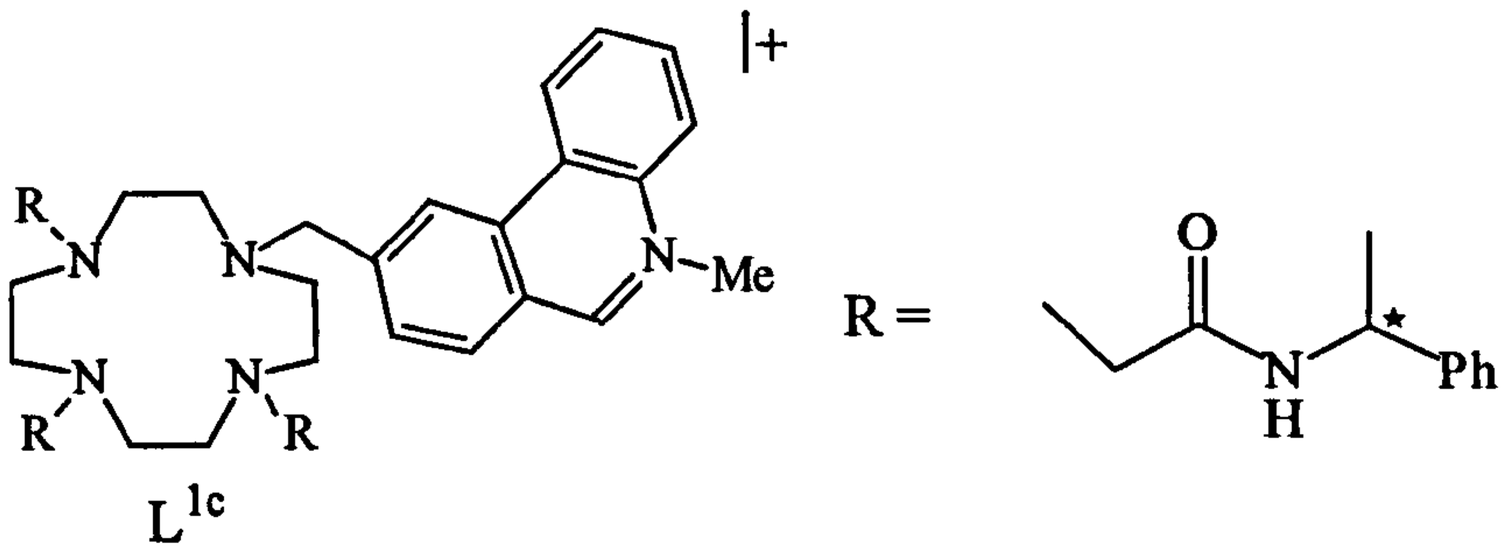

L^{1c}

The circularly polarised and total luminescence spectra of the (*SSS*) –$[EuL^{1c}]^{4+}$ complex was recorded under the same conditions as the L^{1a} and L^{1b} analogues. Unlike the L^{1a} and L^{1b} analogues however, population of the emissive $^5D_0$ state was not achieved by direct excitation (397nm) of the lanthanide chromophore. Instead, the emission was sensitised by excitation of the antenna moiety *ie* the phenthridinium chromophore (365nm).

Figure 4.4 shows the CPL and total emission over the full spectral range (570 to 720nm) of the (*SSS*)- $[EuL^{1c}]^{4+}$ complex as its $3^-0Tf.I^-$ salt.

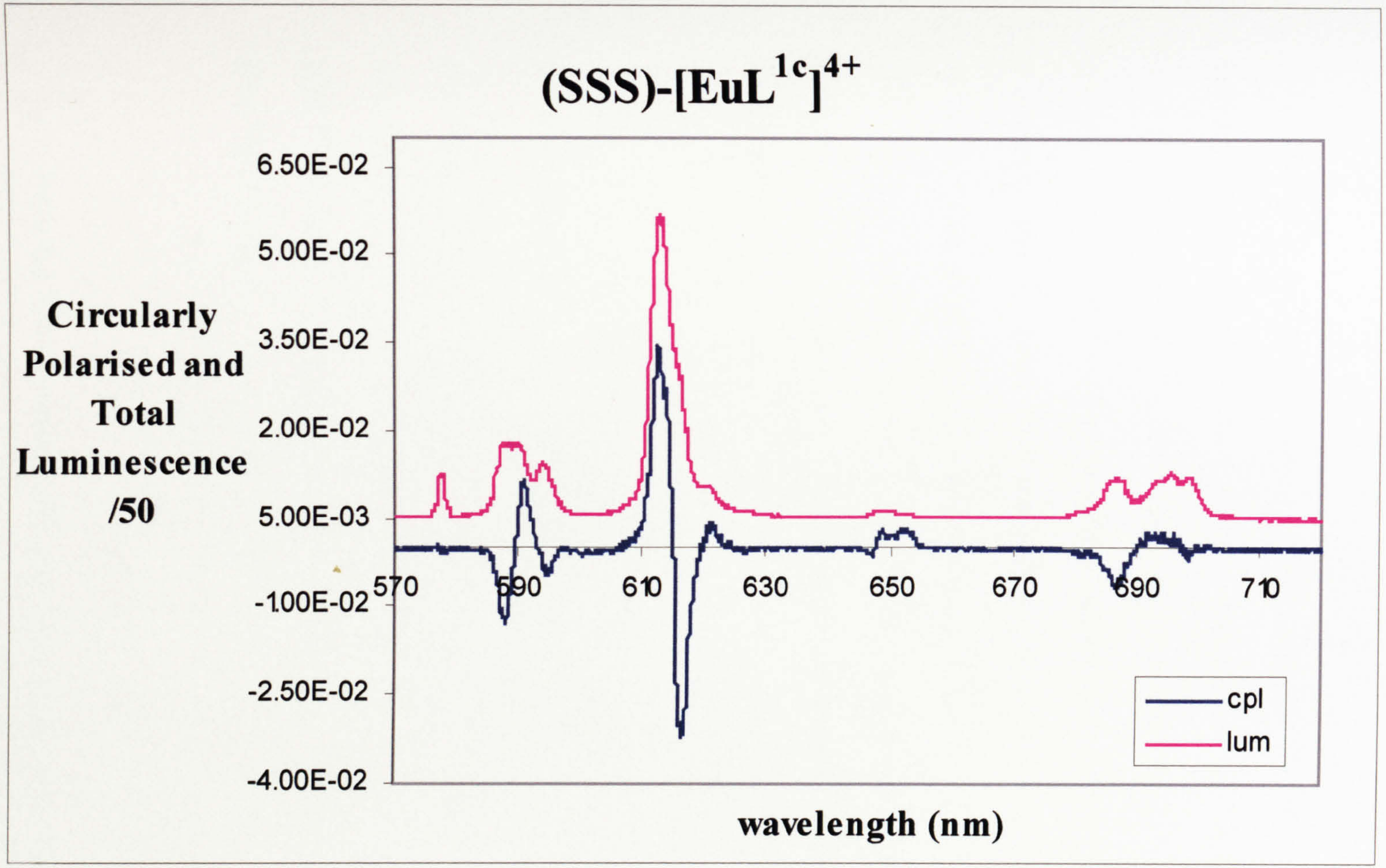

Figure 4.4 *Upper* Total emission of the ΔJ=1,2,3 and 4 transitions of the (SSS)-$[EuL^{1c}]^{4+}$ (2.87mM D_2O solution of complex recorded at 295K and at pD6). *Lower* Circularly polarised emission of the ΔJ=1,2,3 and 4 transitions of the (SSS)-$[EuL^{1b}]^{3+}$ complex under the same conditions.

4.4 Hydration States of the Europium(III) Triaamide Complexes

An evaluation of the hydration state, q , of the europium(III) was carried out by Professor Parker and co-workers at the University of Durham. Derivation of the q value from the rate constants for depopulation of the Eu^{3+} excited state in H_2O and in D_2O is methodology well established (as was described in the preceding introduction section). **Table 4.1** below presents rate constants for depopulation of the europium excited state for the complexes of ligands L^{1a}, L^{1b} and L^{1c} in H_2O and D_2O and the resultant q value. These results were obtained after correcting for the effect of unbound water molecules and amide NH oscillators[65,8] .

Complex/Anion	kH_2O (ms^{-1})	kD_2O (ms^{-1})	Δk_{corr} (ms^{-1})	q
$[EuL^{1a}][CF_3SO_3]_3$	3.85	1.54	1.82	2.2
Cl- / Br- / I-	3.80	1.55	1.76	2.1
$[EuL^{1b}][CF_3SO_3]_3$	2.33	0.53	1.33	1.6
$[EuL^{1c}][CF_3SO_3]_3.I$	1.60	0.28	0.83	1.0

Table 4.1 Rate constants (±10%) for depopulation of the Eu^{3+} excited state of the europium complexes of the ligands L^{1a}, L^{1b} and L^{1c} (295K, 1mM complex) and derived hydration numbers, q (±20%).

Emission Spectra of the Europium(III) Complexes of L^{1a}, L^{1b} and L^{1c}

4.5 Discussion

As expected from previous work on the C_4 symmetric tetraamide complexes, the absolute configuration of the stereogenic centre on the triaamide pendant arm controls the absolute configuration of the complex; an (SSS) - complex gives rise to a Δ configuration, whereas an (RRR) - ligand gives rise to a Λ configuration. The sign the CPL for a given transition also confirms the configuration. This is illustrated by the emission spectra of the enantiomers of the $[EuL^{1a}]^{3+}$ complex as shown in **Figures 4.1** and **4.2** and in **Figure 4.5**, below; the ΔJ=1 and ΔJ=2 transitions of the enantiomers are shown simultaneously .

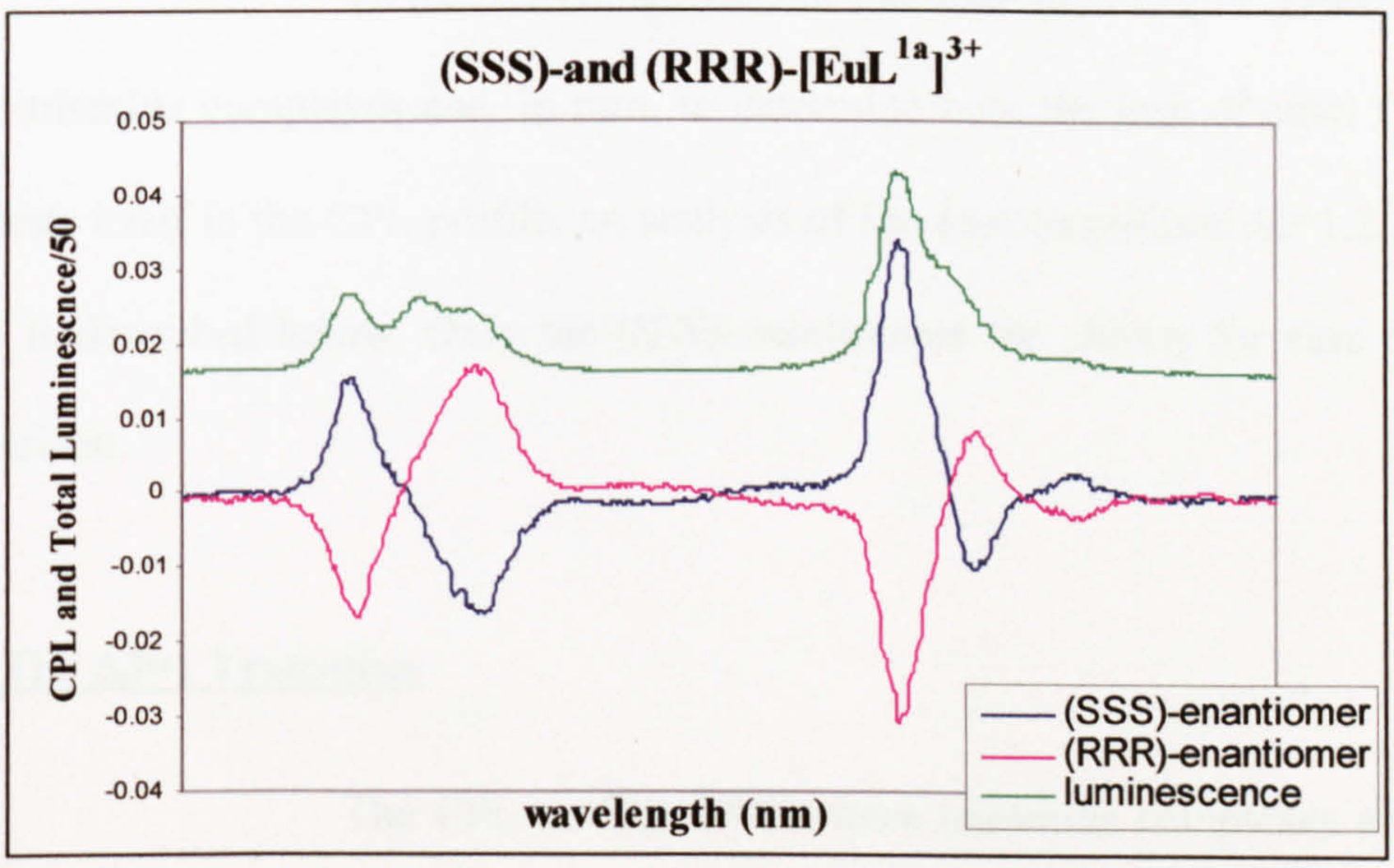

Figure 4.5 *Upper* Total emission of the $[EuL^{1a}]^{3+}$ complex (a 2.87mM D_2O solution recorded at 295K and pD6).
Lower Circularly polarised emission of the $[EuL^{1a}]^{3+}$ enantiomers under the same conditions.

The mirror image nature of the CPL profiles confirms what had been expected – that for any CPL profile of one enantiomer, it could be assumed that the CPL profile of the opposite enantiomer would be identical but inverted.

On inspection of the CPL spectra of the three triamide complexes, it is evident that the $\Delta J=0$ transition carries no CPL in all three cases. This result was expected from previous experiments on C_4 symmetric tetraamide complexes (as discussed in the previous chapter). Of the remaining four transitions observed, all carried a measurable circularly polarised element. The CPL profiles under all four transitions are unique in each case and show significant differences to the CPL profile of the tetraamide complex.

To make a comparison of the three unique CPL profiles of the triamide complexes and, in turn, to determine how the loss of strict C_4 manifests itself in the CPL profile, an analysis of the four transitions $\Delta J=1,2,3,$ and 4 is described below. Only the (*SSS*)-enantiomers are shown for ease of comparison.

4.5.1 The $\Delta J=1$ Transition

The CPL profiles of the three triaamide complexes and of the tetraamide complex under the $\Delta J=1$ transition are shown in **Figure 4.6.** All profiles are drawn to the same scale and wavelength range (580 to 605nm). All profiles indicate CPL ($I_l - I_r$) of arbitrary units which have not been shown.

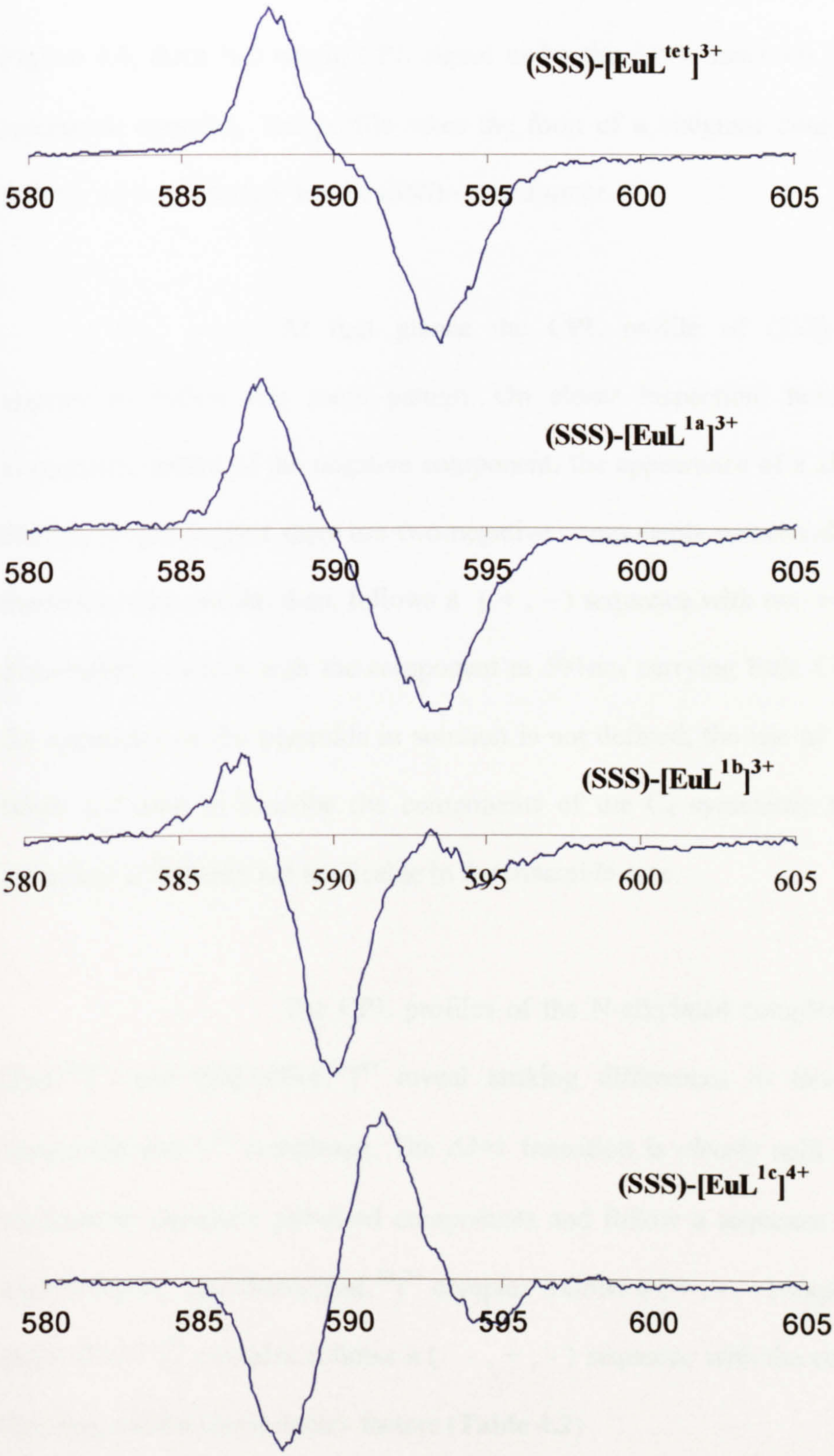

Figure 4.6 CPL profiles of the four europium(III) complexes bearing the ligands L^{tet}, L^{1a}, L^{1b} and L^{1c} under the $\Delta J=1$ transition.

As noted in the previous chapter, and as can be seen in **Figure 4.6,** there is a strong CPL signal under the ΔJ=1 transition for the C_4 symmetric complex. The profile takes the form of a bisignate couplet which follows a (+ , -) pattern for the (*SSS*) – enantiomer.

At first glance the CPL profile of (*SSS*)-$[EuL^{1a}]^{3+}$ appears to follow this same pattern. On closer inspection, however, the asymmetric nature of the negative component, the appearance of a *shoulder* at 591nm, would suggest there are two negative components associated with this transition. The profile, then, follows a (+ , -) sequence with two measurable dissymmetry factors with the component at 591nm carrying little CPL. Since the symmetry of the triaamide in solution is not defined, the use of symmetry labels (as used to describe the components of the C_4 symmetric tetraamide complex) is formally not applicable in the triaamide case.

The CPL profiles of the N-alkylated complexes (*SSS*)-$[EuL^{1b}]^{3+}$ and (*SSS*)-$[EuL^{1c}]^{4+}$ reveal striking differences to those of the tetraamide and L^{1a} complexes. The ΔJ=1 transition is *clearly* split into three measurable circularly polarised components and follow a sequence unique to each complex. The (SSS)-$[EuL^{1b}]^{3+}$ complex follows a (+ , - , -) sequence. The (*SSS*)-$[EuL^{1c}]^{4+}$ complex follows a (- , + , -) sequence with the components showing similar dissymmetry factors **(Table 4.2)**

Complex	Dissymmetry Factor		
	588nm	594nm	
$[EuL^{1a}]^{3+}$	+0.06	-0.14	
	588nm	591nm	595nm
$[EuL^{1b}]^{3+}$	+0.03	-0.07	-0.03
$[EuL^{1c}]^{4+}$	-0.03	+0.05	-0.02

Table 4.2 Dissymmetry Factors of the components resolved under the $\Delta J=1$ transition of the europium complexes of ligands L^{tet}, L^{1a}, L^{1b} and L^{1c}

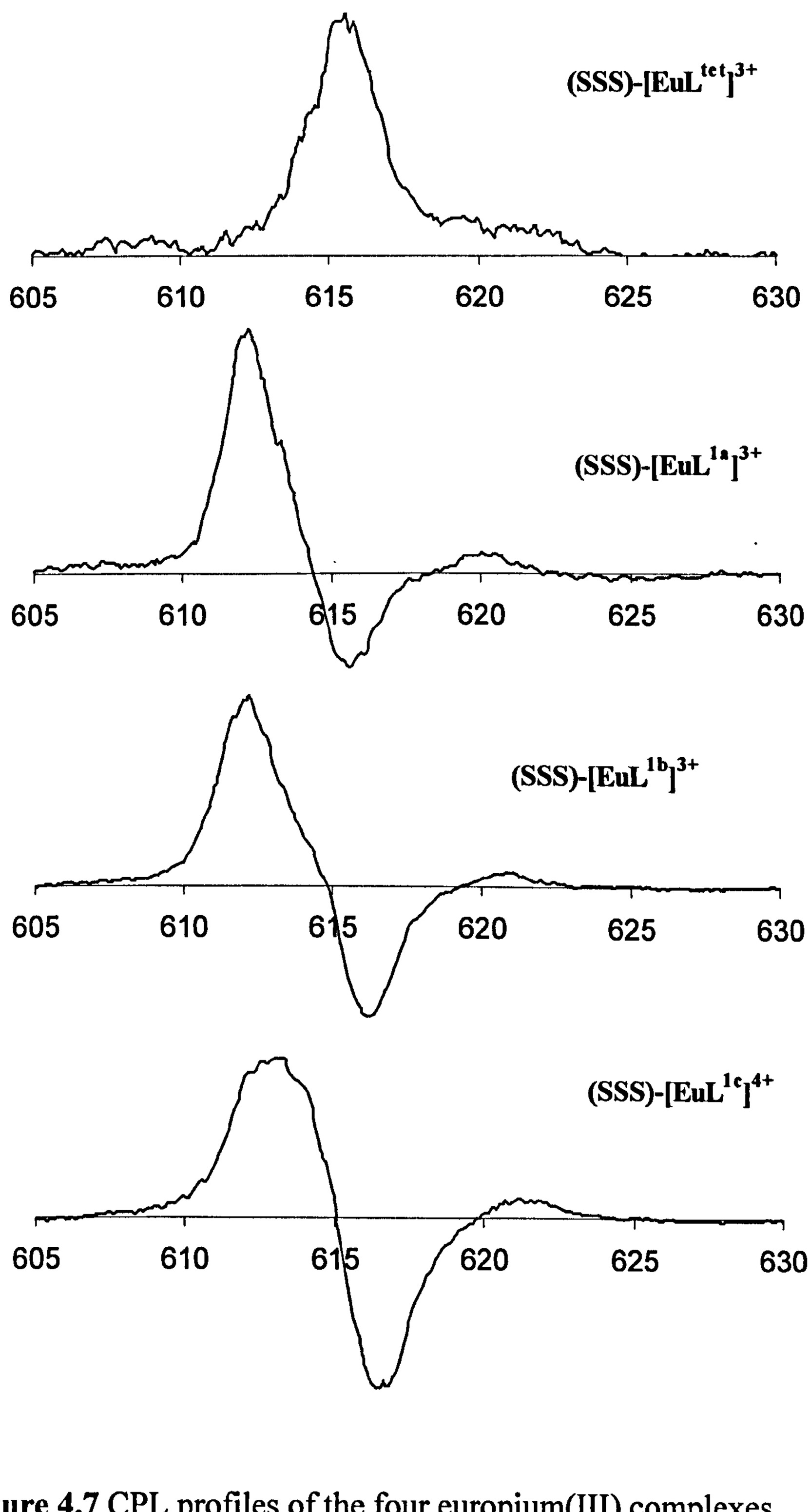

Figure 4.7 CPL profiles of the four europium(III) complexes bearing the ligands L^{tet}, L^{1a}, L^{1b} and L^{1c} under the $\Delta J=2$ transition.

4.5.2 The ΔJ=2 Transition

Even a cursory glance at **Figure 4.7** reveals the striking effect of the loss of C_4 symmetry on the CPL profiles under the hypersensitive ΔJ=2 transition. Whereas the ΔJ=2 transition is resolved into one measurable component for the tetraamide complex, the triaamide is resolved into three, all following a (+ , - , +) sequence. (The asymmetric nature of the initial positive circularly polarised peak suggest there is at least one component in the range 610 to 614nm although the dissymmetry factor of only one can be measured).

The calculated dissymmetry factors of the components of the triaamide complexes under this transition are tabulated below **(Table 4.3).**

Complex	Dissymmetry Factor		
	613nm	617nm	621nm
$[EuL^{1a}]^{3+}$	0.05	0.07	0.08
$[EuL^{1b}]^{3+}$	0.05	0.14	0.08
$[EuL^{1c}]^{4+}$	0.02	0.07	0.03

Table 4.3. Calculated dissymmetry factors of components resolved under the ΔJ=2 transition

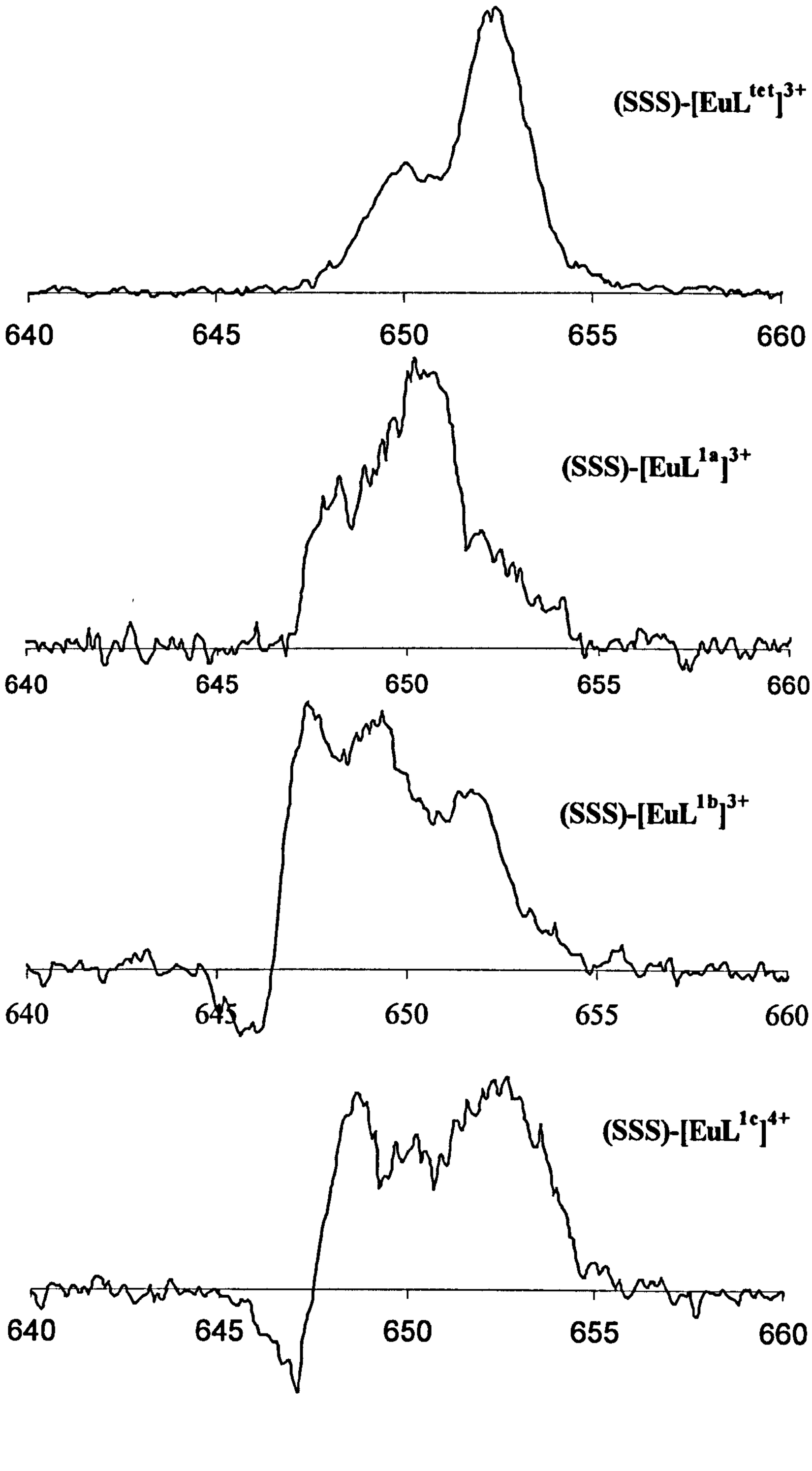

Figure 4.8 CPL profiles of the four europium(III) complexes bearing the ligands L^{tet}, L^{1a}, L^{1b} and L^{1c} under the $\Delta J=3$ transition

4.5.3 The ΔJ=3 Transition

The CPL profiles under the ΔJ=3 transition of the N-alkylated complexes (SSS)-$[EuL^{1b}]^{3+}$ and (SSS)-$[EuL^{1c}]^{4+}$ reveal strong similarities (**Figure 4.8**). Both complexes show a negative circularly polarised component in the range 645 to 648nm. These complexes also appear to have at least three positive components in the range 648 to 645nm. These positive components are not well resolved, however, and so a dissymmetry factor was calculated based on the centre of the positive peak at around 650nm.

The CPL profile of the (SSS)-$[EuL^{1a}]^{3+}$ complex under this same transition reveals no negative component and in this respect resembles the CPL profile of the tetraamide complex. Like the N-alkylated analogues, however, there appears to be at least three components in the range 648 to 645nm, indicated by two *shoulders* flanking the central peak at 650nm. Again, a dissymmetry factor was calculated based on this monosignate peak which is significantly stronger than those of the N-alkylated analogues.

Complex	Dissymmetry Factor (650nm)
$[EuL^{1a}]^{3+}$	0.36
$[EuL^{1b}]^{3+}$	0.12
$[EuL^{1c}]^{4+}$	0.07

Table 4.4. Calculated dissymmetry factors of components resolved under the ΔJ=3 transition

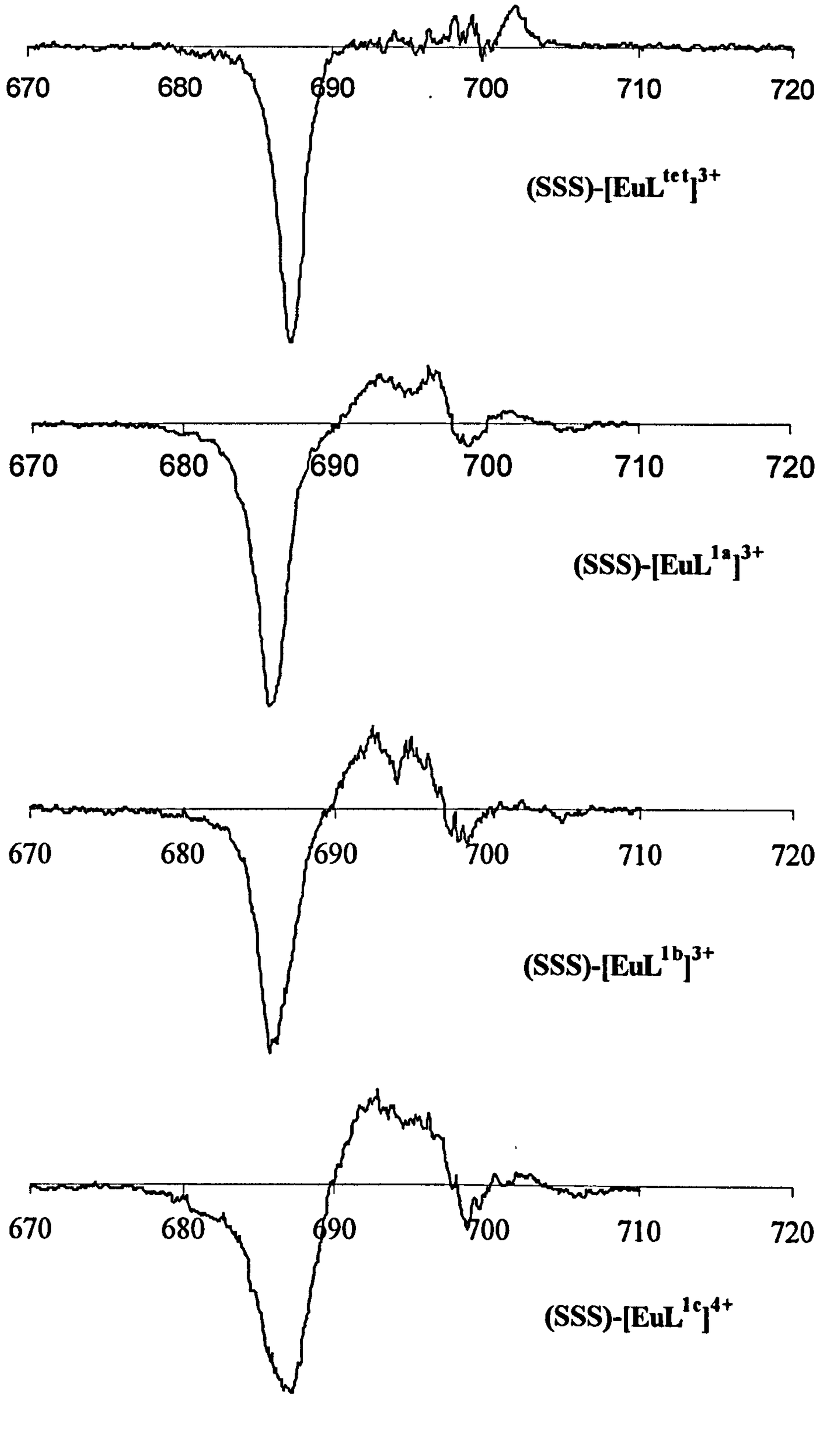

Figure 4.9 CPL profiles of the four europium(III) complexes bearing the ligands L^{tet}, L^{1a}, L^{1b} and L^{1c} under the $\Delta J=4$ transition

4.5.4 The ΔJ=4 Transition

The CPL profiles under the ΔJ=4 transition of all three triaamide complexes are very similar as shown (**Figure 4.9**). Although there appears to be two positive components in the range 690 to 688nm in all cases, they cannot be distinguished sufficiently to calculated individual dissymmetry factors. The profiles generally follow a (- , + , - , + , -) sequence in all cases with the most prominent component being the first. The dissymmetry factor of this component around 685nm was calculated for each complex can be compared to the analogous component of the tetraamide complex which is slightly stronger, $g_{em} = 0.11$.

Complex	Dissymmetry Factor (685nm)
$[EuL^{1a}]^{3+}$	-0.09
$[EuL^{1b}]^{3+}$	-0.07
$[EuL^{1c}]^{4+}$	-0.03

Table 4.5. Calculated dissymmetry factors of components resolved under the ΔJ=4 transition

4.5.5 Hydration States of the Europium(III) Triaamide Complexes

The hydration state of the tetraamide complex is clearly defined; the observed q value being confirmed by observation of the *capping* water molecule as shown by the crystal structure. The results of a similar evaluation of the hydration state of the triaamide complexes as their triflate salts are outlined by Table 4.1 and show the differing q values for each complex.

A value of $q = 2.2$ for the L^{1a} complex suggests that the complex exists as a diaqua species in solution and that the triflate ion does not bind to the europium ion. Similarly, although a lower value of $q = 1.6$ was observed for the L^{1b} complex, it is assumed that this too exists as a diaqua species in solution. The data for the L^{1c} complex suggests the presence of only one bound water molecule in solution ($q = 1$). The reduced hydration state of the N-alkyllated can be explained in terms of a steric effect; the bulky alkyl groups restricting the access of water molecules to the europium centre.

Table 4.1 also shows the observed data for the europium(III) L^{1a} complex in the presence of chloride, bromide and iodide. In the presence of all three anions, the diaqua nature of the complex is maintained, indicating that these anions, as the case with triflate, **do not** interact with the metal centre.

4.5.6 Summary

In summary, although axial symmetry has been lost, the correlation of ligand chirality to the observed CPL profile as observed in the tetraamide complexes is maintained in the triaamide complexes. On inspection of the CPL profiles of the triaamide complexes, particularly those under the $\Delta J=1$ and 2 transitions, the loss of axial symmetry is evident. These transitions are split by the ligand field into three measurable components in each case (compared to the splitting into two and one component for the $\Delta J=1$ and 2 transitions respectively in the tetraamide case).

It is also clear that the CPL profiles of all three triamide complexes are unique, and represent a *fingerprint* of the chiral environment about the luminescent ion. The evaluation of the hydration state is also an important tool in an analysis of this local environment.

Chapter 5

5. Emission Spectra of the $[EuL^{1a}]^{3+}$ System in the Presence of Selected Anions

5.1 The $[EuL^{1a}]^{3+}$ System in the Presence of $NaHCO_3$

The (*SSS*)-enantiomer of the $[EuL^{1a}]^{3+}$ complex was exposed to a ten-fold molar excess of sodium hydrogen carbonate, and the CPL and total emission of the complex were observed at pD6 and 298K. **Figure 5.1** shows the CPL and total emission of the complex over the full spectral range 570 to 720nm.

5.2 The $[EuL^{1a}]^{3+}$ System in the Presence of Na_2HPO_4

The (*SSS*)-enantiomer of the $[EuL^{1a}]^{3+}$ complex was exposed to a ten-fold molar excess of disodium hydrogen phosphate, and the CPL and total emission of the complex were observed under the same conditions as the previous experiments. **Figure 5.2** shows the CPL and total emission of the complex over the full spectral range 570 to 720nm.

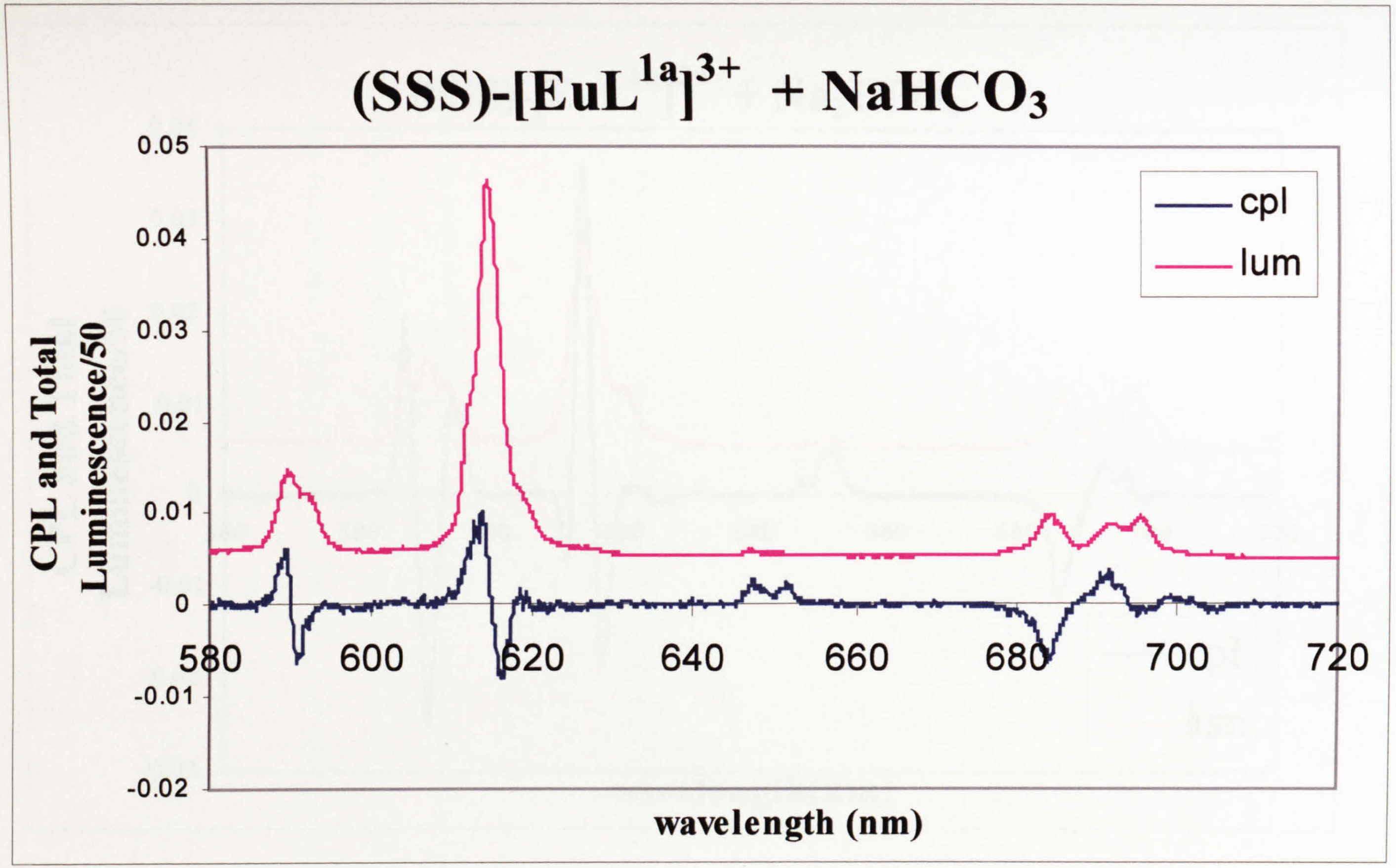

Figure 5.1 *Upper* Total emission of the ΔJ=1,2,3 and 4 transitions of the (SSS)- $[EuL^{1a}]^{3+}$ complex in the presence of $NaHCO_3$ (2.87mM D_2O solution of complex, 28.70mM salt recorded at 295K and at pD6). *Lower* Circularly polarised emission of the ΔJ=1,2,3 and 4 transitions of the (SSS)-$[EuL^{1a}]^{3+}$ complex under the same conditions.

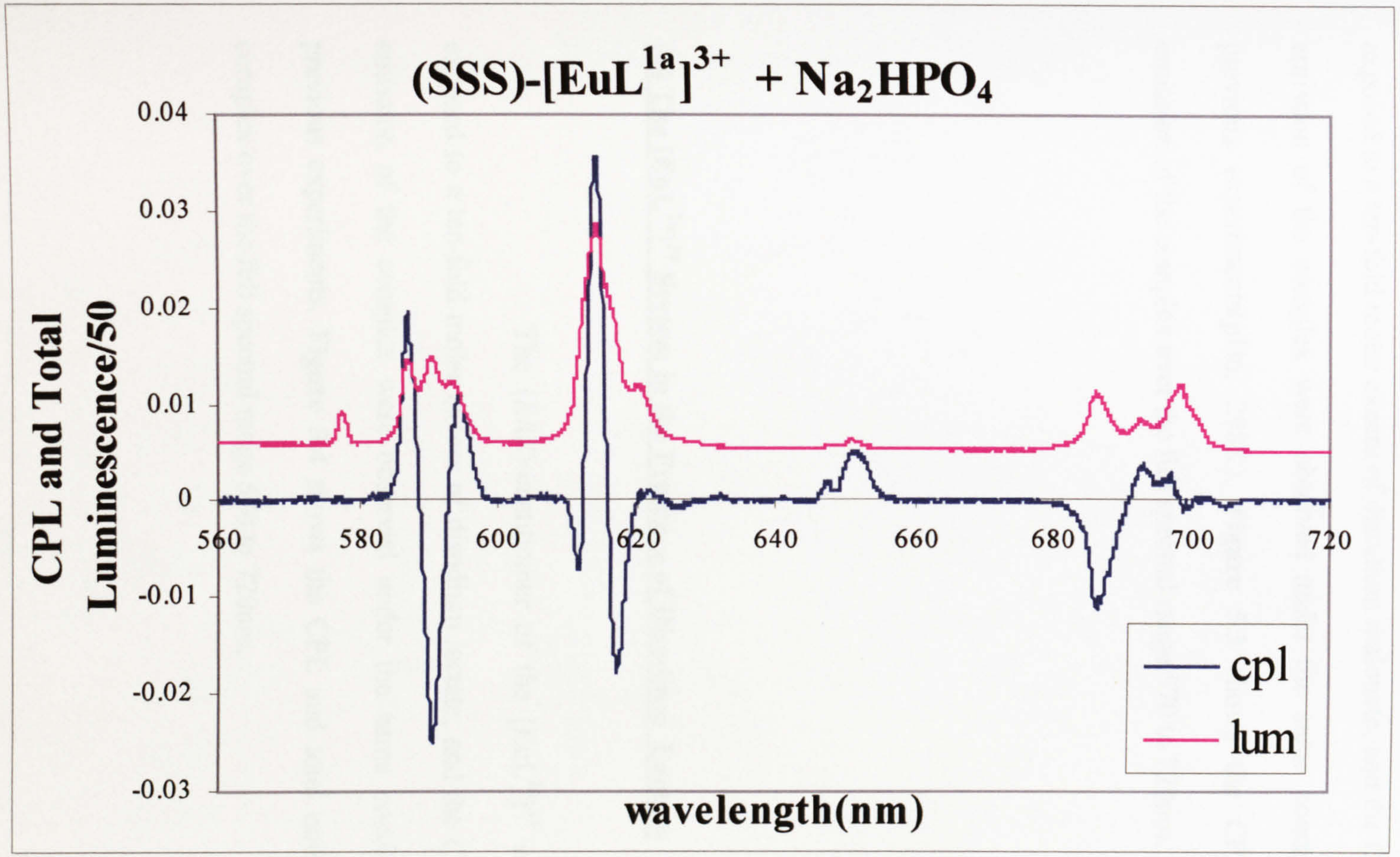

Figure 5.2 *Upper* Total emission of the ΔJ=1,2,3 and 4 transitions of the (SSS)- $[EuL^{1a}]^{3+}$ complex in the presence of Na_2HPO_4 (2.87mM D_2O solution of complex, 28.70mM salt recorded at 295K and at pD6). *Lower* Circularly polarised emission of the ΔJ=1,2,3 and 4 transitions of the (SSS)-$[EuL^{1a}]^{3+}$ complex under the same conditions.

5.3 The $[EuL^{1a}]^{3+}$ System in the Presence of Disodium Malonate

The (*RRR*)-enantiomer of the $[EuL^{1a}]^{3+}$ complex was exposed to a ten-fold molar excess of disodium malonate, and the CPL and total emission of the complex were observed under the same conditions as the previous experiments(pD6, 298K). **Figure 5.3** shows the CPL and total emission of the complex over the full spectral range 570 to 720nm.

5.4 The $[EuL^{1a}]^{3+}$ System in the Presence of Disodium Lactate

The (*RRR*)-enantiomer of the $[EuL^{1a}]^{3+}$ complex was exposed to a ten-fold molar excess of disodium lactate, and the CPL and total emission of the complex were observed under the same conditions as the previous experiments. **Figure 5.4** shows the CPL and total emission of the complex over the full spectral range 570 to 720nm.

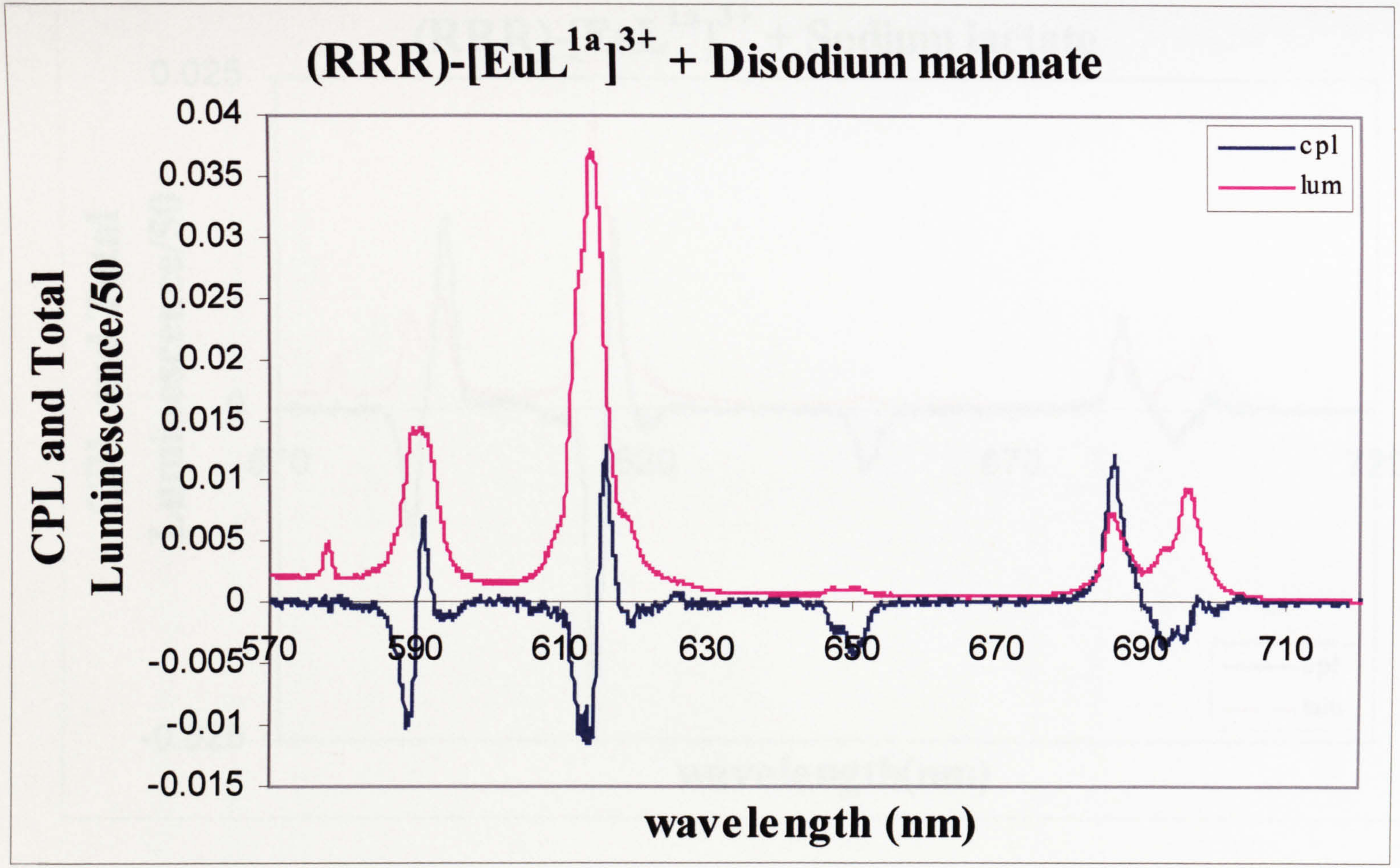

Figure 5.3 *Upper* Total emission of the ΔJ=1,2,3 and 4 transitions of the (RRR)-$[EuL^{1a}]^{3+}$ complex in the presence of $Na_2C_3H_6O_2$ (2.87mM D_2O solution of complex, 28.70mM salt recorded at 295K and at pD6). *Lower* Circularly polarised emission of the ΔJ=1,2,3 and 4 transitions of the (RRR)-$[EuL^{1a}]^{3+}$ complex under the same conditions.

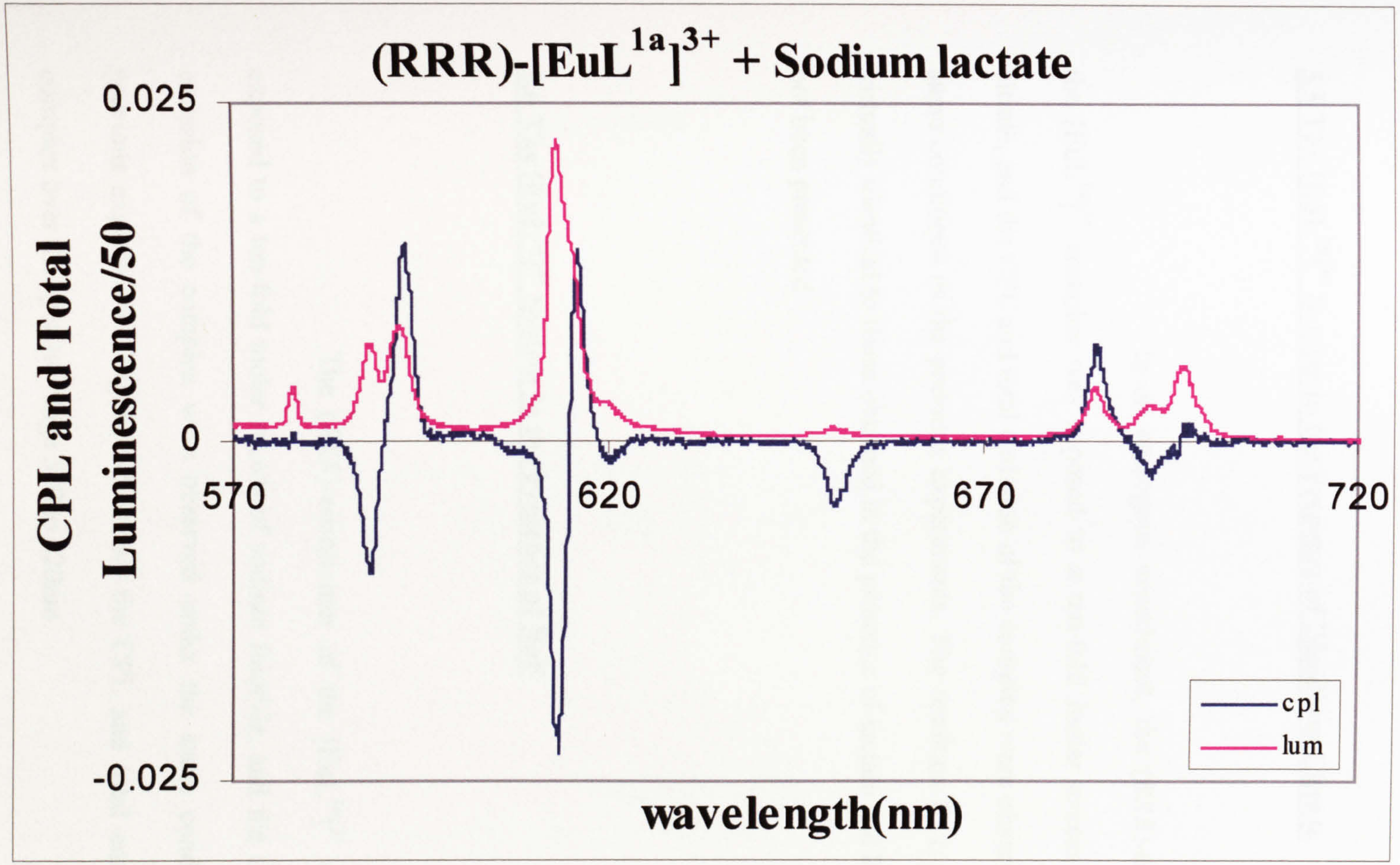

Figure 5.4 *Upper* Total emission of the ΔJ=1,2,3 and 4 transitions of the (RRR)- $[EuL^{1a}]^{3+}$ complex in the presence of disodium (s) - lactate (2.87mM D_2O solution of complex, 28.70mM salt recorded at 295K and at pD6)*Lower* Circularly polarised emission of the ΔJ=1,2,3 and 4 transitions of the (RRR)-$[EuL^{1a}]^{3+}$ complex under the same conditions.

5.5 The $[EuL^{1a}]^{3+}$ System in the Presence of Disodium Citrate

In an analogous experiment, the (*RRR*)-enantiomer of the $[EuL^{1a}]^{3+}$ complex was exposed to a ten-fold molar excess of disodium citrate, and the CPL and total emission of the complex were observed under the same conditions as the previous experiments. The resultant CPL profiles were virtually identical to those obtained in the presence of lactate and have therefore not been presented

5.6 The $[EuL^{1a}]^{3+}$ System in the Presence of NaF

The (*RRR*)-enantiomer of the $[EuL^{1a}]^{3+}$ complex was exposed to a ten-fold molar excess of sodium fluoride, and the CPL and total emission of the complex were observed under the same conditions as the previous experiments. **Figure 5.5** shows the CPL and total emission of the complex over the spectral range 570 to 620nm.

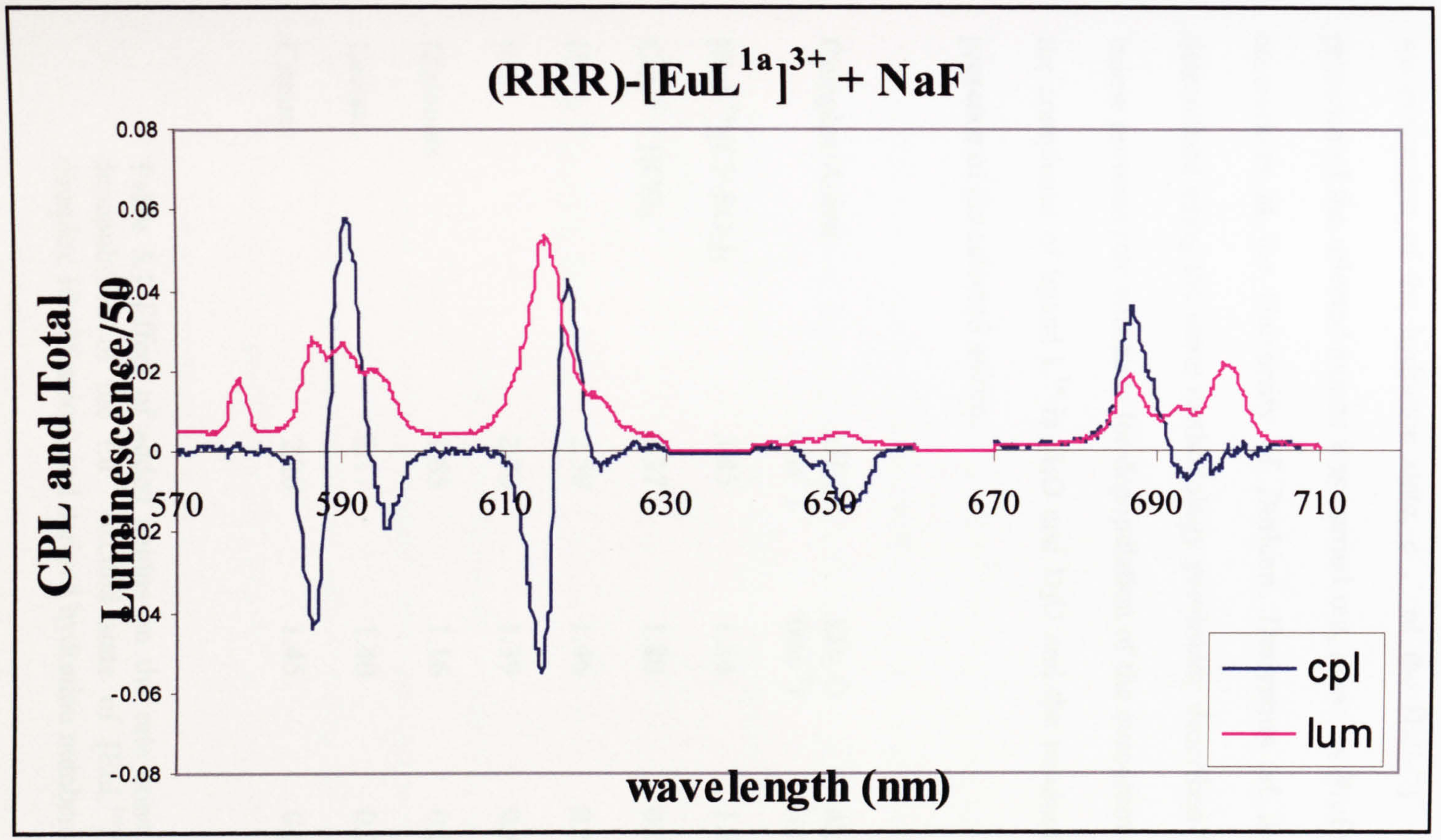

Figure 5.5 *Upper* Total emission of the ΔJ=1,2,3 and 4 transitions of the (RRR)-$[EuL^{1a}]^{3+}$ complex in the presence of NaF(2.87mM D_2O solution of complex, 28.70mM salt recorded at 295K and at pD6). *Lower* Circularly polarised emission of the ΔJ=1,2,3 and 4 transitions of the (RRR)-$[EuL^{1a}]^{3+}$ complex under the same conditions.

5.8 Hydration States of the Europium(III) Triaamide Complexes

An evaluation of the hydration state, q , of the $[EuL^{1a}]^{3+}$ complex in the presence of the selected anions was carried out, again by Professor Parker and co-workers at the University of Durham. Derivation of the q value was determined using the same methodology previously described [65,8] . **Table 5.1** below presents rate constants for depopulation of the europium excited state for the complexes of ligand L^{1a} in H_2O and D_2O and the resultant q value in the presence of the selected anions.

Complex/Anion	kH_2O (ms^{-1})	kD_2O (ms^{-1})	Δk_{corr} (ms^{-1})	q
$[EuL^{1a}][CF_3SO_3]_3$	3.85	1.54	1.82	2.2
CO_3^{2-} / HCO_3^-	2.37	1.80	0.08	0.1
HPO_4^{2-}	2.50	1.46	0.55	0.7
F^-	2.70	1.39	0.82	1.0
Malonate	1.65	1.16	0.00	0.0
Lactate	2.17	1.40	0.28	0.3
Citrate	2.20	1.45	0.26	0.3

Table 5.1 Effect of added anions on the rate constants (±10%) for depopulation of the Eu^{3+} excited state of $[EuL^{1a}]^{3+}$ (295K, 1mM complex 10mM anion) and derived hydration numbers, q (±20%).

5.9 Discussion

Exposure of a ten-fold excess of selected anion to the europium complex of ligand L^{1a} produced dramatic changes in the strength and in the form of the circular polarised emission. In all cases, no CPL was observed under the $\Delta J=0$ transition as expected. Of the remaining four transitions observed, all carried a measurable circularly polarised element.

As discussed previously, for any CPL profile of one enantiomer, it could be assumed that the CPL profile of the opposite enantiomer would be identical but inverted. To be able, therefore, to make a more accessible and straightforward comparison of the CPL profiles under each of the following four transitions, the profiles of the (*RRR*)- enantiomers of the complex have been inverted.

5.9.1 The $\Delta J=1$ Transition

The CPL profiles of the L^{1a} complex in the presence of a ten molar excess of carbonate, phosphate, malonate, lactate and fluoride under the $\Delta J=1$ transition are shown in **Figure 5.6.** All profiles are drawn to the same scale and wavelength range (580 to 605nm). All profiles indicate CPL ($I_l - I_r$) of arbitrary units which have not been shown.

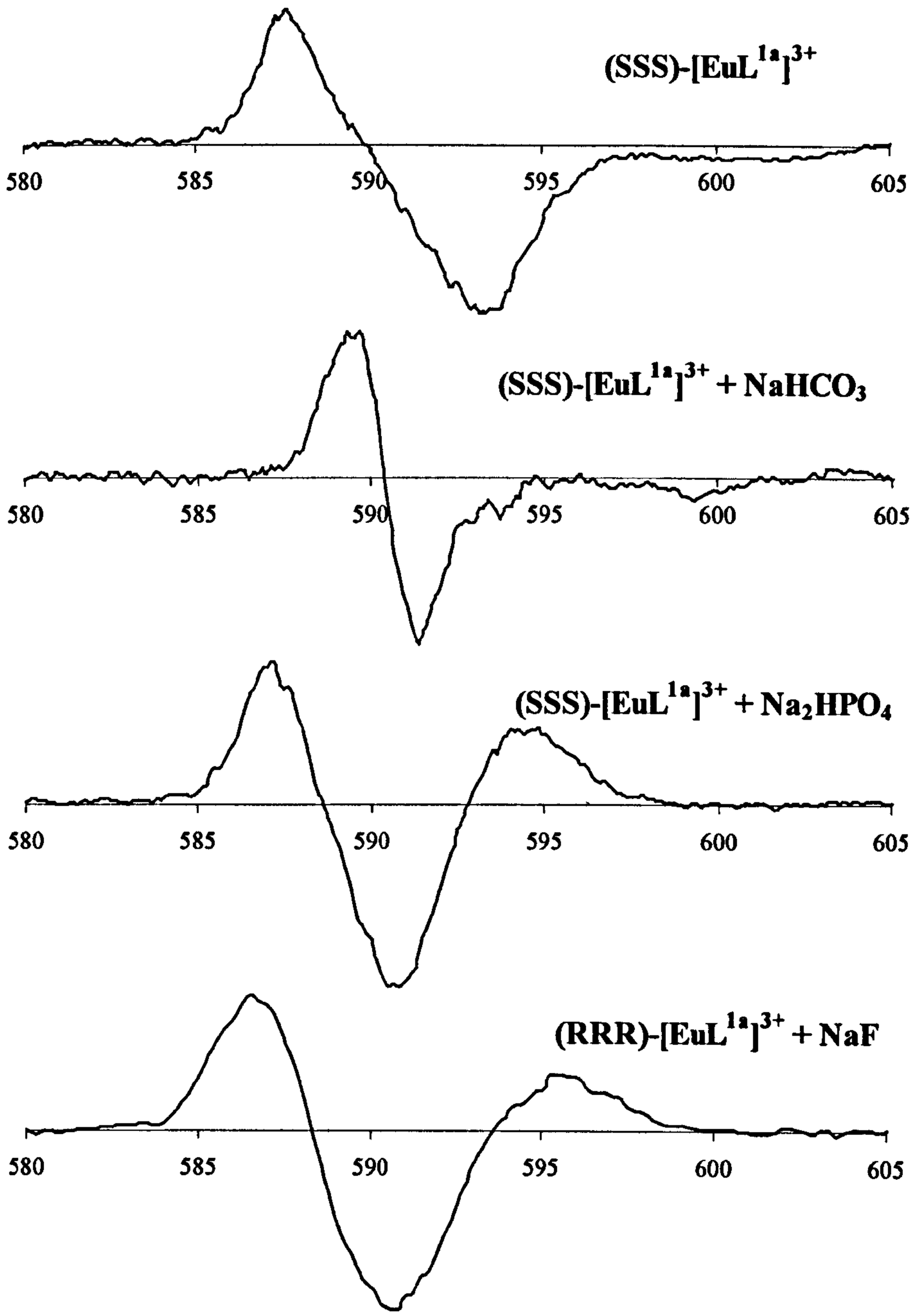

Figure 5.6. CPL profiles of the $[EuL^{1a}]^{3+}$ complex under the $\Delta J=1$ transition in the absence and presence of selected anions.

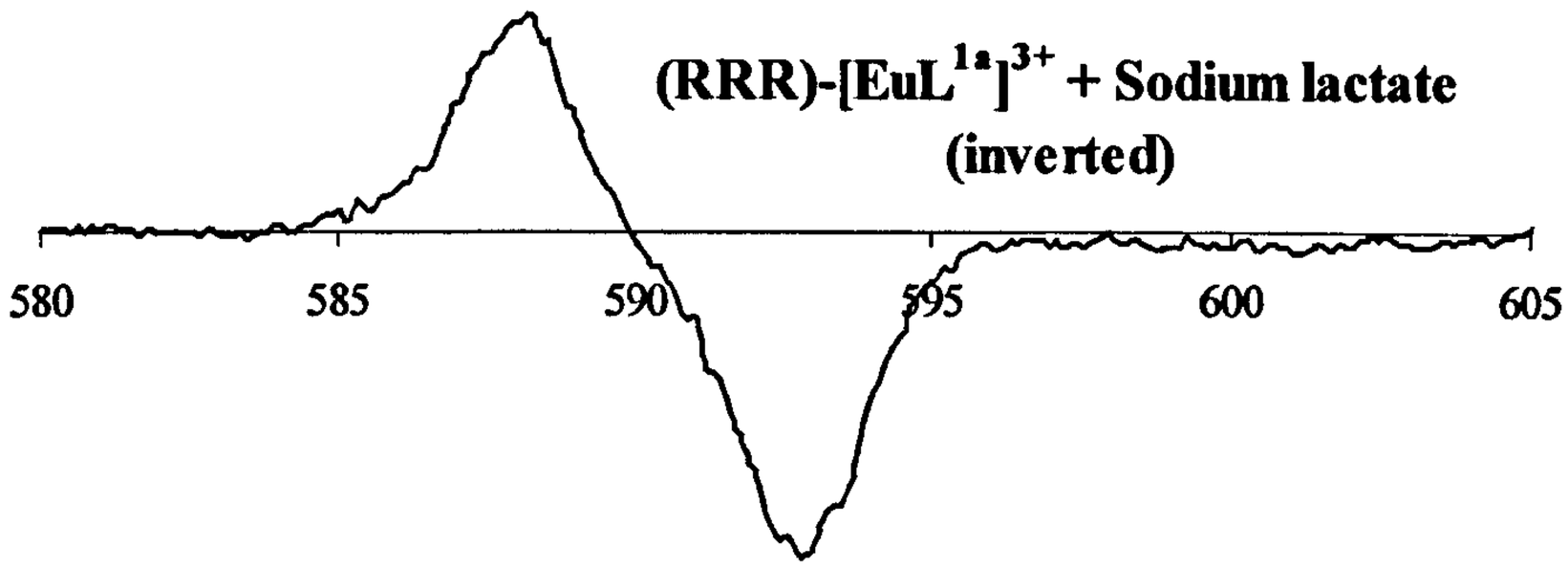

Figure 5.6 (cont.). CPL profiles of the $[EuL^{1a}]^{3+}$ complex under the $\Delta J=1$ transition in the absence and presence of selected anions

As observed in the previous chapter, the CPL profile of the L^{1a} complex under the $\Delta J=1$ transition follows a (+ , -) pattern for the two measurable components at 588 and 594nm with a second negative component indicated by a shoulder at around 591nm.

The CPL profiles of the L^{1a} complex in the presence of sodium lactate, and citrate also follow this same pattern. The similarity of the pattern is also reflected in the strength of the circularly polarised emission as indicated by the comparable dissymmetry factors.

The nature of the emission follows a distinctly different profile for the L^{1a} complex in the presence of phosphate, fluoride and malonate. These profiles follow a (+ , - , +) sequence with the component peaks at around 587, 591 and 595nm. Although the complex in the presence of these salts follow the same pattern, consideration of the relative strength of the circularly polarised emission reveals a difference in the phosphate and fluoride profile with those of malonate.

The circularly polarised emission of the L^{1a} complex in the presence of carbonate is the most unique of the profiles presented under the $\Delta J=1$ transition. The emission also follows the same (+ , -) sequence as the L^{1a} complex in the absence of any anion, however, the component peaks are now found at 589 and 592nm.

Anion	Dissymmetry Factor		
	588/589nm	593nm	
Lactate/Citrate	+0.06	-0.10	
Carbonate	+0.03	-0.04	
	587nm	591nm	595nm
Fluoride	+0.10	-0.11	+0.05
Malonate	+0.03	-0.02	+0.02
Phosphate	+0.09	-0.11	+0.06

Table 5.2 Dissymmetry factors of the resolved components under the $\Delta J=1$ transition in the presence of selected anion

5.9.2 The $\Delta J=2$ Transition

The unique nature of the effect of carbonate on the EuL^{1a} system as noted under the $\Delta J=1$ transition is again evident under the $\Delta J=2$ transition (**Figure 5.7**). Whereas the CPL profile of the complex in the absence of any excess anion and in the presence phosphate, malonate, citrate and lactate is resolved into three components, the $\Delta J=2$ transition is resolved into only two. The bisignate couplet observed in the presence of carbonate follows a (+ , -) sequence with component peaks at 614 and 617nm.

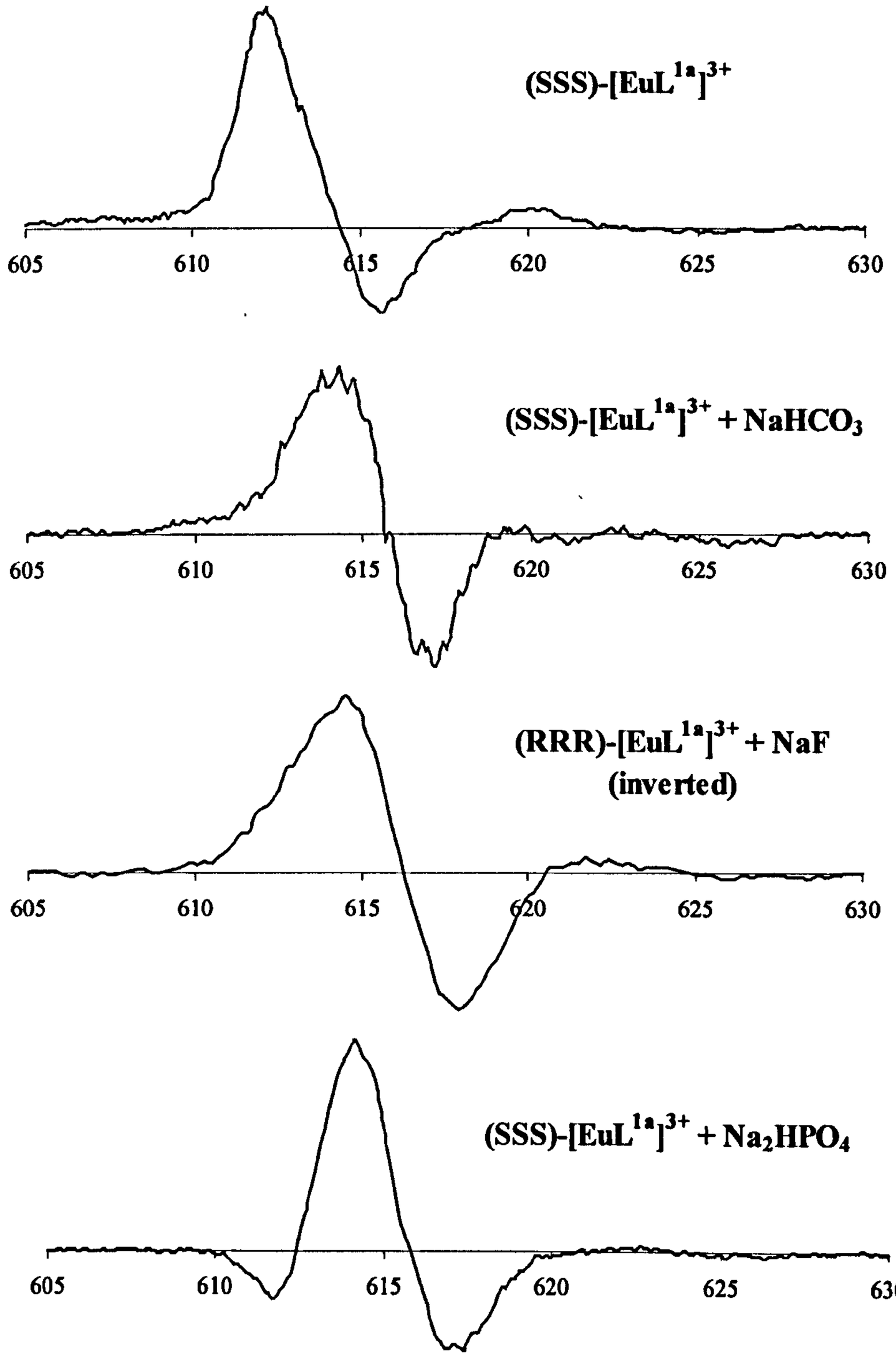

Figure 5.7. CPL profiles of the $[EuL^{1a}]^{3+}$ complex under the $\Delta J=2$ transition in the absence and presence of selected anions.

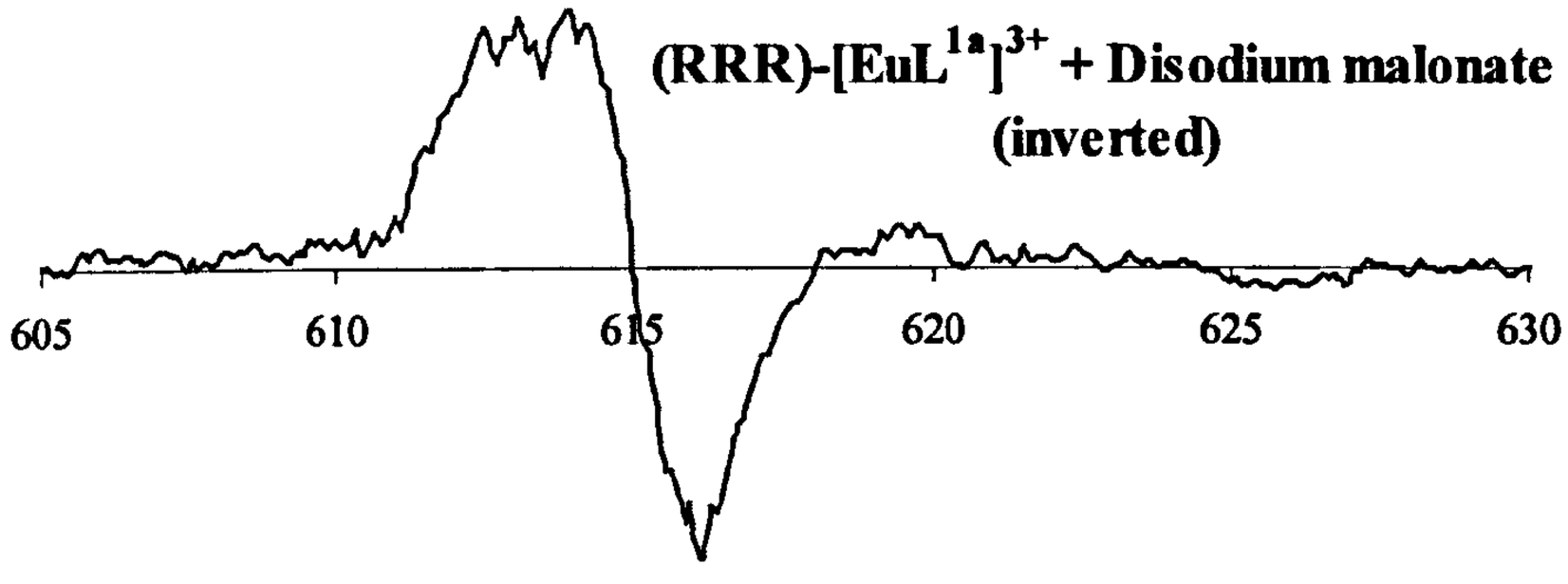

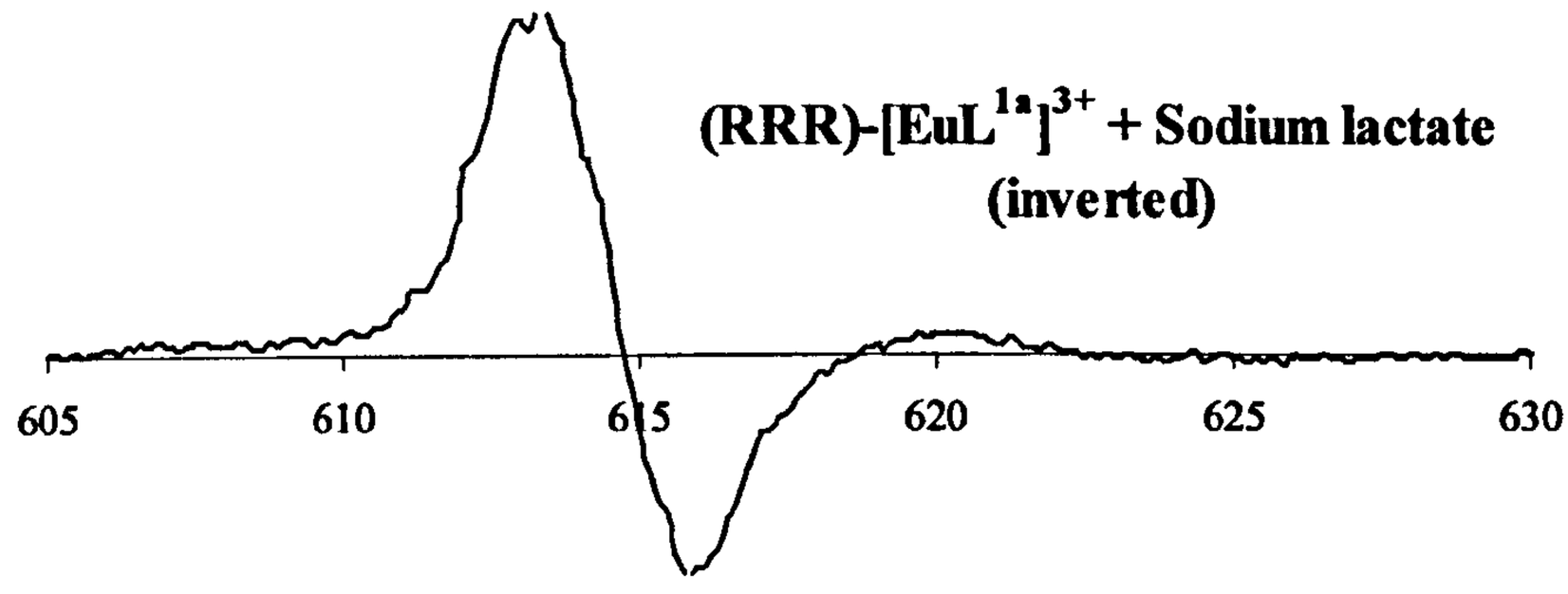

Figure 5.7 (cont.). CPL profiles of the $[EuL^{1a}]^{3+}$ complex under the $\Delta J=2$ transition in the absence and presence of selected anions.

Of the remaining profiles, all are resolved into three components. All, with the exception of phosphate, follow a (+ , - , +) sequence with the component peaks occurring at around 613/614nm (positive), 616/617nm (negative) and around 620nm (positive). Again, the form of the profiles of the complex in the presence of lactate is closely related to the profile of the complex in the absence of any anion in terms of the relative height of the components. The associated dissymmetry factors are more wide ranging, however, and are cited in the table below **Table 5.3**.

Anion	Dissymmetry Factor		
	614nm	617nm	
Carbonate	+0.01	+0.01	
	613/614nm	616/617nm	620nm
Fluoride	+0.04	-0.07	+0.01
Malonate	+0.02	-0.02	+0.02
Lactate/Citrate	+0.04	-0.05	+0.04

Table 5.3 Dissymmetry factors of the resolved components under the $\Delta J=2$ transition in the presence of selected anion

In the presence of phosphate, however, the trisignate sequence observed above, (+ , - , +), sequence is reversed. Three distinct components are resolved at 612, 614 and 617nm, all with relatively strong dissymmetry factors.

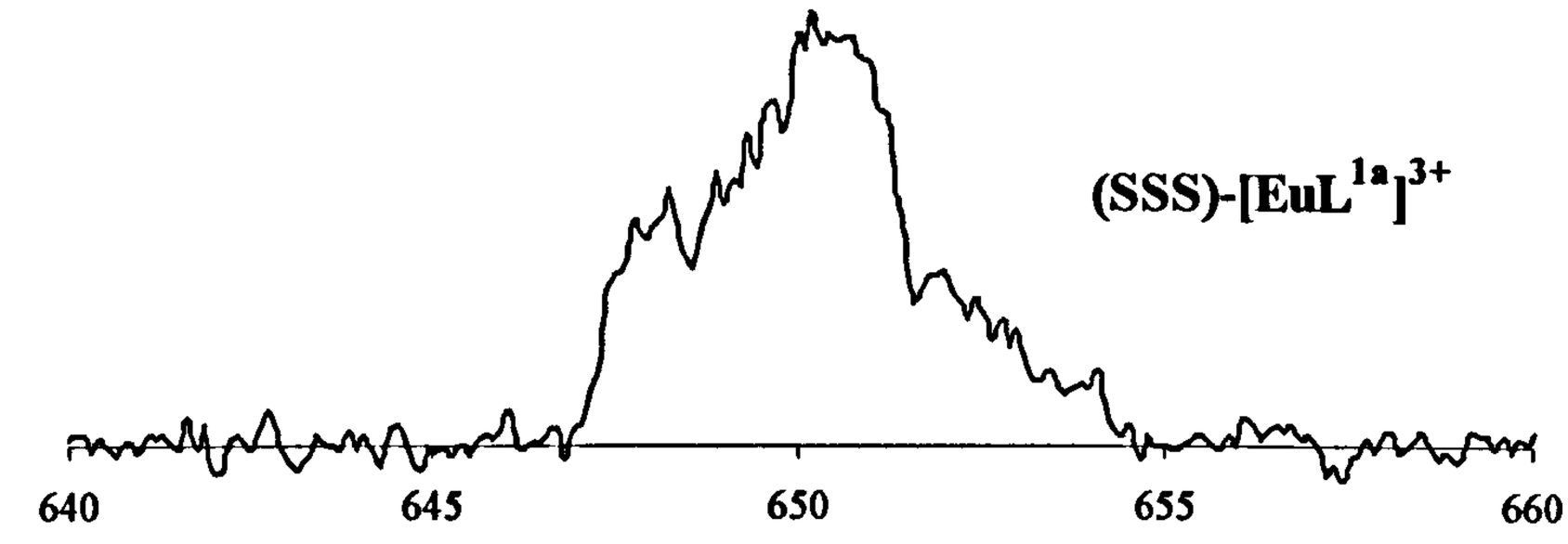

Figure 5.8. CPL profiles of the $[EuL^{1a}]^{3+}$ complex under the $\Delta J=3$ transition in the absence and presence of selected anions.

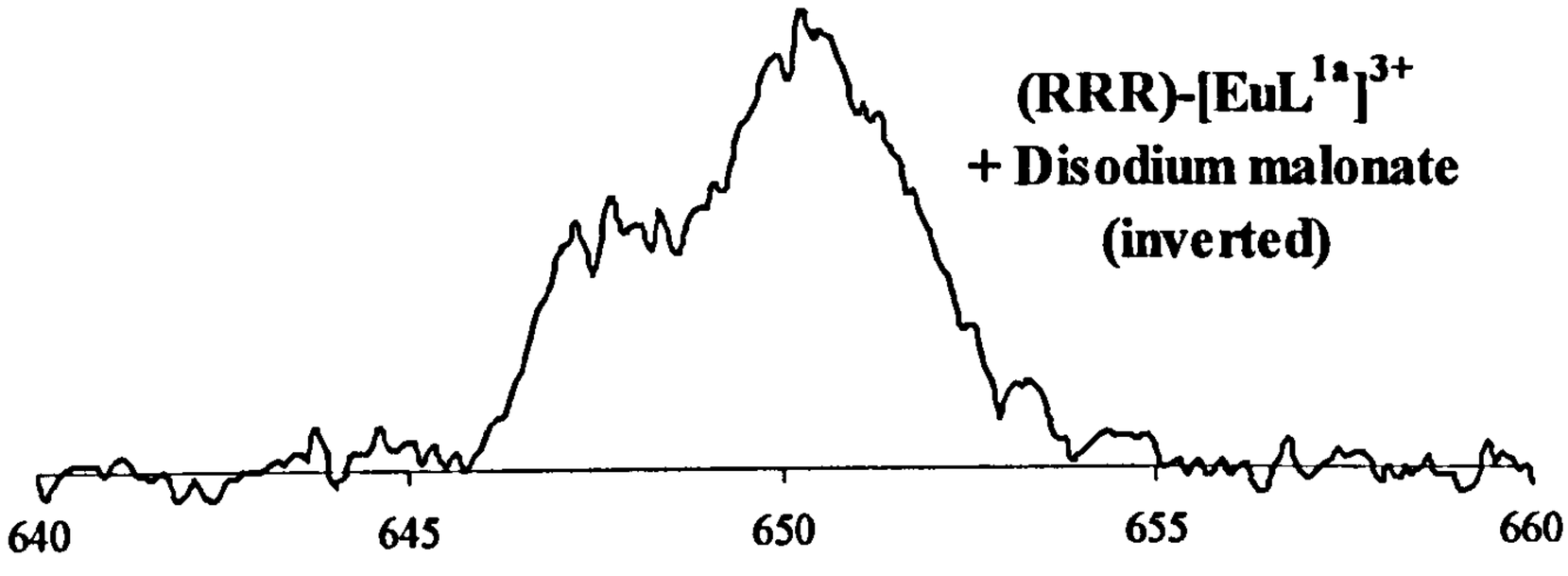

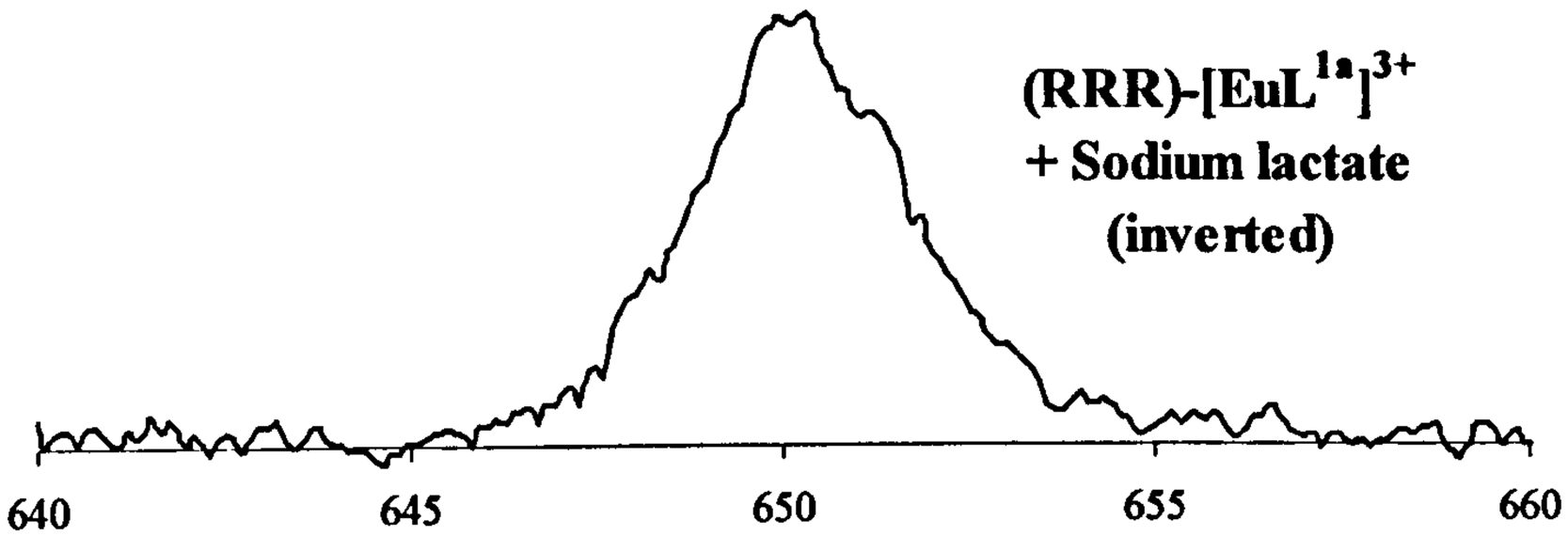

Figure 5.8 (cont.). CPL profiles of the $[EuL^{1a}]^{3+}$ complex under the $\Delta J=3$ transition in the absence and presence of selected anions.

5.9.3 The ΔJ=3 Transition

The CPL profiles of the L^{1a} complex in the presence of the selected anions under the ΔJ=3 transition are shown in **Figure 5.8.**

The CPL profile of the (SSS)-$[EuL^{1a}]^{3+}$ complex under the ΔJ=3 transition reveals no negative component. There appears to be at least three components in the range 648 to 645nm, indicated by two *shoulders* flanking the central peak at 650nm. A dissymmetry factor was calculated based on this monosignate peak a strong signal with g_{em} (650nm)= 0.12.

The profiles of the complex in the presence of the selected anions (with the exception of carbonate) are strikingly similar. All have a main peak around 651nm with the emergence of a shoulder at around 647nm. The similarity is also reflected in the calculated dissymmetry factors associated with the main peak of roughly 0.10.

The profile of the complex in the presence of carbonate is again unique. The transition appears to be resolved into two components occurring at 647 and 652nm, with dissymmetry factors roughly equivalent to those quoted above.

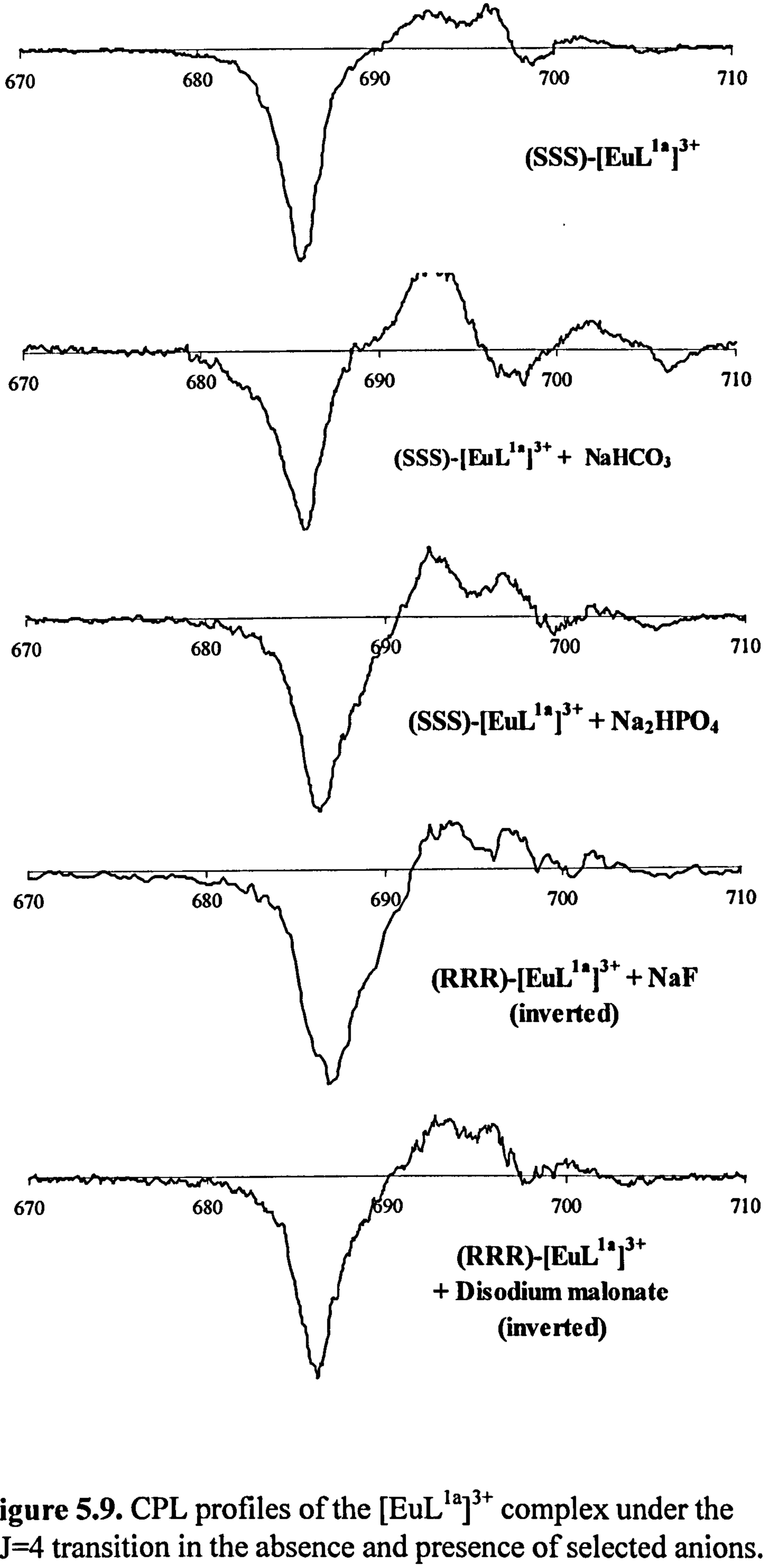

Figure 5.9. CPL profiles of the $[EuL^{1a}]^{3+}$ complex under the $\Delta J=4$ transition in the absence and presence of selected anions.

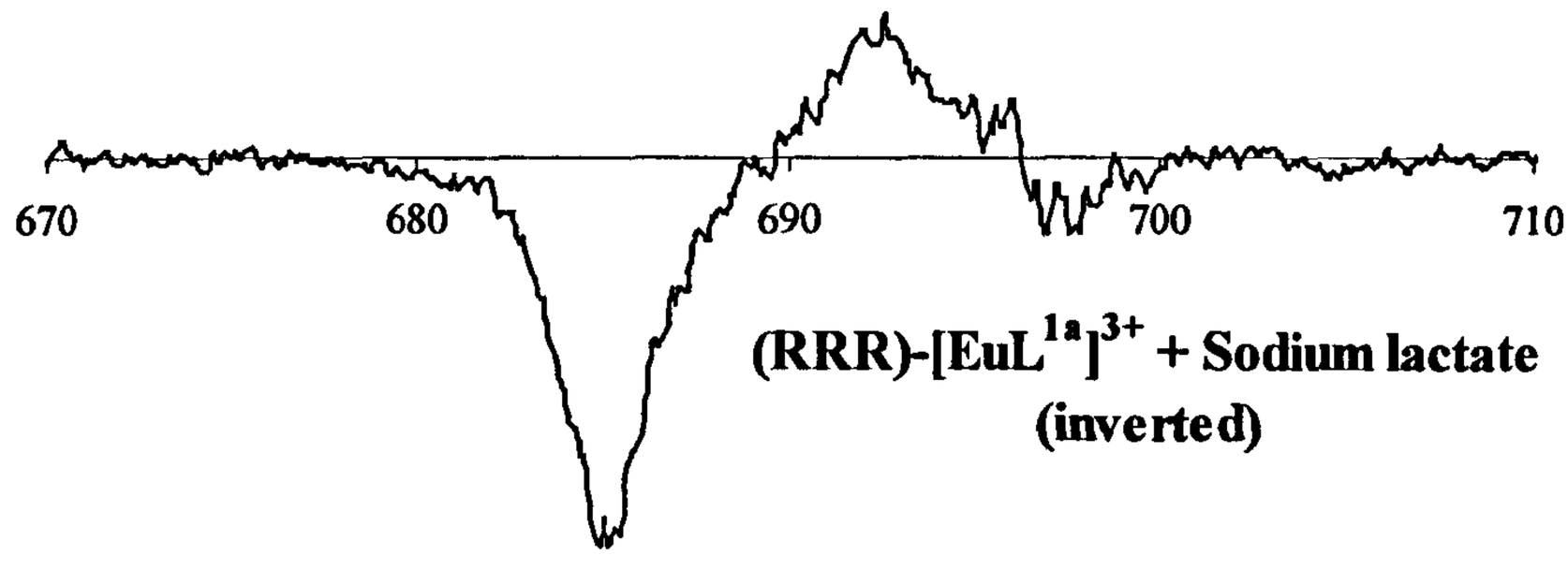

Figure 5.9 (cont.). CPL profiles of the $[EuL^{1a}]^{3+}$ complex under the $\Delta J=4$ transition in the absence and presence of selected anions.

5.9.4 The ΔJ=4 Transition

The components resolved under the ΔJ=4 transition for the complex in the presence and absence of selected anion are shown in **Figure 5.9.** All profiles show a clear, prominent and negative peak at around 686nm. There are a multitude of components which are not well resolved in the spectral region 690 to 710nm but all profiles seem to follow the same general form. The associated dissymmetry factor of the main peak at 686nm was calculated for each profile and the results are tabulated below **Table 5.4.**

Anion	Dissymmetry Factor g_{em} (686nm)
Carbonate	0.06
Phosphate	0.08
Malonate	0.07
Lactate/Citrate	0.06
Fluoride	0.08

Table 5.4 Dissymmetry factors of the resolved components under the ΔJ=4 transition in the presence of selected anion.

5.9.5 Summary

It is clear that the CPL profile of the $[EuL^{1a}]^{3+}$ diaqua complex changes significantly on exposure to the selected anion as discussed at length above. The change in profile and in the calculated dissymmetry factors of the components resolved under each transition implies in the very least that a complex-anion interaction has occurred. However, in conjunction with the evaluation of the hydration state of the molecule in the presence of these anions, it can be stated that the anions *bind* to the metal centre, displacing at least one of the two bound water molecules in all cases.

The hydration states of the $[EuL^{1a}]^{3+}$ complex in the presence of the selected anions suggest that one of the two bound water molecules is displaced when the $[EuL^{1a}]^{3+}$ diaqua species is exposed to phosphate and fluoride ($q \approx 1$) and that both are replaced when exposed to carbonate, malonate, citrate and lactate ($q \approx 0$).

This data would suggest the formation of a six-membered chelate ring for the malonate-bound complex, a five membered ring structure for the both the complex-lactate and complex-citrate adducts and a four membered chelate ring in the complex-carbonate case.

Chapter 6

6. CPL and Total Lumniescence Spectra of $[EuL^{1b}]^{3+}$ in the Presence of Selected Anions

6.1 The$[EuL^{1b}]^{3+}$ System in the presence of $NaHCO_3$

The (*SSS*)-enantiomer of the $[EuL^{1b}]^{3+}$ complex was exposed to a ten-fold molar excess of sodium hydrogen carbonate, and the CPL and total emission of the complex were observed under the same conditions as the previous experiments, that is pD 6 and 298K. **Figure 6.1** shows the CPL and total emission of the complex over the full spectral range 570 to 720nm.

6.2 The $[EuL^{1b}]^{3+}$ System in the presence of Na_2HPO_4

The (*SSS*)-enantiomer of the $[EuL^{1b}]^{3+}$ complex was exposed to a ten-fold molar excess of disodium hydrogen phosphate, and the CPL and total emission of the complex were observed under the same conditions as the previous experiments. **Figure 6.2** shows the CPL and total emission of the complex over the full spectral range 570 to 720nm.

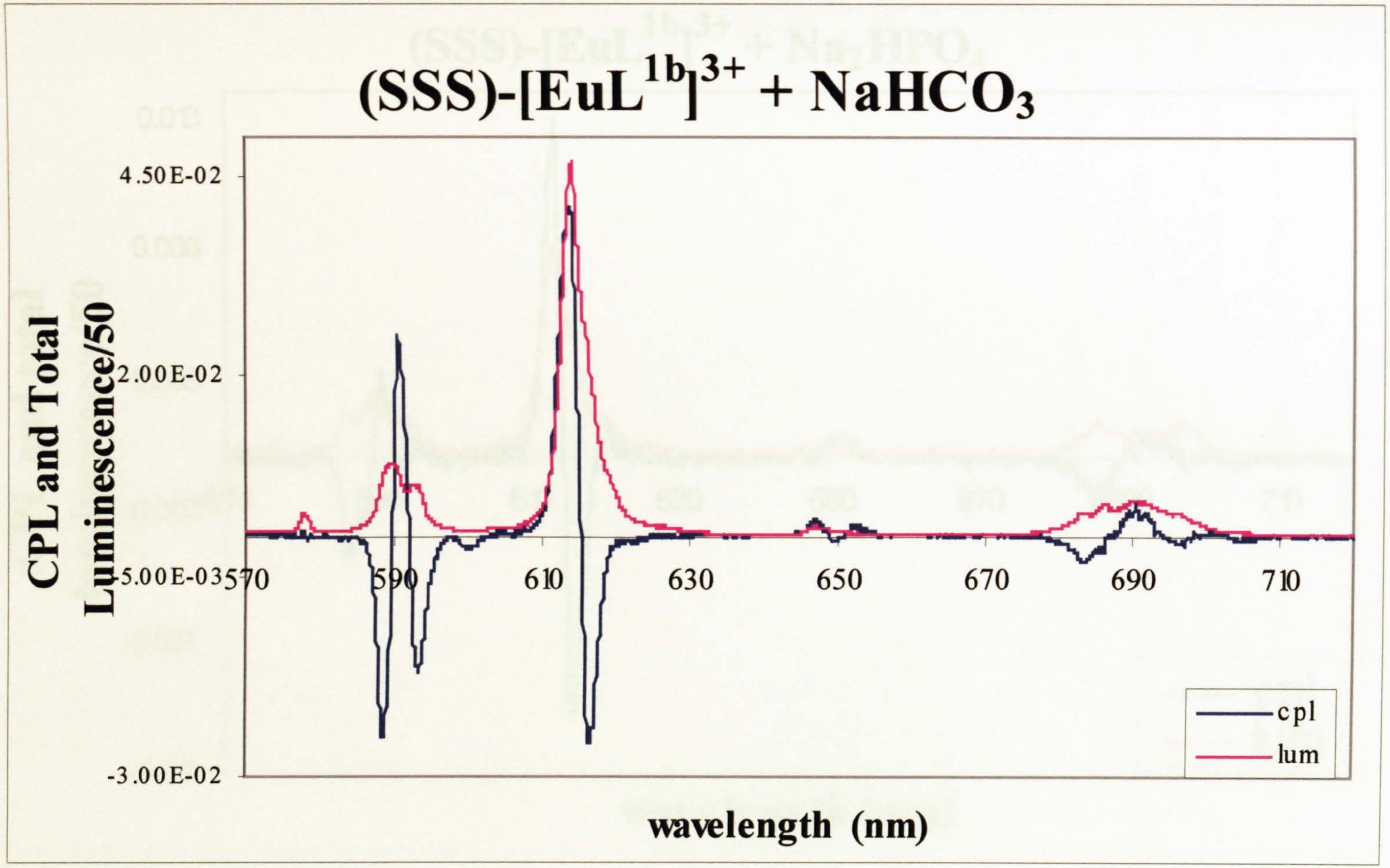

Figure 6.1 *Upper* Total emission of the ΔJ=1,2,3 and 4 transitions of the (SSS)- $[EuL^{1b}]^{3+}$ complex in the presence of $NaHCO_3$ (2.87mM D_2O solution of complex, 28.70mM salt recorded at 295K and at pD6). *Lower* Circularly polarised emission of the ΔJ=1,2,3 and 4 transitions of the (SSS)-$[EuL^{1b}]^{3+}$ complex under the same conditions.

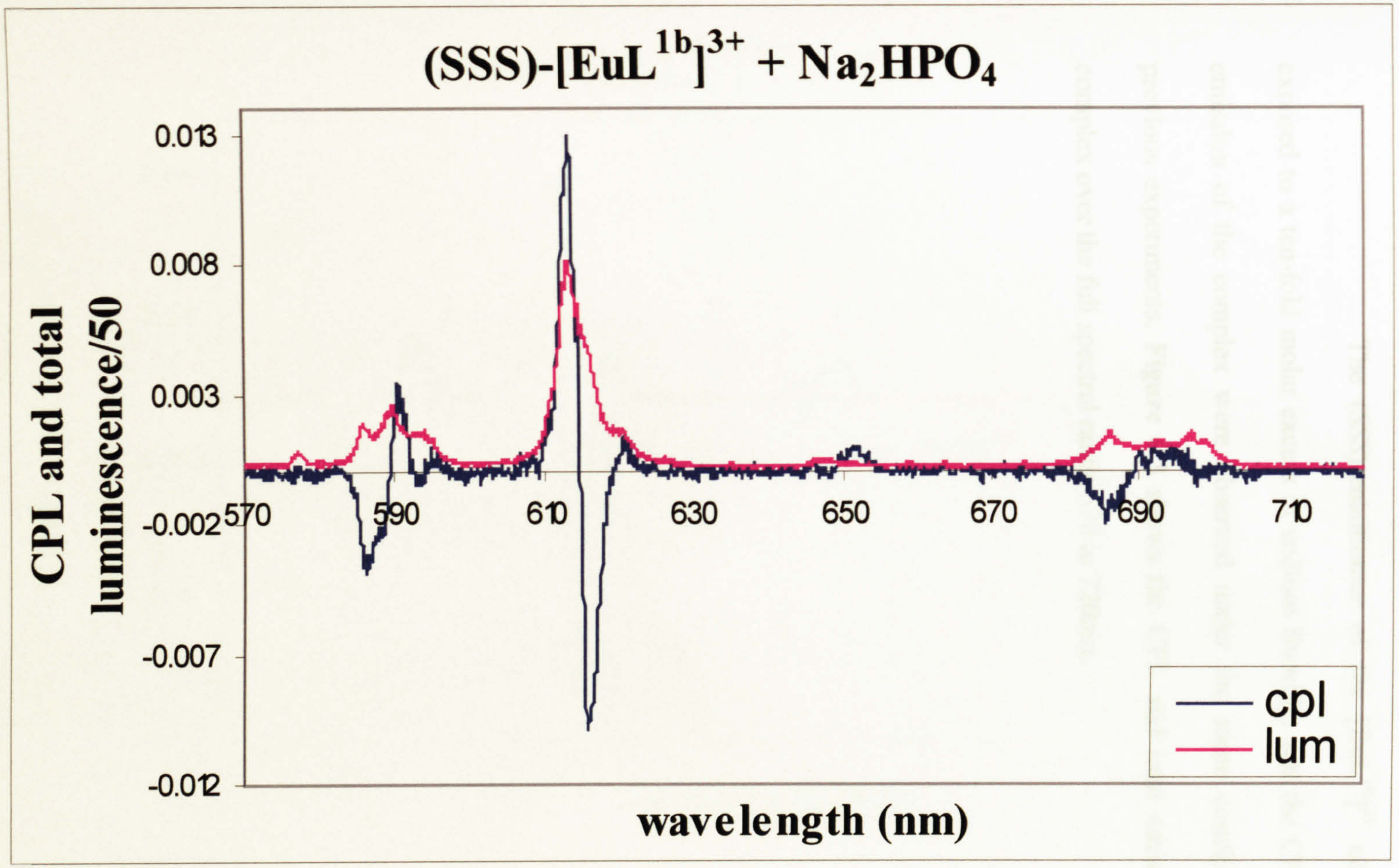

Figure 6.2 *Upper* Total emission of the ΔJ=1,2,3 and 4 transitions of the (SSS)- $[EuL^{1b}]^{3+}$ complex in the presence of Na_2HPO_4 (2.87mM D_2O solution of complex, 28.70mM salt recorded at 295K and at pD6). *Lower* Circularly polarised emission of the ΔJ=1,2,3 and 4 transitions of the (SSS)-$[EuL^{1b}]^{3+}$ complex under the same conditions.

6.3 The $[EuL^{1b}]^{3+}$ System in the presence of NaF

The (*SSS*)-enantiomer of the $[EuL^{1b}]^{3+}$ complex was exposed to a ten-fold molar excess of sodium fluoride, and the CPL and total emission of the complex were observed under the same conditions as the previous experiments. **Figure 6.3** shows the CPL and total emission of the complex over the full spectral range 570 to 720nm.

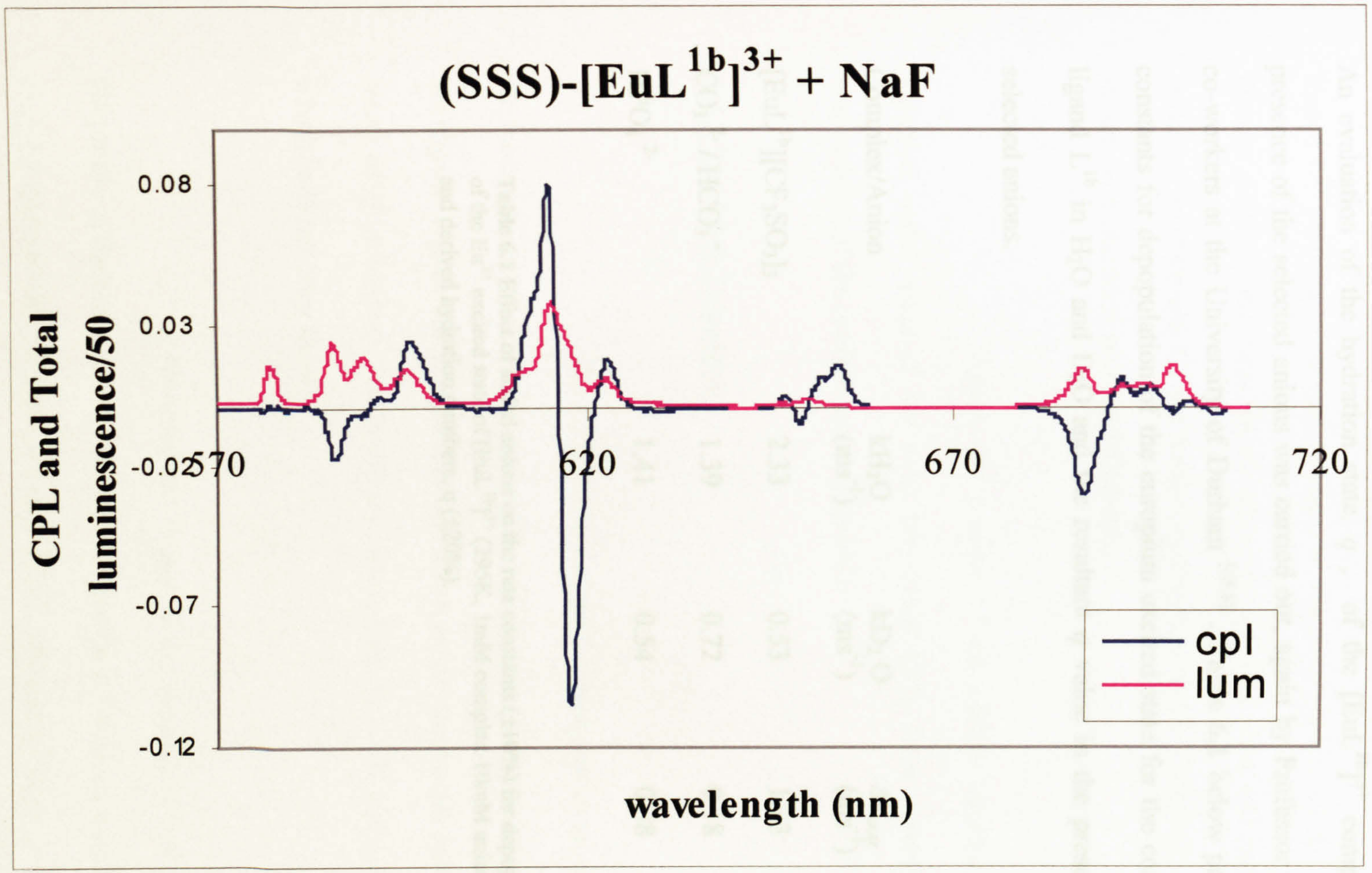

Figure 6.3 *Upper* Total emission of the ΔJ=1,2,3 and 4 transitions of the (SSS)- $[EuL^{1b}]^{3+}$ complex in the presence of NaF (2.87mM D_2O solution of complex, 28.70mM salt recorded at 295K and at pD6). *Lower* Circularly polarised emission of the ΔJ=1,2,3 and 4 transitions of the (SSS)-$[EuL^{1b}]^{3+}$ complex under the same conditions.

6.6 Hydration States of the $[EuL^{1b}]^{3+}$ Complex

An evaluation of the hydration state, q , of the $[EuL^{1b}]^{3+}$ complex in the presence of the selected anions was carried out, again by Professor Parker and co-workers at the University of Durham [65,8] . **Table 6.1** below presents rate constants for depopulation of the europium excited state for the complexes of ligand L^{1b} in H_2O and D_2O and the resultant q value in the presence of the selected anions.

Complex/Anion	kH_2O (ms^{-1})	kD_2O (ms^{-1})	Δk_{corr} (ms^{-1})	q
$[EuL^{1b}][CF_3SO_3]_3$	2.33	0.53	1.33	1.6
CO_3^{2-} / HCO_3^-	1.39	0.72	0.18	0.2
HPO_4^{2-}	1.41	0.54	0.38	0.5

Table 6.1 Effect of added anions on the rate constants (±10%) for depopulation of the Eu^{3+} excited state of $[EuL^{1b}]^{3+}$ (295K, 1mM complex 10mM anion) and derived hydration numbers, q (±20%).

6.7 Discussion

Exposure of a ten-fold excess of selected anion to the europium complex of ligand L^{1b} produced dramatic changes in the strength and in the form of the circular polarised emission. In all cases, no CPL was observed under the $\Delta J=0$ transition as expected. Of the remaining four transitions observed, all carried a measurable circularly polarised element.

Again, the profiles of the (*RRR*)- enantiomers of the complex under each of the four transitions have been inverted to make comparisons of the profiles more accessible.

6.7.1 The $\Delta J=1$ Transition

The CPL profiles of the L^{1b} complex in the presence of a ten molar excess of carbonate, phosphate and fluoride under the $\Delta J=1$ transition are shown **Figure 6.4.** All profiles are drawn to the same scale and wavelength range (580 to 605nm). All profiles indicate CPL ($I_l - I_r$) of arbitrary units which have not been shown.

As noted previously, in the absence of any added anion, the profile of the europium complex of the ligand L^{1b} follows a well defined (+ , - , -) sequence with component peaks at 587, 590 and 595nm.

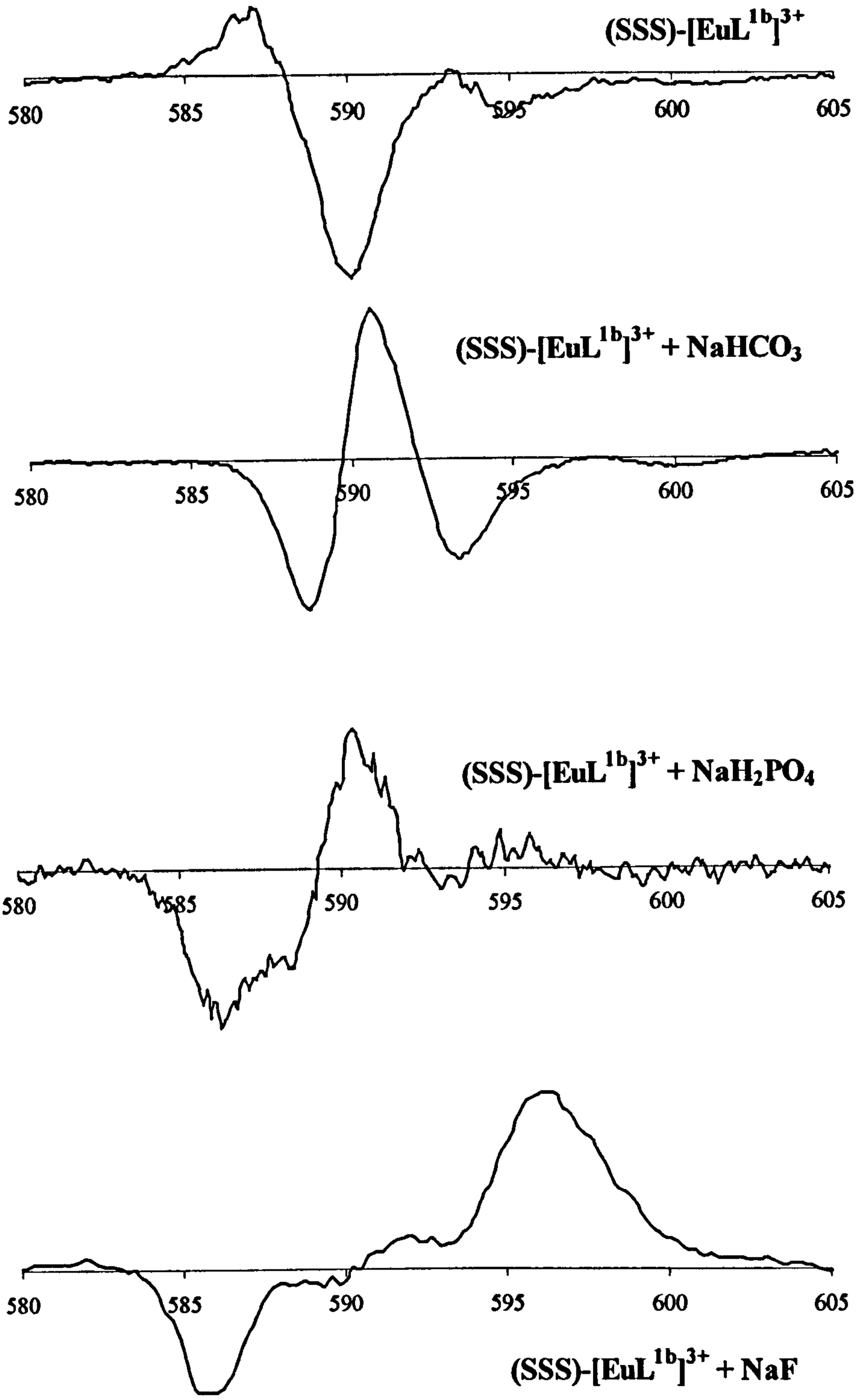

Figure 6.4. CPL profiles of the $[EuL^{1b}]^{3+}$ complex under the $\Delta J=1$ transition in the absence and presence of selected anions.

On exposure to bicarbonate, the circularly polarised emission of the complex remains well defined, following a (- , + , -) sequence, the component peaks occurring at 588,591 and 594nm.

The CPL profile in the presence of phosphate is well less defined but appears to follow a (- , +) pattern, the transition seemingly being resolved into three components peaks at 586 and 591nm. The third component appears to be partially 'hidden' by the negative component at 586nm, visible only as a shoulder at 588nm. This particular profile is difficult to interpret, however, owing to the poor quality of the spectrum.

The components of the complex under this transition appear to be resolved into three on exposure to fluoride. In this case a (- , + , +) sequence with component peaks at 586, 592 and 596nm.

6.7.2 The ΔJ=2 Transition

The CPL profiles of the L^{1b} complex in the presence of the selected anions under the ΔJ=2 transitions are shown in **Figure 6.5.** Again, the profiles are drawn to the same scale and wavelength range (605 to 630nm) and all profiles indicate CPL ($I_l - I_r$) of arbitrary units.

The profile of the complex in the presence of bicarbonate is resolved into at least two components. The profile follows a (+ , -) pattern with the peaks of the bisignate couplets occuring around 614 and 617nm.

The remaining profiles appear to be resolved into at least three components (the shoulder at around 613nm in the fluoride case in particular would suggest the possibility of a 'hidden' component).

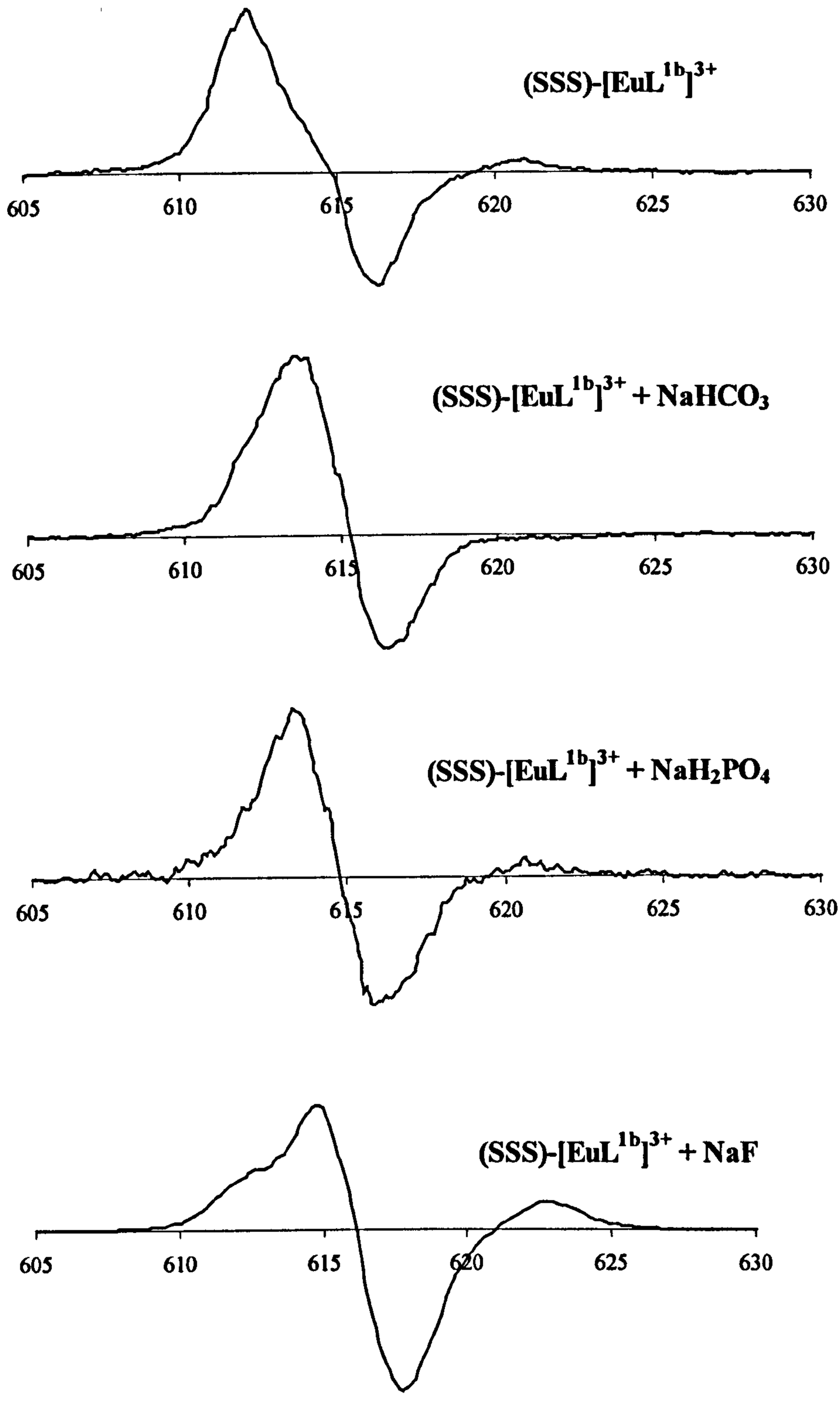

Figure 6.5. CPL profiles of the $[EuL^{1b}]^{3+}$ complex under the $\Delta J=2$ transition in the absence and presence of selected anions.

6.7.3 The ΔJ=3 Transition

The CPL profiles of the L^{1b} complex in the presence of the selected anions under the ΔJ=3 transition are shown in **Figure 6.6.** The profile of the emission in the presence of both bicarbonate and fluoride are multisignate in nature with the bicarbonate profile being resolved into at least three components following a (+ , - , +) pattern with peaks at around 647, 650 and 653nm. The fluoride profile is the most clearly defined, appearing to be resolved into at least four components in a (+ , - , + , +) pattern. The associated dissymmetry factors under this transition are again all characteristically strong, with the main component in the spectral region 650 to 655nm having typical values of 0.23 to 0.30.

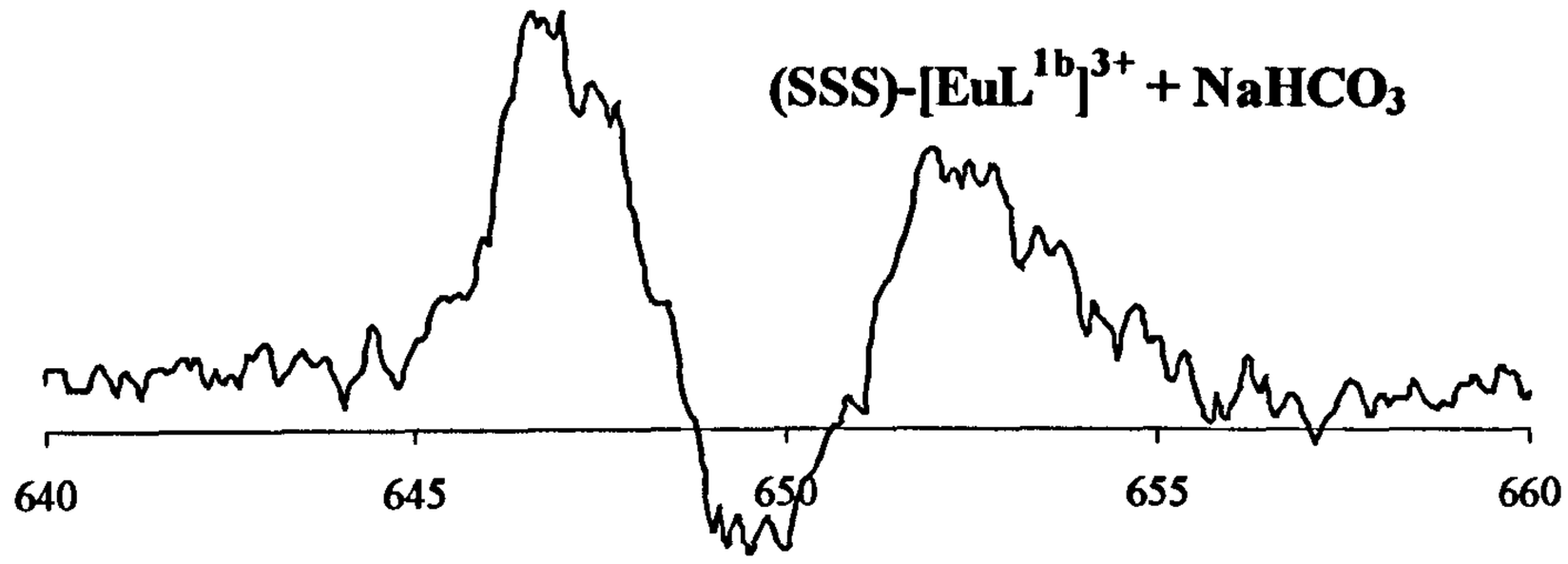

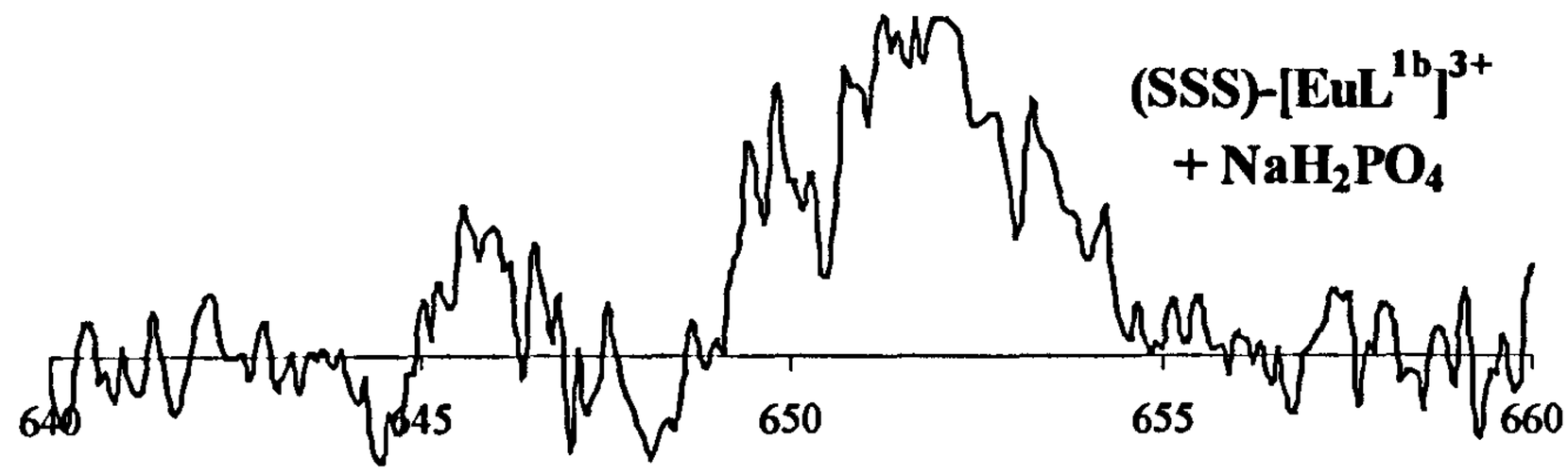

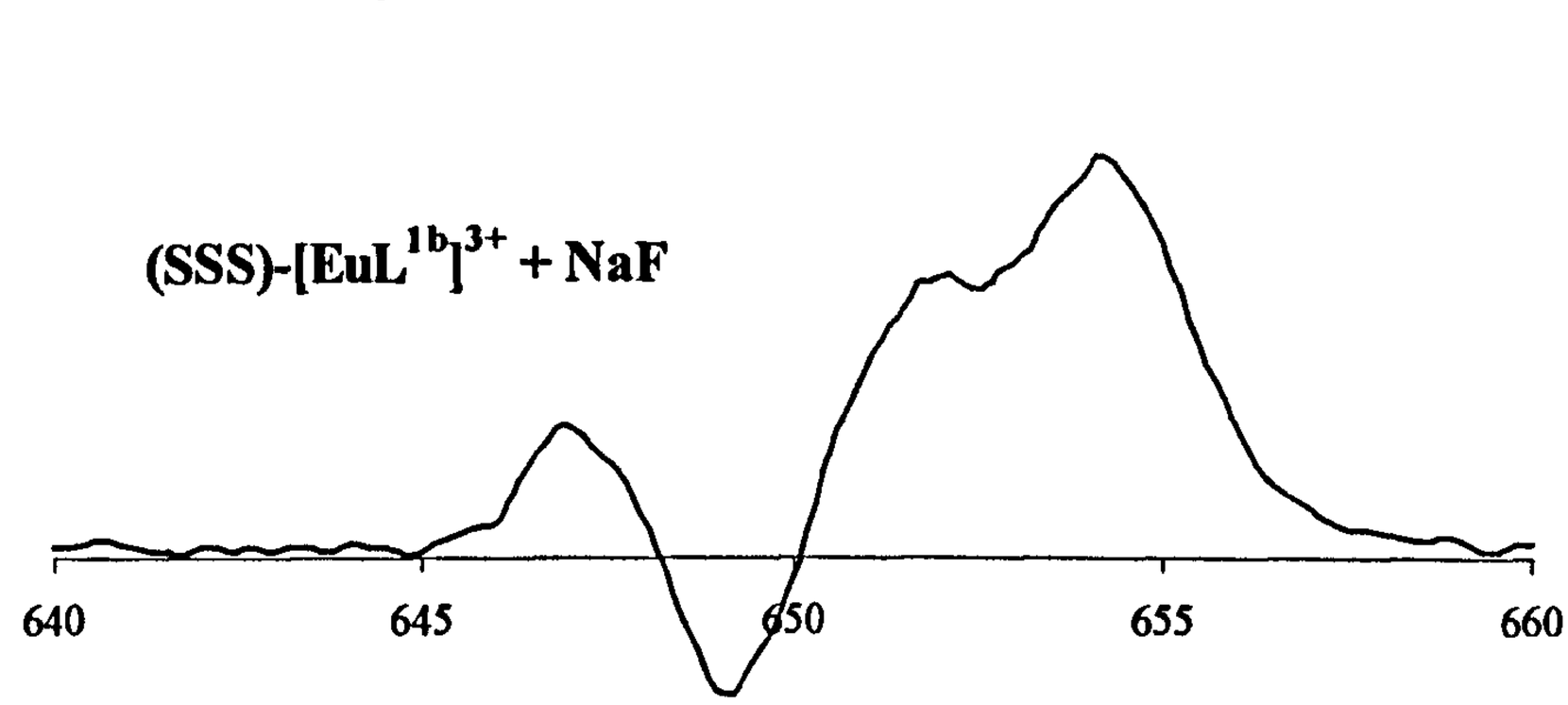

Figure 6.6. CPL profiles of the $[EuL^{1b}]^{3+}$ complex under the $\Delta J=3$ transition in the absence and presence of selected anions.

6.7.4 The ΔJ=4 Transition

The components resolved under the ΔJ=4 transition for the complex in the presence and absence of selected anion are shown in **Figure 6.7.** All profiles show a clear, prominent and negative peak at around 686nm. There are several components which are not well resolved in the spectral region 690 to 710nm but all profiles seem to follow the same general form. The associated dissymmetry factor of the main peak at 686nm was calculated for each profile and the results are tabulated below **Table 6.2.**

Anion	Dissymmetry Factor g_{em} (686nm)
Carbonate	0.05
Phosphate	0.05
Fluoride	0.05

Table 6.2. Calculated dissymmetry factors for the component occurring at 686nm under the ΔJ=4 transition.

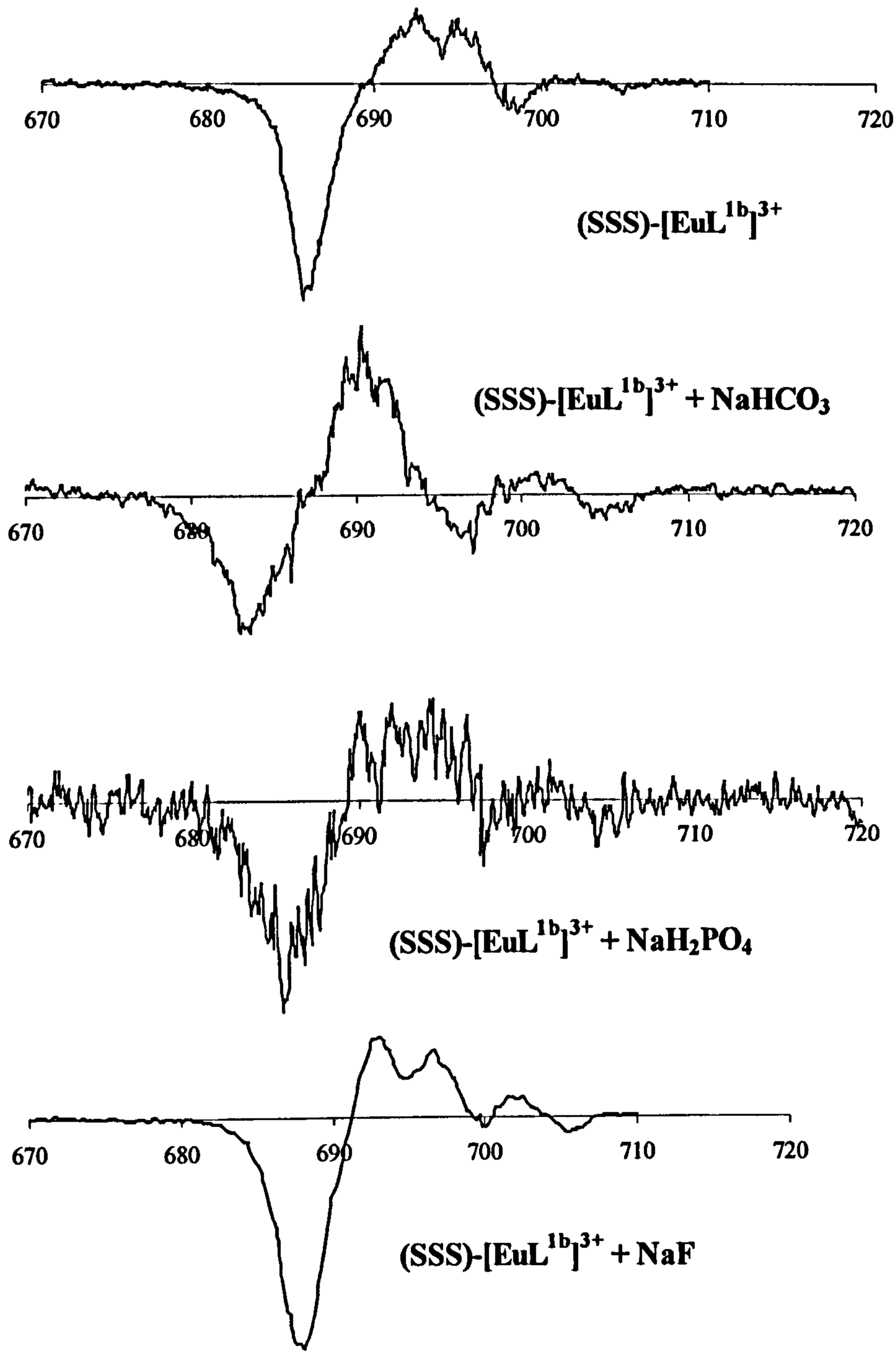

Figure 6.7. CPL profiles of the $[EuL^{1b}]^{3+}$ complex under the $\Delta J=4$ transition in the absence and presence of selected anions.

6.7.5 Summary

Again it is clear that the CPL profile of the $[EuL^{1b}]^{3+}$ diaqua complex changes significantly on exposure to the selected anion . This change in profile, in conjunction with the evaluation of the hydration state of the molecule in the presence of the anions suggest a binding of the anions to the europium centre

The hydration states of the $[EuL^{1b}]^{3+}$ complex in the presence of the selected anions show that one of the two bound water molecules is displaced when the $[EuL^{1b}]^{3+}$ diaqua species is exposed to phosphate ($q \approx 1$) and that both are replaced when exposed to carbonate ($q \approx 0$) suggesting the formation of a four-membered complex-carbonate adduct.

Chapter 7

7.0 Emission Spectra of $[EuL^{1c}]^{4+}$ in the Presence of Selected Anions

7.1 The $[EuL^{1c}]^{4+}$ System in the Presence of Disodium Malonate

The (*SSS*)-enantiomer of the $[EuL^{1c}]^{4+}$ complex was exposed to a ten-fold molar excess of disodium malonate, and the CPL and total emission of the complex were observed at pD6 and 298K with excitation wavelength of 365nm. **Figure 7.1** shows the CPL and total emission of the complex over the full spectral range 570 to 720nm.

7.2 The $[EuL^{1c}]^{4+}$ System in the Presence of Na_2HPO_4

The (*SSS*)-enantiomer of the $[EuL^{1c}]^{4+}$ complex was exposed to a ten-fold molar excess of disodium hydrogen phosphate, and the CPL and total emission of the complex were observed under the same conditions as the previous experiment described above. **Figure 7.2** shows the CPL and total emission of the complex over the full spectral range 570 to 720nm.

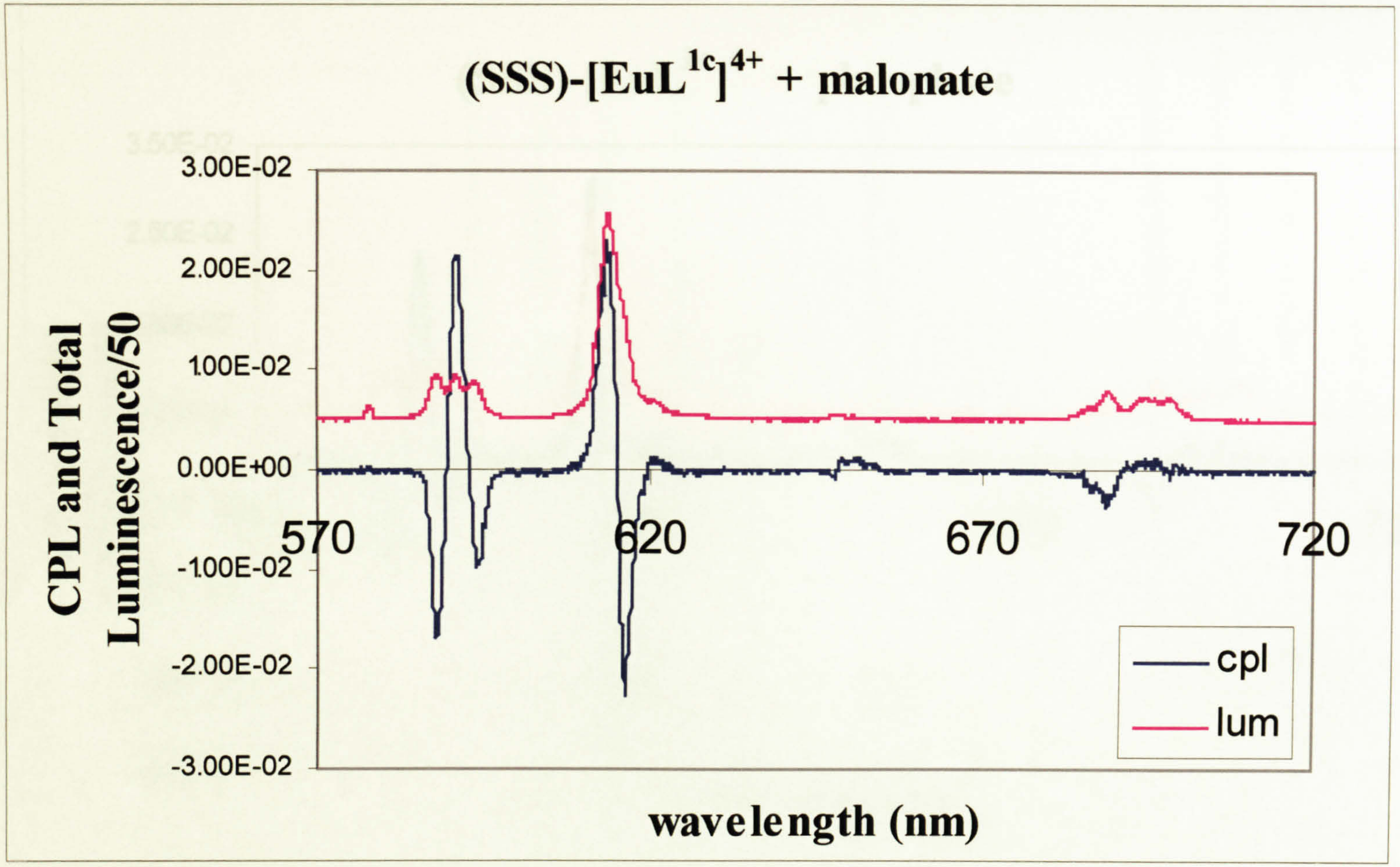

Figure 7.1 *Upper* Total emission of the ΔJ=1,2,3 and 4 transitions of the (SSS)- $[EuL^{1c}]^{4+}$ complex in the presence of $Na_2C_3H_6O_2$ (2.87mM D_2O solution of complex, 28.70mM salt recorded at 295K and at pD6). *Lower* Circularly polarised emission of the ΔJ=1,2,3 and 4 transitions of the (SSS)-$[EuL^{1c}]^{4+}$ complex under the same conditions.

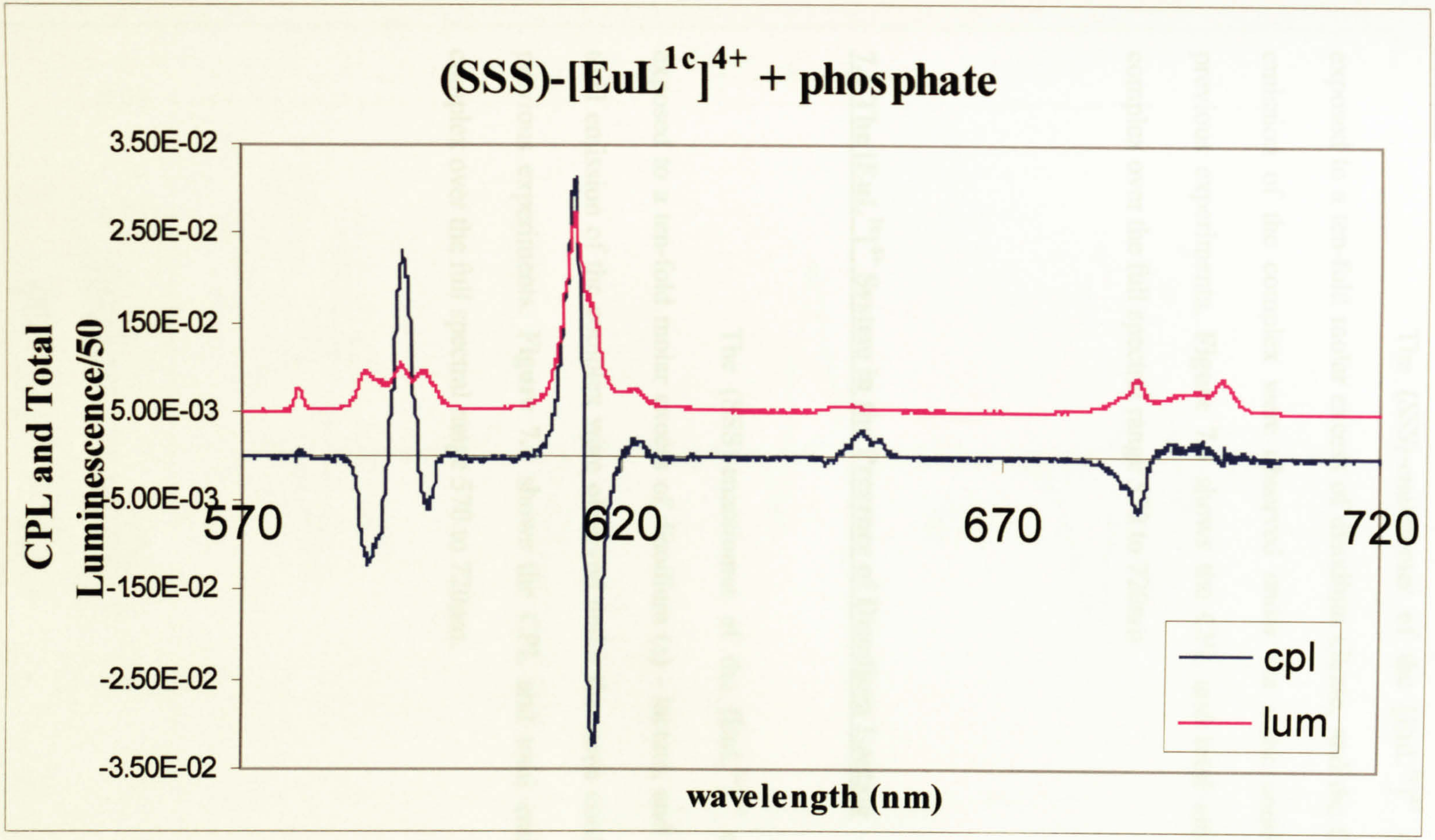

Figure 7.2 *Upper* Total emission of the ΔJ=1,2,3 and 4 transitions of the (SSS)- $[EuL^{1c}]^{4+}$ complex in the presence of Na_2HPO_4 (2.87mM D_2O solution of complex, 28.70mM salt recorded at 295K and at pD6). *Lower* Circularly polarised emission of the ΔJ=1,2,3 and 4 transitions of the (SSS)-$[EuL^{1c}]^{4+}$ complex under the same conditions.

7.3 $[EuL^{1c}]^{4+}$ in the presence of Disodium Citrate

The (*SSS*)-enantiomer of the $[EuL^{1c}]^{4+}$ complex was exposed to a ten-fold molar excess of disodium citrate, and the CPL and total emission of the complex were observed under the same conditions as the previous experiments. **Figure 7.3** shows the CPL and total emission of the complex over the full spectral range 570 to 720nm

7.4 The $[EuL^{1c}]^{4+}$ System in the Presence of Disodium Lactate

The (SSS)-enantiomer of the $[EuL^{1c}]^{4+}$ complex was exposed to a ten-fold molar excess of disodium (s) - lactate, and the CPL and total emission of the complex were observed under the same conditions as the previous experiments. **Figure 7.4** shows the CPL and total emission of the complex over the full spectral range 570 to 720nm.

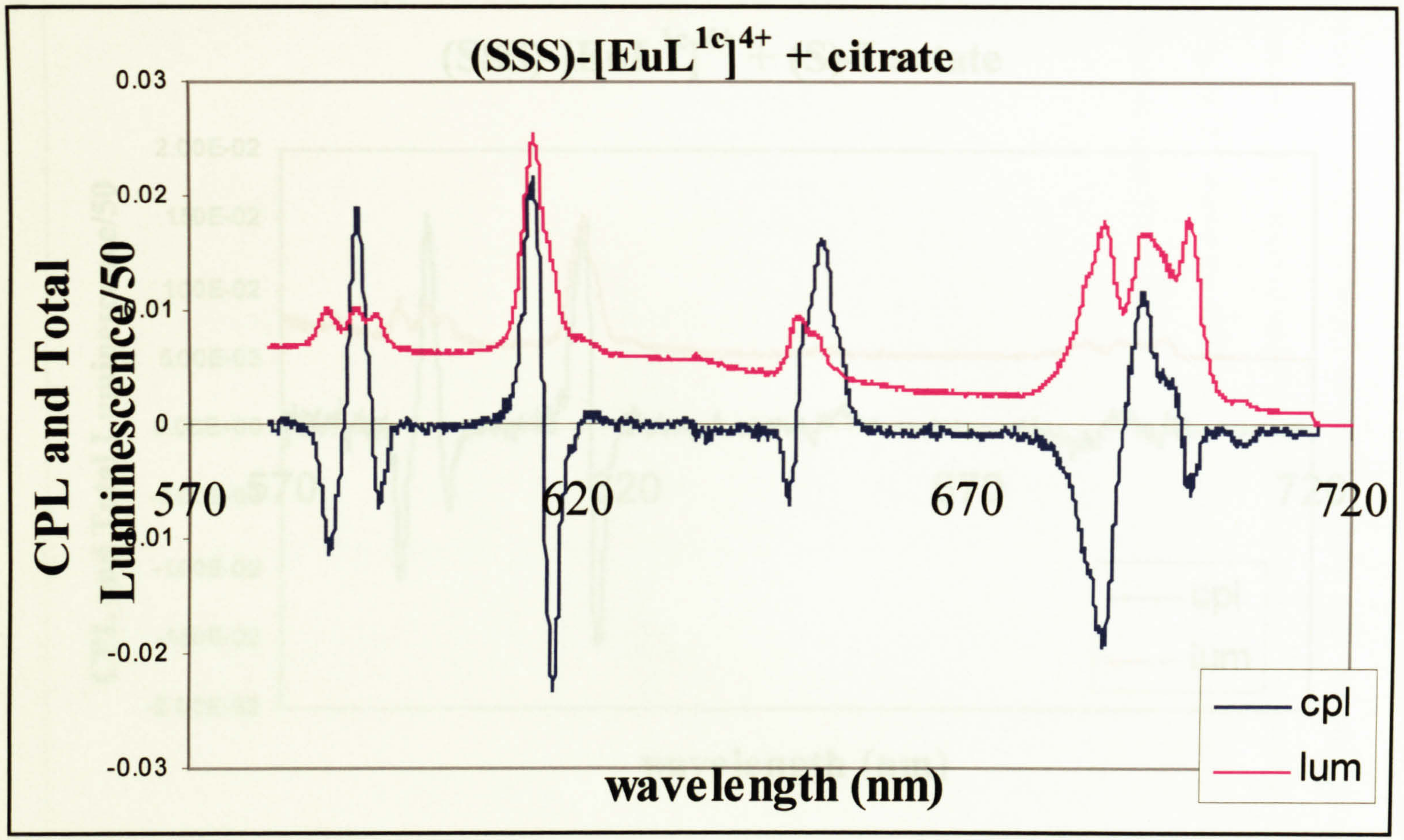

Figure 7.3 *Upper* Total emission of the ΔJ=1,2,3 and 4 transitions of the (SSS)- $[EuL^{1c}]^{4+}$ complex in the presence of Sodium Citrate (2.87mM D_2O solution of complex, 28.70mM salt recorded at 295K and at pD6). *Lower* Circularly polarised emission of the ΔJ=1,2,3 and 4 transitions of the (SSS)-$[EuL^{1c}]^{4+}$ complex under the same conditions.

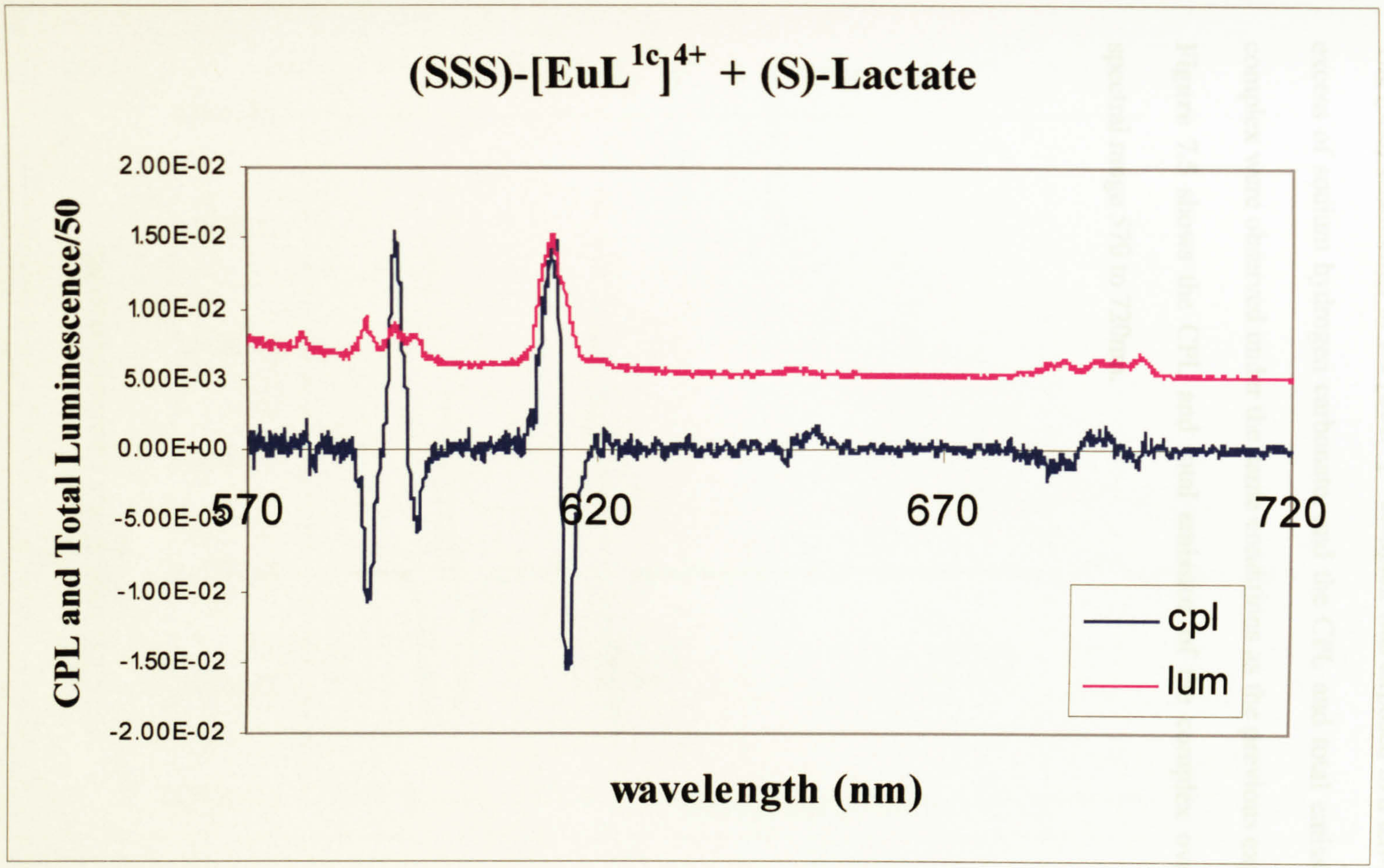

Figure 7.4 *Upper* Total emission of the ΔJ=1,2,3 and 4 transitions of the (SSS)- $[EuL^{1c}]^{4+}$ complex in the presence of disodium (s) - lactate (2.87mM D_2O solution of complex, 28.70mM salt recorded at 295K and at pD6). *Lower* Circularly polarised emission of the ΔJ=1,2,3 and 4 transitions of the (SSS)-$[EuL^{1c}]^{4+}$ complex under the same conditions.

7.5 The $[EuL^{1c}]^{4+}$ System in the Presence of $NaHCO_3$

The (*SSS*)-enantiomer of the $[EuL^{1c}]^{4+}$ complex was exposed to a ten-fold molar excess of sodium hydrogen carbonate, and the CPL and total emission of the complex were observed under the same conditions as the previous experiments. **Figure 7.5** shows the CPL and total emission of the complex over the full spectral range 570 to 720nm.

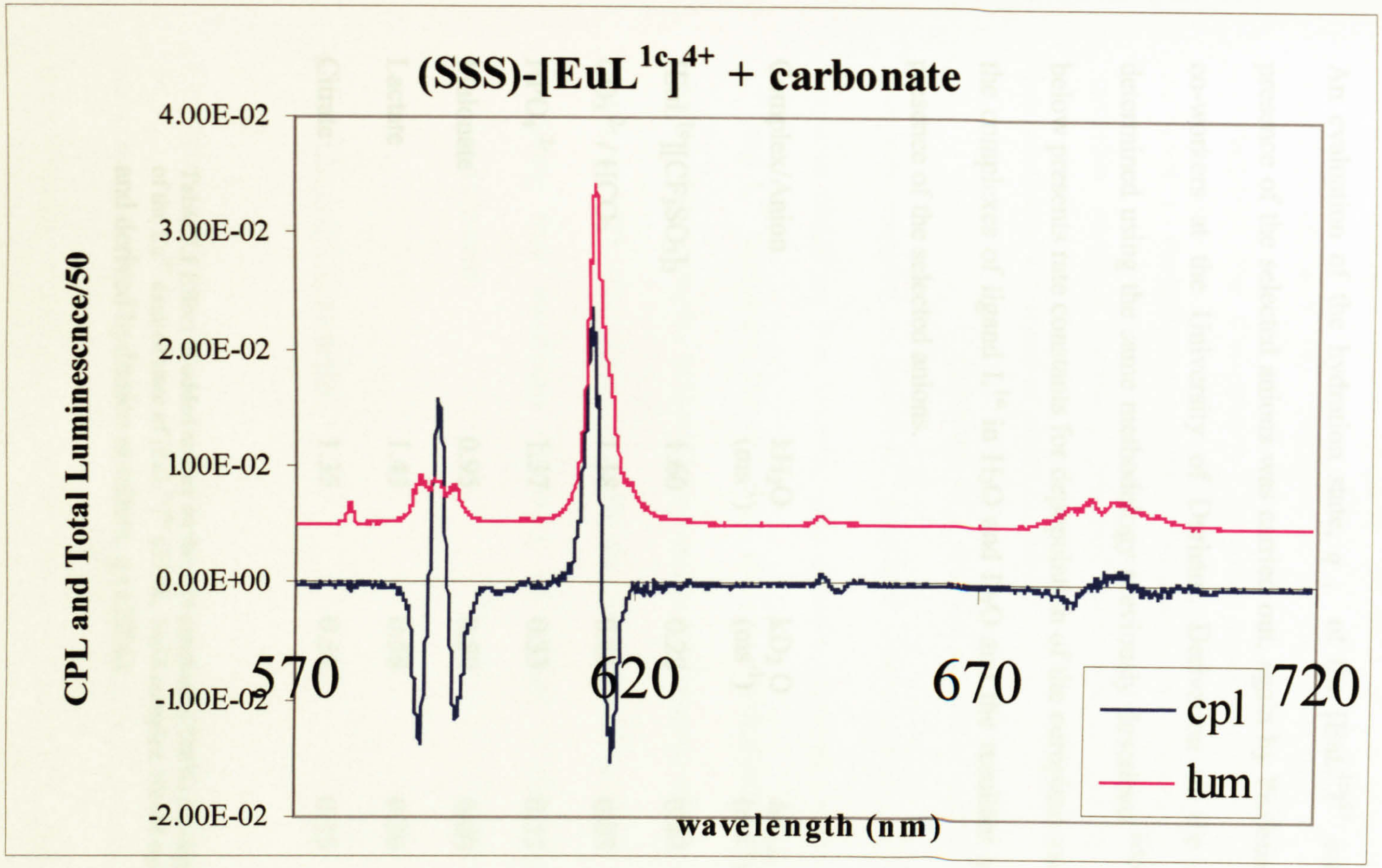

Figure 7.5 *Upper* Total emission of the ΔJ=1,2,3 and 4 transitions of the (SSS)-$[EuL^{1c}]^{4+}$ complex in the presence of $NaHCO_3$ (2.87mM D_2O solution of complex, 28.70mM salt recorded at 295K and at pD6). *Lower* Circularly polarised emission of the ΔJ=1,2,3 and 4 transitions of the (SSS)-$[EuL^{1c}]^{4+}$ complex under the same conditions.

7.6 Hydration States of the $[EuL^{1c}]^{4+}$ Complex

An evaluation of the hydration state, q , of the $[EuL^{1c}]^{4+}$ complex in the presence of the selected anions was carried out, again by Professor Parker and co-workers at the University of Durham. Derivation of the q value was determined using the same methodology previously described [65,8] . **Table 7.1** below presents rate constants for depopulation of the europium excited state for the complexes of ligand L^{1c} in H_2O and D_2O and the resultant q value in the presence of the selected anions.

Complex/Anion	kH_2O (ms^{-1})	kD_2O (ms^{-1})	Δk_{corr} (ms^{-1})	q
$[EuL^{1c}][CF_3SO_3]_3$	1.60	0.28	0.83	1.0
CO_3^{2-} / HCO_3^-	1.18	0.66	0.03	0.0
HPO_4^{2-}	1.37	0.33	0.55	0.7
Malonate	0.95	0.50	0.00	0.0
Lactate	1.43	0.58	0.36	0.4
Citrate	1.35	0.51	0.35	0.4

Table 7.1 Effect of added anions on the rate constants (±10%) for depopulation of the Eu^{3+} excited state of $[EuL^{1c}]^{4+}$ (295K, 1mM complex 10mM anion) and derived hydration numbers, q (±20%).

7.7 Discussion

The presence of the light harvesting phenanthridinium moiety of the ligand L^{1c} allowed population of the emissive $^5D_0$ state of the europium(III) ion by sensitised emission via excitation at 365nm. Excitation of the lanthanide chromophore was also achieved by direct means with excitation at 397nm. Although all the spectra presented in this chapter were obtained using sensitised emission, identical circularly polarised luminescence spectra were obtained irrespective of sensitised or direct excitation.

Exposure of a ten-fold excess of selected anion to the europium complex of ligand L^{1c} produced changes in the circular polarised emission which are less dramatic than changes observed for complexes of the L^{1a} and L^{1b} analogues. Nevertheless, there are noticeable differences in the spectra of the complex in the absence and in the presence of these anions. In all cases, no CPL was observed under the $\Delta J=0$ transition once again. Of the remaining four transitions observed, all carried a measurable circularly polarised element.

7.7.1 The $\Delta J=1$ Transition

On exposure to a ten–fold excess of malonate, phosphate, citrate, lactate and carbonate, the $\Delta J=1$ transition of the complex is split into three components (as is the complex without any substrate). This is illustrated by **Figure 7.6,** where all profiles are drawn to the same scale and spectral range (x-axis) and the y-axis indicates CPL (arbitrary units).

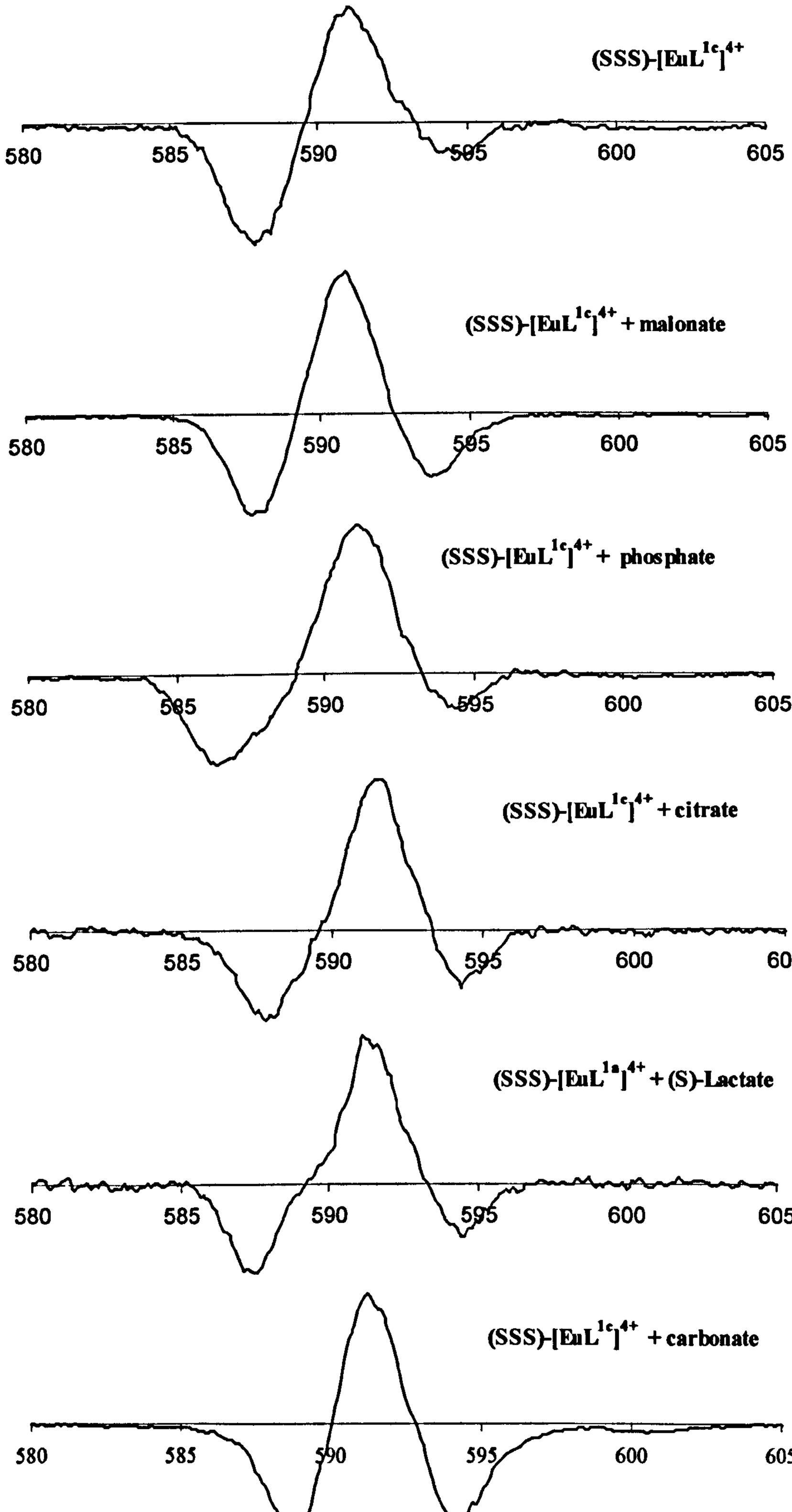

Figure 7.6 CPL profiles under the ΔJ=1 transition of the (SSS)-$[EuL^{1c}]^{4+}$ complex in the absence and presence of selected anions

The splitting of the transition follows a (- , + , -) sequence for the (SSS)-enantiomer. As is shown, the circularly polarised components change on introduction of an anion. In some cases the position of the component peak is shifted, and there is a change in intensity of all components. This change in intensity can be quantified by measuring the ratio of the positive component around 592nm to the first negative component occurring at roughly 588nm.

In the absence of any substrate, the ratio of the peaks, I_{592nm} / I_{588nm} (cpl) is 0.67. The ratio obtained for the complex in the presence of the selected anions is tabulated below **Table 7.2.**

Anion	Intensity Ratio (I_{592nm} / I_{588nm} (cpl))
Malonate	1.40
Phosphate	1.69
Citrate	1.69
Lactate	1.69
Carbonate	1.19

Table 7.2. Intensity ratio of the CPL peaks found at 592 and 588nm

The ratio of the peaks is consistent for phosphate, citrate and lactate, but is markedly different for the complex in the presence of malonate and particularly carbonate. A similar treatment of the peaks at 592 and 594nm was carried out. The intensity ratio I_{592nm} / I_{594nm} (cpl) in the absence of any substrate is 2.4. The ratio obtained for the complex in the presence of the selected anions is tabulated below **Table 7.3.**

The splitting of the transition follows a (- , + , -) sequence for the (SSS)-enantiomer. As is shown, the circularly polarised components change on introduction of an anion. In some cases the position of the component peak is shifted, and there is a change in intensity of all components. This change in intensity can be quantified by measuring the ratio of the positive component around 592nm to the first negative component occurring at roughly 588nm.

In the absence of any substrate, the ratio of the peaks, I_{592nm} / I_{588nm} (cpl) is 0.67. The ratio obtained for the complex in the presence of the selected anions is tabulated below **Table 7.2.**

Anion	Intensity Ratio (I_{592nm} / I_{588nm} (cpl))
Malonate	1.40
Phosphate	1.69
Citrate	1.69
Lactate	1.69
Carbonate	1.19

Table 7.2. Intensity ratio of the CPL peaks found at 592 and 588nm

The ratio of the peaks is consistent for phosphate, citrate and lactate, but is markedly different for the complex in the presence of malonate and particularly carbonate. A similar treatment of the peaks at 592 and 594nm was carried out. The intensity ratio I_{592nm} / I_{594nm} (cpl) in the absence of any substrate is 2.4. The ratio obtained for the complex in the presence of the selected anions is tabulated below **Table 7.3.**

7.7.2 The ΔJ=2 Transition

The change in the CPL profile of the complex when exposed to carbonate is again evident when we look at the ΔJ=2 transition of the (*SSS*)- enantiomer. **Figure 7.7** shows the CPL profiles of the ΔJ=2 transitions of the L^{1c} complex with no substrate and in the presence of the selected anions.

With the exception of carbonate, the components follow a (+ , - , +) pattern. The initial positive component is strong in all cases and occurs at 613nm in the absence of an anion and in the presence of malonate. The same component occurs at 614nm in the presence of all other anions. The negative component is again strong in all cases and occurs in the range 616 to 618nm. The second positive component (620 to 622nm) is much weaker and is harder to discern in the cases of citrate and lactate, although the signal appears to be real. The ratio of the two strong CPL components is consistent for all spectra.

This consistency is also exhibited in the measured dissymmetry factors of the components (with the exception of a stronger signal at 617 and 621nm for lactate) **Table 7.5.** The values are also stronger than the measured values for the complex in the absence of any anion.

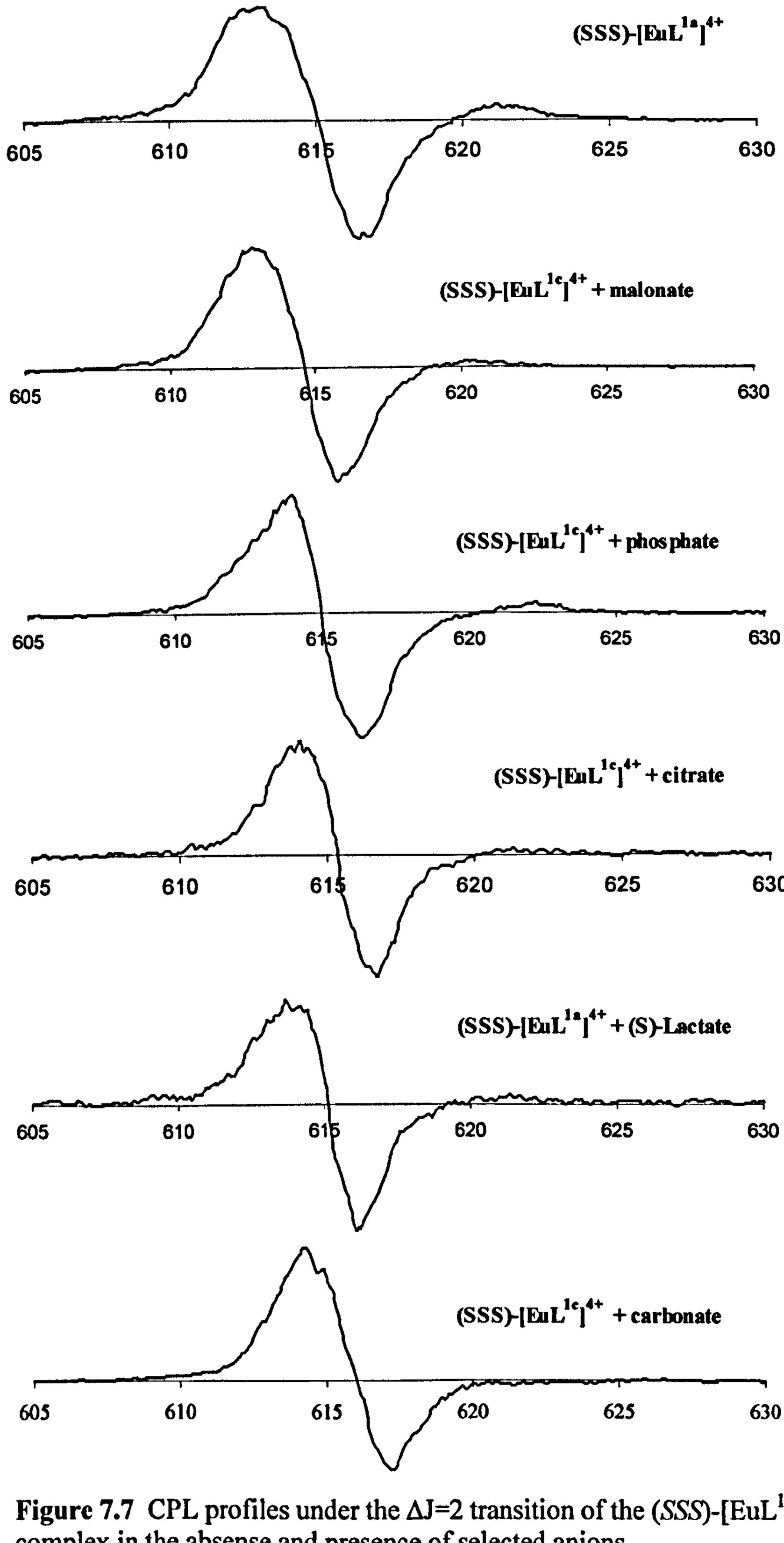

Figure 7.7 CPL profiles under the ΔJ=2 transition of the (*SSS*)-$[EuL^{1c}]^{4+}$ complex in the absense and presence of selected anions

Anion	Dissymmetry Factor		
	614nm	617nm	621nm
Malonate	+0.04	-0.09	+0.02
Phosphate	+0.06	-0.11	+0.02
Citrate	+0.05	-0.12	+0.04
Lactate	+0.06	-0.17	+0.08
Carbonate	+0.03	-0.05	

Table 7.5. Measured dissymmetry factors for components under the $\Delta J=2$ transition.

7.7.3 The $\Delta J=3$ Transition

The $\Delta J=3$ transition also highlights the effect that carbonate has on the L^{1c} system. The resultant CPL profile of the complex under this transition is unique for each anion as shown in (**Figure 7.8**).

With the exception of the carbonate spectrum, there is one negative component around 647nm and there appears to be at least three positive components under the $\Delta J=3$ transition in the range 648 to 655nm giving a (- , + , + , +) sequence. These components, however, are not well defined in the presence of the anions; there appears to be a central circularly polarised component around 652nm which is flanked by two components of lesser intensity (indicated by two shoulders at 648 and 653nm). In the absence

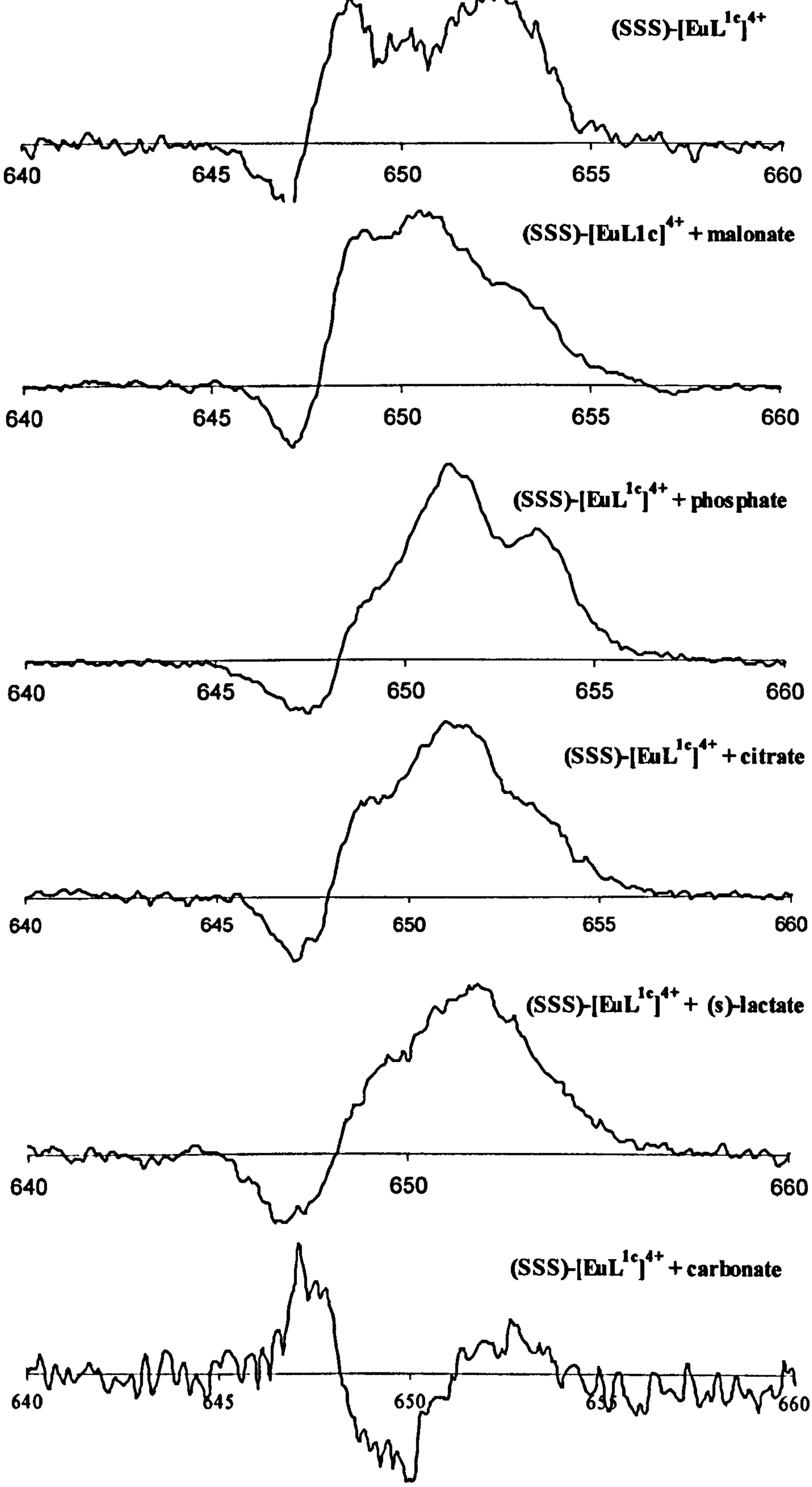

Figure 7.8 CPL profiles under the ΔJ=3 transition of the (*SSS*)-$[EuL^{1c}]^{4+}$ complex in the absense and presence of selected anions

of any anion, the components at 648 and 653nm are more intense than the central components at 650nm.

The carbonate spectrum, although particularly noisy, appears to be resolved into three components following a (+ , - , +) pattern which is distinct from all others.

Calculated dissymmetry factors for the central peak at around 650nm again showed that the signal was stronger in the presence of a substrate.

7.7.4 The ΔJ=4 Transition

The CPL profile of the complex under the ΔJ=4 transition in the presence of carbonate is the most well defined of all profiles obtained. A comparison of the profiles in the absence and in the presence of the selected anions is shown by **Figure 7.9**. The carbonate spectrum shows what appears to be two negative components in the range 680 to 690nm, two positive components (690 to 697nm) with two further negative components at 699 and 707nm and a positive components at 702nm. The components follow a (- , - , + , + , - , + , -) sequence. The profile of the transition in the absence and in the presence of the other anions follow this same sequence although the position of the CPL peaks change slightly. This similarity is also reflected in the measured dissymmetry factors for the prominent peak at around 687nm.

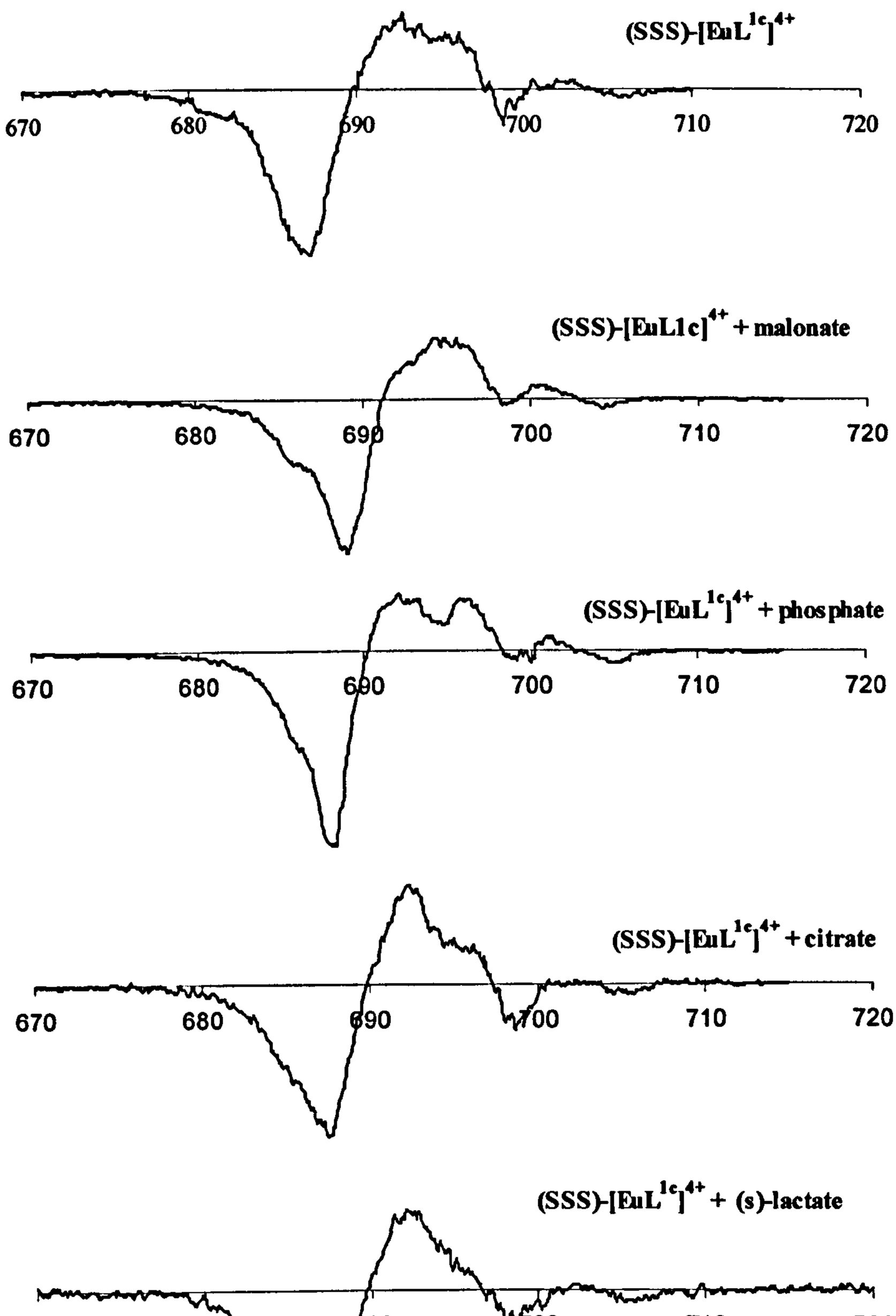

Figure 7.9 CPL profiles under the ΔJ=4 transition of the (*SSS*)-$[EuL^{1c}]^{4+}$ complex in the absense and presence of selected anions

7.7.5 Chapter 7 - Summary

In summary, it can be said that the change in the CPL profile of the L^{1c} system induced by the introduction of an anion substrate is most pronounced in the case of carbonate. This is shown by an analysis of all transitions observed which carry a measurable circularly polarised component. Although the change in the CPL profile on the interaction of the other anions is less pronounced, it is nonetheless a real and measurable interaction.

The evaluation of the hydration state for the L^{1c} complex in the presence of the anions is consistent with the data obtained for the L^{1a} and L^{1b} analogues suggesting the formation of the analogous complex-anion adducts.

Chapter 8

8. Binding Studies Europium(III) Complexes with Bicarbonate

As discussed in the preceding results chapters, exposure of the selected anions to the europium complexes of the ligands L^{1a} L^{1b} and L^{1c} changed, in many cases dramatically, the nature of the circularly polarised emission of the europium complex. Throughout the preceding discussions, however, it was the change in the behaviour of the europium systems on exposure to sodium bicarbonate that was most noteworthy.

Carbon Dioxide is of vital importance in the chemistry of biological processes [66] and has been much studied [67] . When carbon dioxide dissolves in water, it forms a weak acid, carbonic acid although only a small amount is formed. Depending on pH, the four forms present in aqueous solution are H_2CO_3 , CO_2 HCO_3^- and CO_3^{3-} . At physiological pH the major form present is bicarbonate.

The change in the conventional luminescence spectra of these complexes on exposure to bicarbonate was first noted after luminescence experiments were conducted (primarily on the europium L^{1a} system) at the University of Durham. It was noticed that exposure of a molar excess of bicarbonate to the L^{1a} system produced roughly a three-fold increase in the intensity of the hypersensitive $\Delta J=2$ transition. After an analysis of the hydration state of the complex reported a q value equal to zero, it was proposed that bicarbonate/carbonate had displaced the two bound water molecules of the europium L^{1a} system to form a complex-carbonate adduct.

Further experiments were conducted which involved the monitoring of the intensity of the ΔJ=2 transition as a function of added sodium bicarbonate. This was done at pH 7.4 in aqueous media using a 0.1M collidine/HCl buffer solution. The resulting plot produced in effect a binding curve which was used to calculate the affinity of the europium complex for bicarbonate resulting in a binding constant of 400±50 Ms^{-1} . This plot is shown in below **Figure 8.1.**

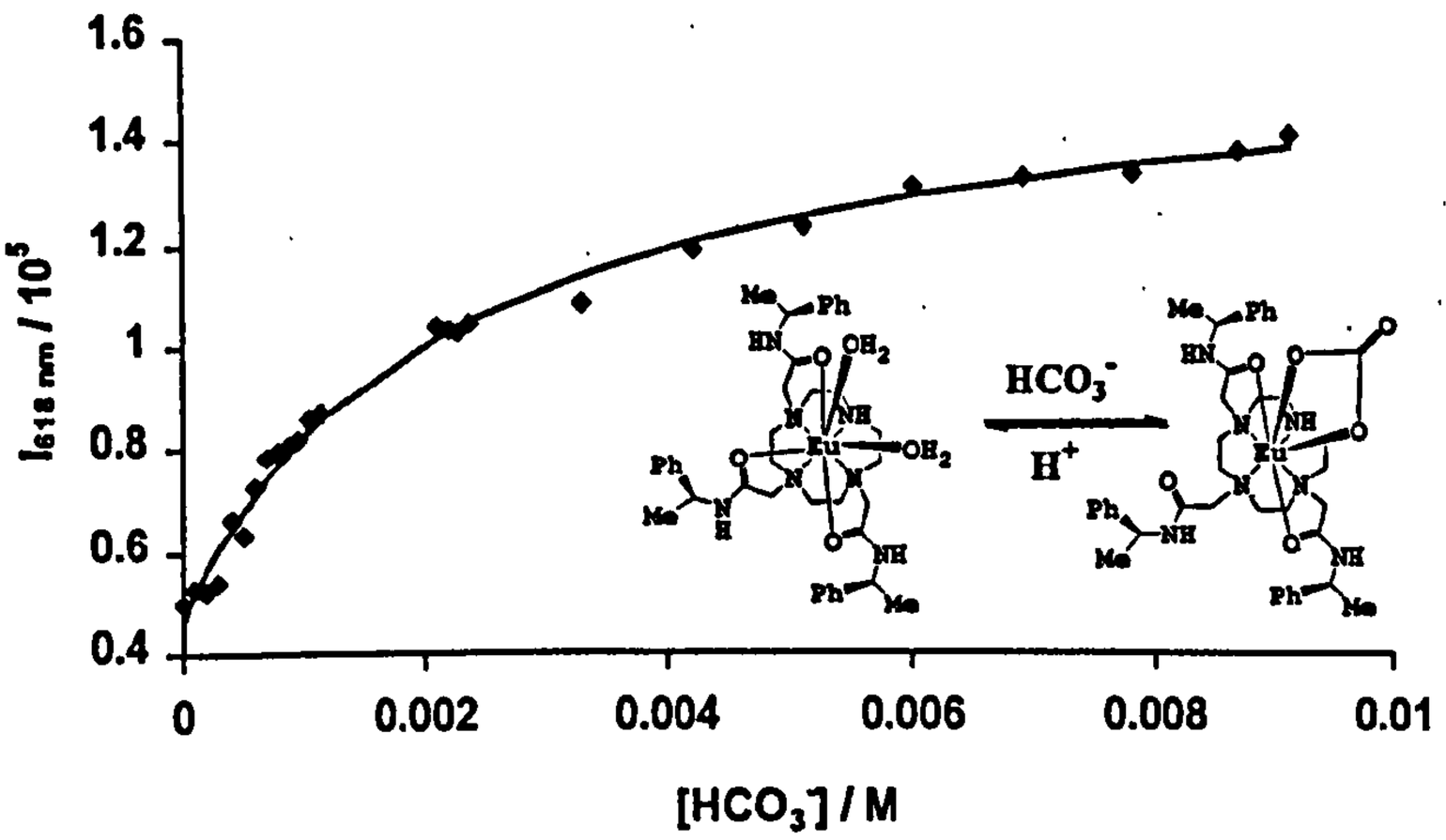

Figure 8.1. Variation of the europium emission intensity (618nm) of the $[EuL^{1a}]^{3+}$ complex as a function of added bicarbonate (1mM complex, pH 7.4, 0.1M collidine/HCl buffer solution). (Data recorded by Professor Parker and co-workers at the University of Durham).

With the experiment discussed above in mind, an analogous experiment was designed to monitor the *polarisation* of the emission of the europium L^{1a} complex as a function of added sodium bicarbonate.

8.1 Binding of Bicarbonate Titration to the $[EuL^{1a}]^{3+}$ System

As is shown in **Figure 8.1**, the intensity of the $\Delta J=2$ peak increases on addition of sodium bicarbonate. Addition also has the effect of decreasing the intensity of the CPL signals under the $\Delta J=1$ and 2 transitions by a factor of roughly two. It was this feature that was exploited to produce a plot polarisation against added bicarbonate.

The polarisation value was calculated in an analogous manner to the calculation of the dissymmetry factors and can be thought of as a pseudo-dissymmetry factor. In the context of this experiment, and considering **Figure 8.2** (a pictorial representation of the observed emission spectra), polarisation is defined as the sum of the two component peaks under the $\Delta J=1$ transition (*ie* a + c) divided by the total luminescence of the same transition (*ie* c x 50) shown by **Equation 8.1.**

$$Polarisation = \frac{a+c}{b\times 50} \qquad \textbf{Equation 8.1}$$

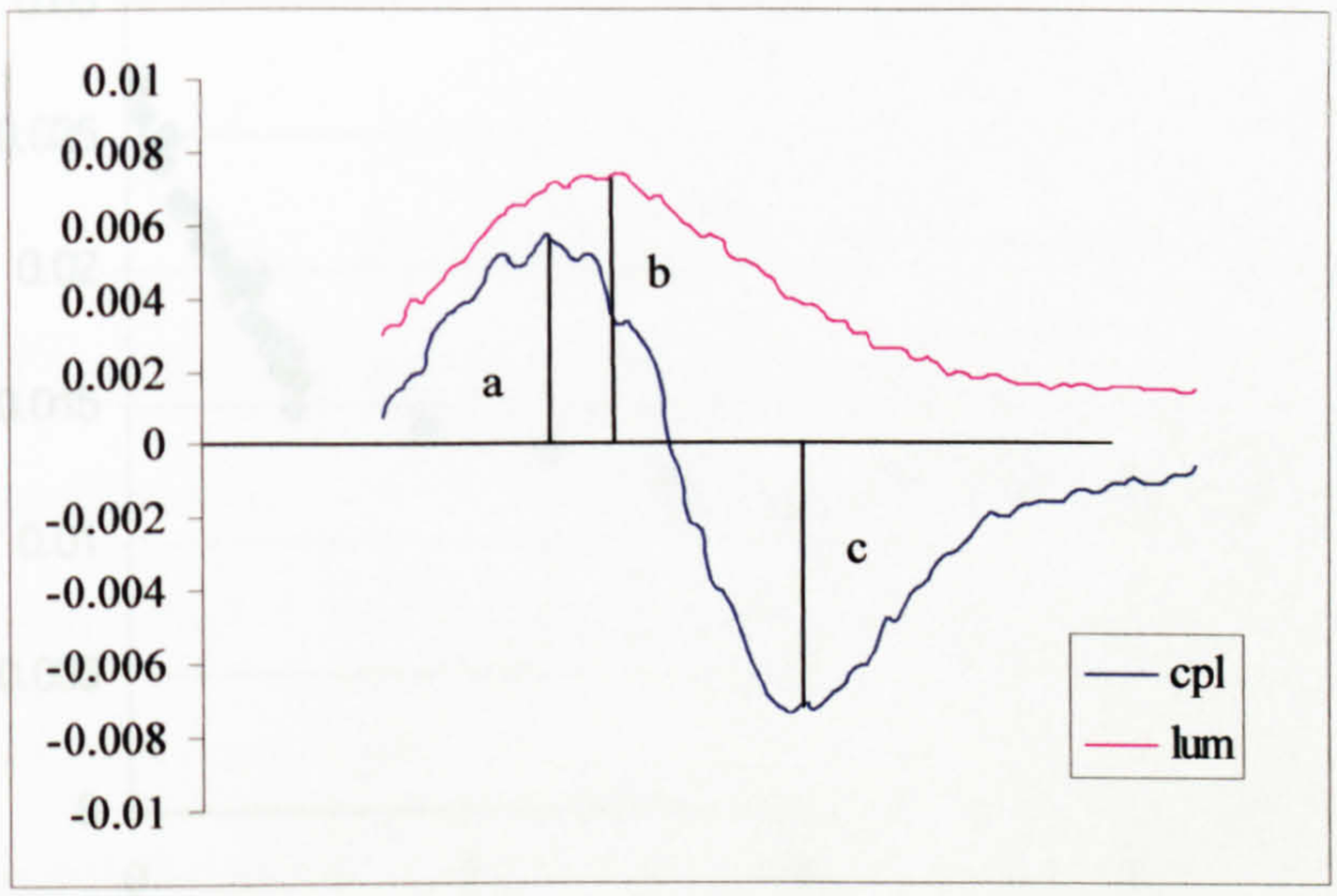

Figure 8.2. Pictorial representation of the observed emission spectra of the ΔJ=1 transition of the (*SSS*)- $[EuL^{1a}]^{3+}$complex.Labels a,b and c depict the measurements taken to calculate a pseudo-dissymmetry factor.

The CPL profile was of the complex was recorded in the absence of sodium bicarbonate and after every 10μL addition of a previously prepared sodium bicarbonate solution (as described in the experimental section).

An analysis of the CPL and luminescence signals recorded was then carried out as described above to give the plot of polarisation (arbitrary units) as a function of added bicarbonate **Figure 8.3.**

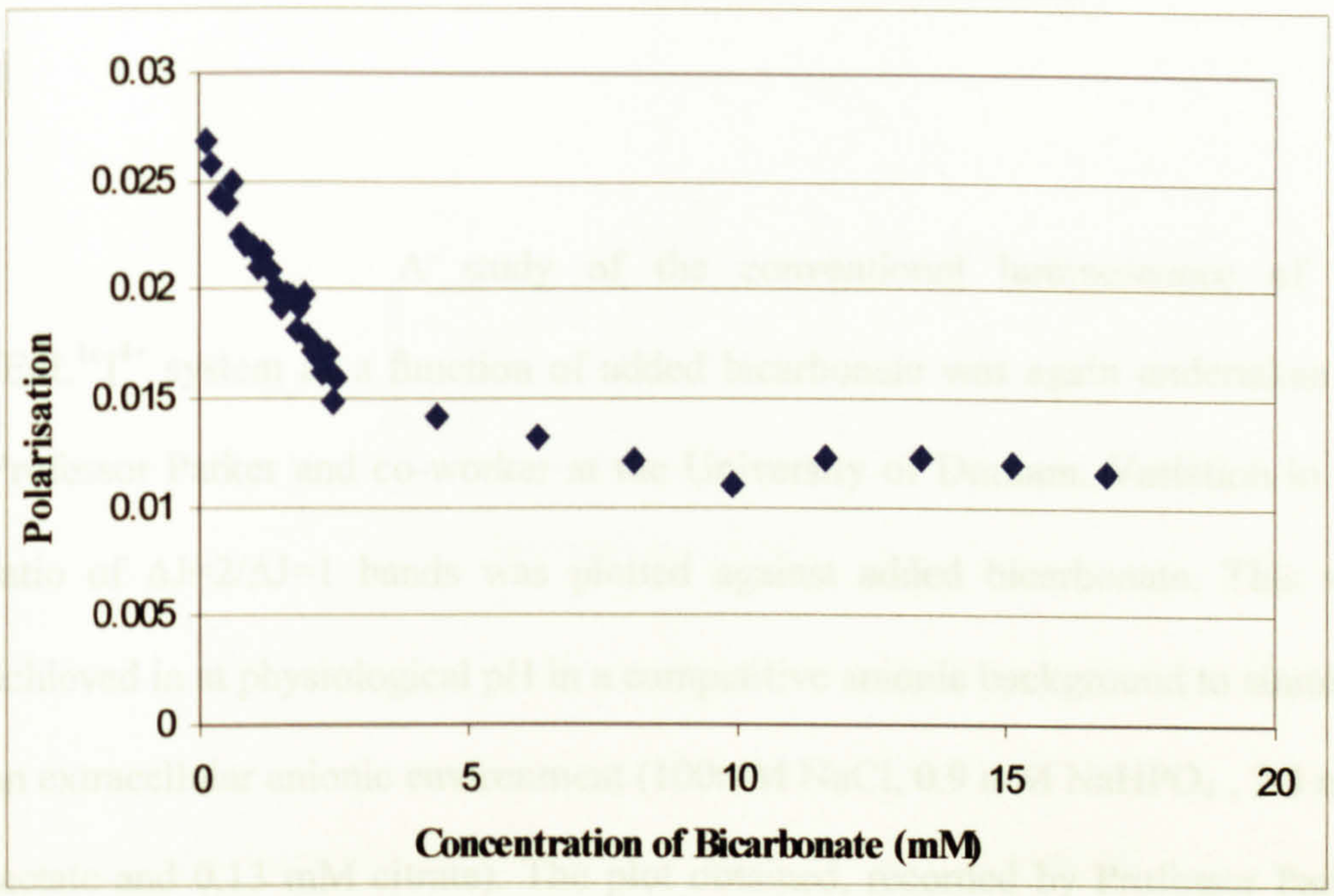

Figure 8.3. Polarisation of the ΔJ=1 transition of the (SSS)- $[EuL^{1a}]^{3+}$ complex as a function of added sodium bicarbonate. (2.5mM complex, 0.1M collidine/HCl buffer pH7.4)

As was expected, the plot of polarisation as a function of added bicarbonate (**Figure 8.3**) reflects the plot of luminescence intensity under the same conditions (**Figure 8.1**), the turning point of the plot confirming a 1:1 binding stoichiometry for complex:carbonate.

8.2 Binding of Bicarbonate Titration to the $[EuL^{1c}]^{4+}$ System

A study of the conventional luminescence of the $[EuL^{1c}]^{4+}$ system as a function of added bicarbonate was again undertaken by Professor Parker and co-worker at the University of Durham. Variation in the ratio of $\Delta J=2/\Delta J=1$ bands was plotted against added bicarbonate. This was achieved in at physiological pH in a competitive anionic background to simulate an extracellular anionic environment (100mM NaCl, 0.9 mM $NaHPO_4$, 2.3 mM lactate and 0.13 mM citrate). The plot obtained, recorded by Professor Parker and co-worker at the University of Durham is described by **Figure 8.4.**

An analogous experiment to measure polarisation of emission of the $[EuL^{1c}]^{4+}$ system as a function of added bicarbonate was carried out at the University of Glasgow. In the context of this experiment, polarisation is defined as the dissymmetry factor, g_{em}, of the resolved component occurring at 614nm under the $\Delta J=1$ transition. The experiment was carried out in the same competitive anionic background as used in the analogous conventional luminescence study and similarly at pH 7.4. The resultant plot is shown below **Figure 8.5.**

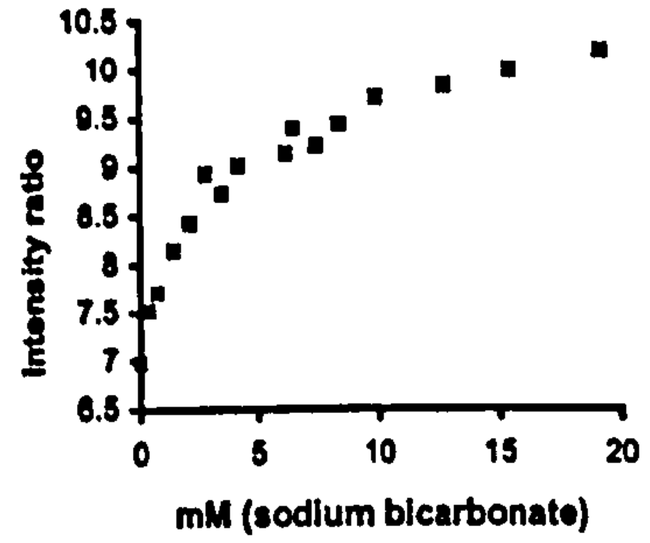

Figure 8.4. Variation in the ratio of the $\Delta J=2/\Delta J=1$ bands for the $[EuL^{1c}]^{4+}$ system as a function of added bicarbonate (1.5mM complex, 0.1M collidine/HCl buffer, pH7.4, 100mM NaCl, 0.9 mM $NaHPO_4$, 2.3 mM lactate and 0.13 mM citrate). (Data recorded by Prof.Parker and co-workers at the University of Durham).

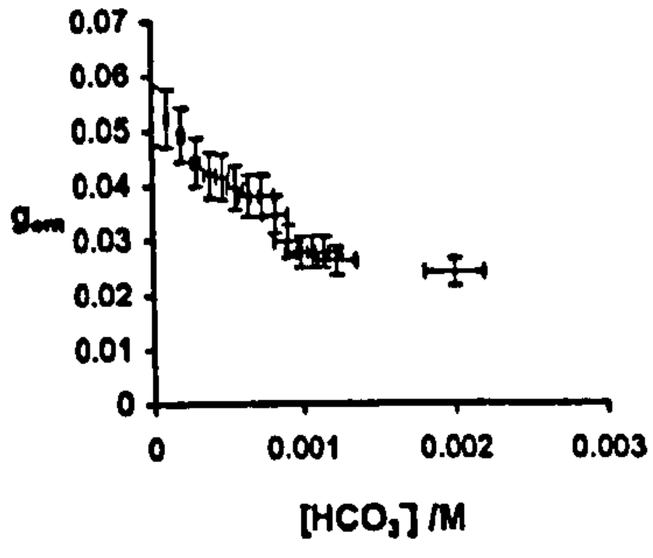

Figure 8.5. Variation in emission polarisation (g_{em}) for the $\Delta J=1$ transition of the $[EuL^{1c}]^{4+}$ system as a function of added bicarbonate (1.0mM complex, pH7.4, 100mM NaCl, 0.9 mM $NaHPO_4$, 2.3 mM lactate and 0.13 mM citrate). (Data recorded at the University of Glasgow).

8.3 Chapter 8 Discussion

As shown above, the binding of the bicarbonate/carbonate substrate to complexes of europium(III) has been successfully monitored by following the change in the polarisation of the observed emission. Furthermore, this has been achieved, in the case of the $[EuL^{1c}]^{4+}$ system, in a competitive anionic background. It is the $[EuL^{1a}]^{+}$ system, however, that provides most scope for discussion.

Various ^{1}H NMR experiments carried out on the $[EuL^{1a}]^{+}$ system as its triflate salt (*ie* a diaqua species) and with bound carbonate revealed very different spectra [8] . Proton shifts of the diaqua species closely resembled the shifts observed for a monocapped square antiprismatic cyclen complex whereas the spectra of the carbonate bound species exhibited characteristics of a twisted square antiprismatic arrangement [39] . A mechanism for the formation of the L^{1a} complex-carbonate adduct is proposed in **Figure 8.6.**

This data would suggest that bicarbonate/carbonate chelation has changed the helicity of the coordinating ligand about the metal ion. The degree of twist about the principle axis given by the twist angle, θ, is equal approximately to 40° in the square antiprismatic and approximately 29° in the twisted square antiprismatic structure. **Figure 8.7.**

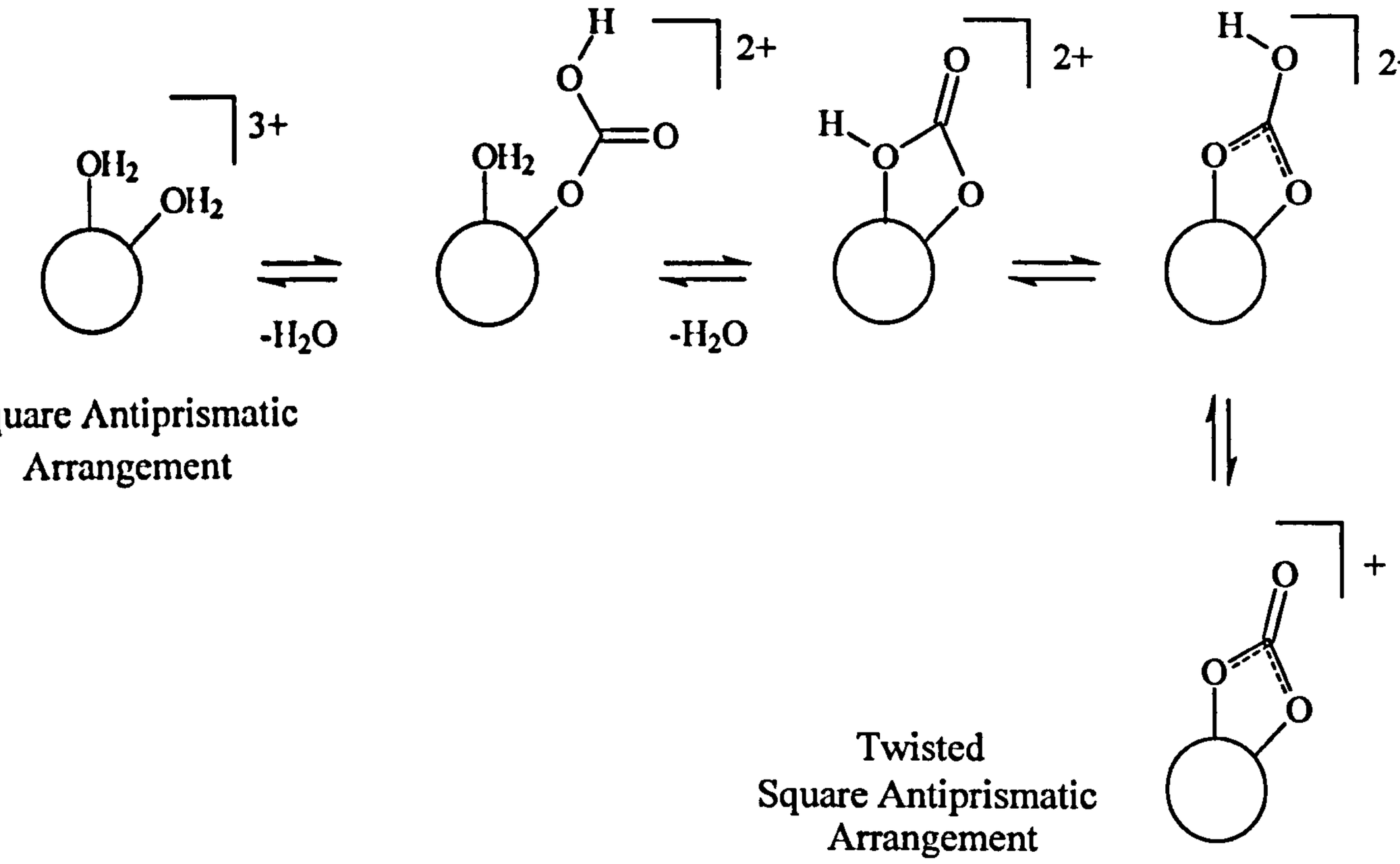

Figure 8.6. Proposed mechanism for the binding mode of bicarbonate/ carbonate.

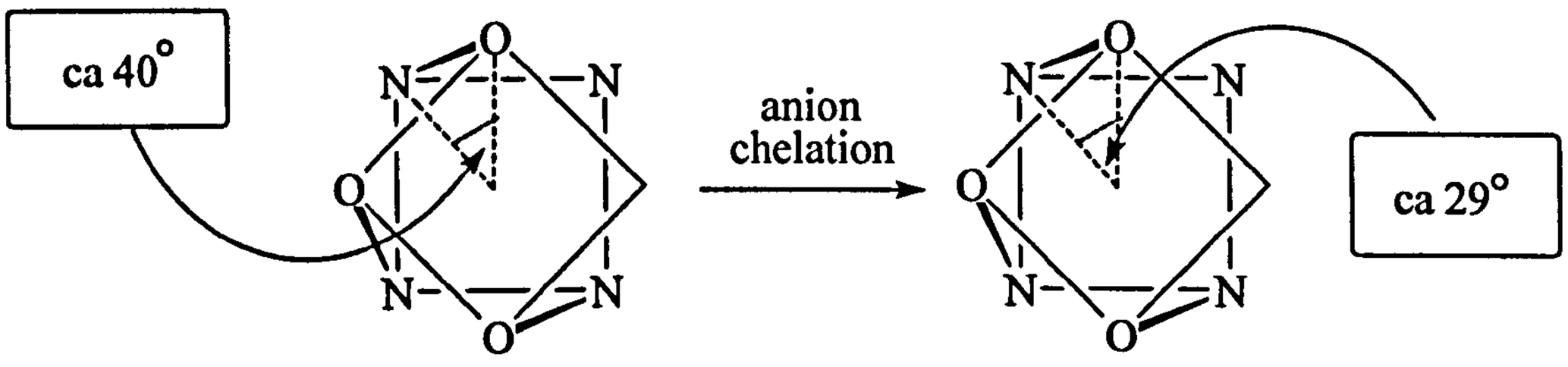

Figure 8.7. Representation of the differing twist angles in square antiprismatic and twisted square antiprismatic confirmations.

At first glance this change in twist from a higher (40°) to lower (29°) value would explain the observed reduction in the CPL intensity and dissymmetry factors. One would expect the change in twist would inherently produce a change in the observed CPL since the twist angle determines the angle between the magnetic and electric dipole transition moment vectors and hence the rotary strengths of the transitions in complexes of this kind. Theory would suggest, however, that there should be an *increase* in the CPL intensity as opposed to the measured decrease.

Reproducing **Equation 1.7** from the introduction section, the rotary strength, a measure of the sign and magnitude of the of a transition is given by

$$R_{ab} = \mid P_{ab} \parallel M_{ba} \mid \cos\tau_{ab} \qquad (1.7)$$

R_{ab} is equal to zero therefore when $\tau_{ab} = 90°$. This condition is met when the degree of twist about the priciple axis, θ, is 0° or 90° (ie when the planes are eclipsed) or 45°. **Figure 8.8.**

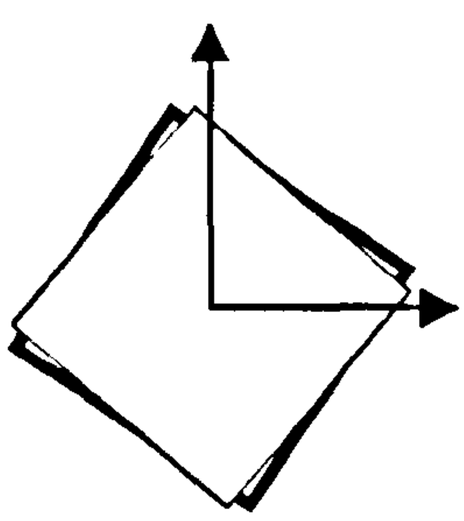

Square prism: twist = 0° or 90°

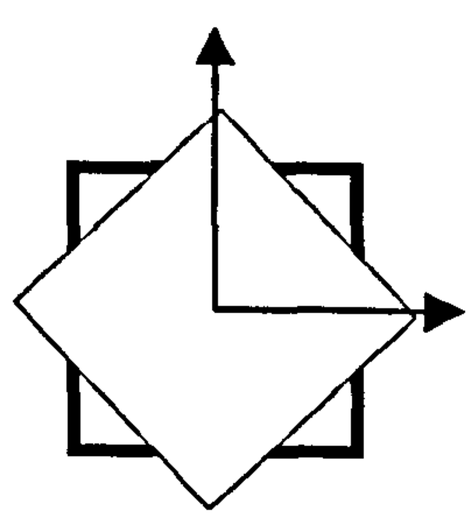

Square prism: twist = 45°

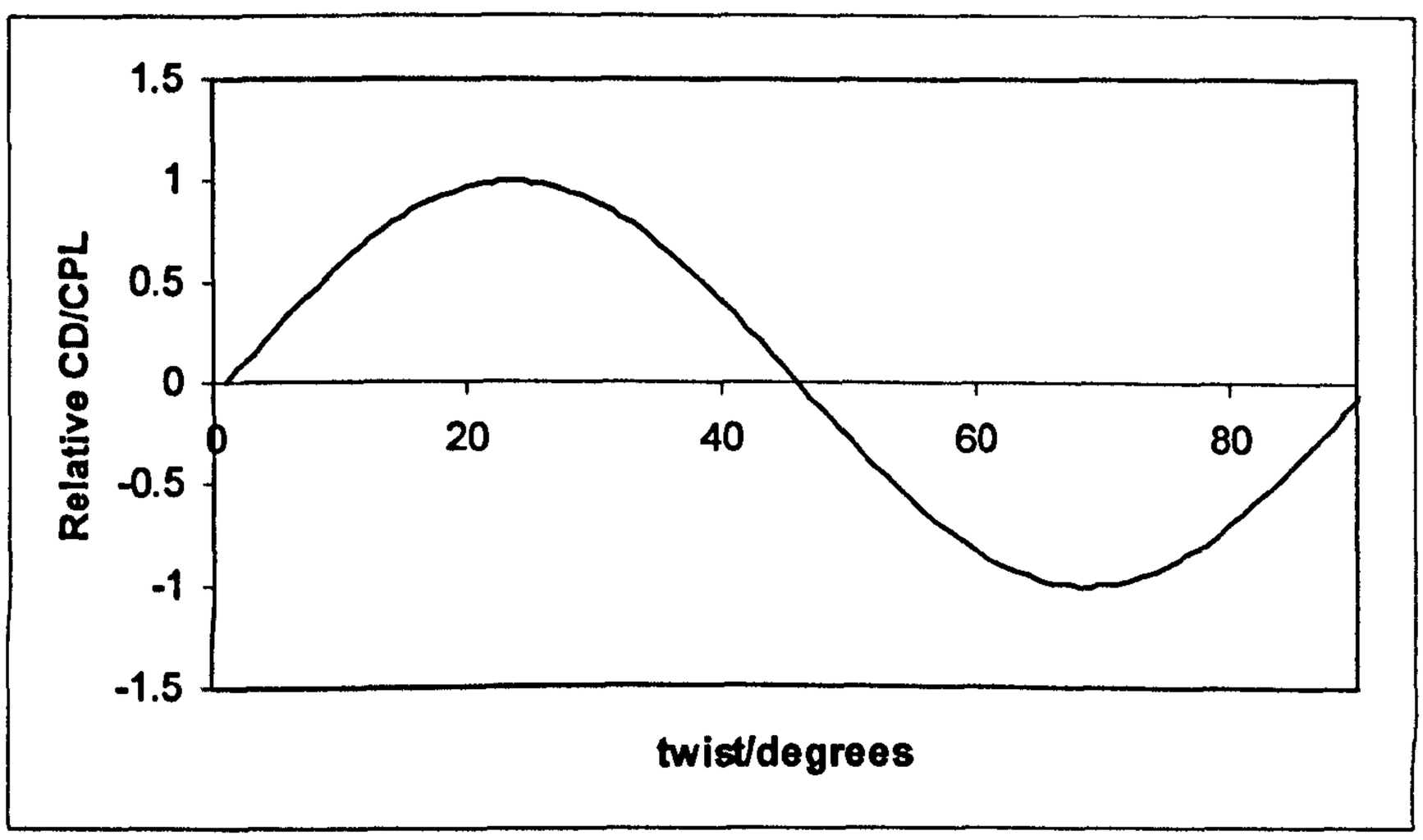

Figure 8.8. Correlation of the effect of twist angle in symmetric antiprismatic lanthanide complexes on their CPL or CD intensity.

The relative CPL is therefore defined by a sin2θcos2θ (or sin 40) function and a maximum CPL signal should be observed when 0=±22.5°. For a twist angle θ = 29° (twisted square antiprismatic structure) we would therefore expect a larger CPL signal than for the case when θ = 40° (square antiprismatic) since this angle is closer to the optimal angle of 0=±22.5°.

Clearly, this is an area which requires further investigation. Although the triaamide complex shows characteristics of a square antiprismatic structure it is not subject to the same strict axial symmetry. Furthermore, residual optical activity associated with the chiral nature of the ligand have not been accounted for in this discussion.

PAGE NUMBERING AS ORIGINAL

Chapter 9. Conclusions

9.Conclusions

Although the symmetry of the $[EuL^{1a}]^{3+}$ complex has not been established definitively, it can be argued that the complex approximates to a C_2-symmetric species. For the pseudo- C_2-symmetric molecule we can then tentatively assign symmetry labels (by the same analysis as used in Chapter 3) to the circularly polarised components of the lanthanide transitions (**Figure 9.1**).

Since the symmetry of the binding site does not change on carbonate binding (as alluded to by **Figure 9.2**), it is not unexpected that the complex-carbonate adduct retains the pseudo C_2 type symmetry of the diaqua species. This is reflected in the almost identical nature of the CPL spectrum, the only observable change being the reduction in the strength of the emission (g_{em}). This reduction can be attributed to the *tightening* of the helical twist of the ligand on carbonate chelation as discussed in the preceding chapter.

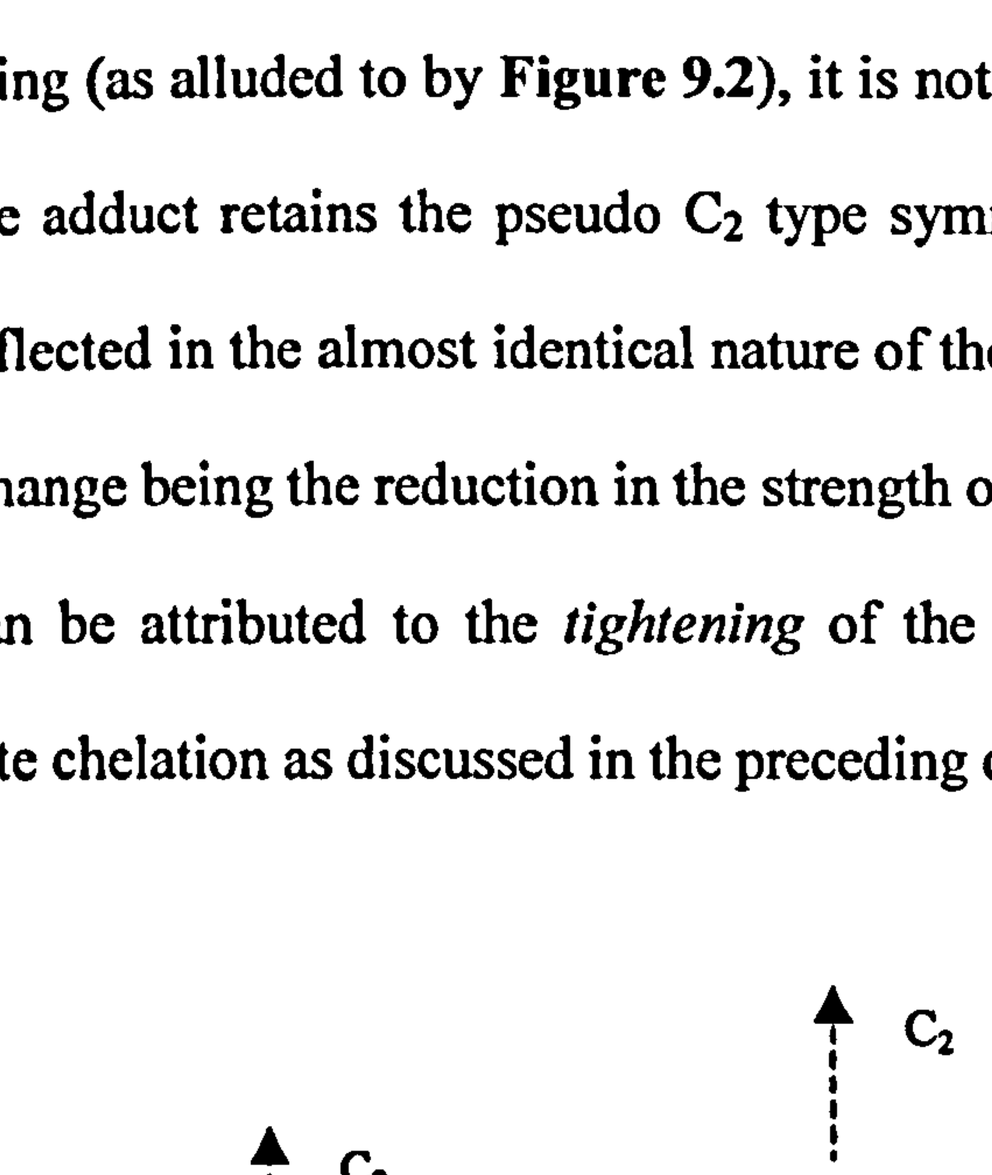

Figure 9.2 Pictorial representation of the pseudo C_2-symmetry of the $[EuL^{1a}]^{3+}$ complex and its carbonate adduct.

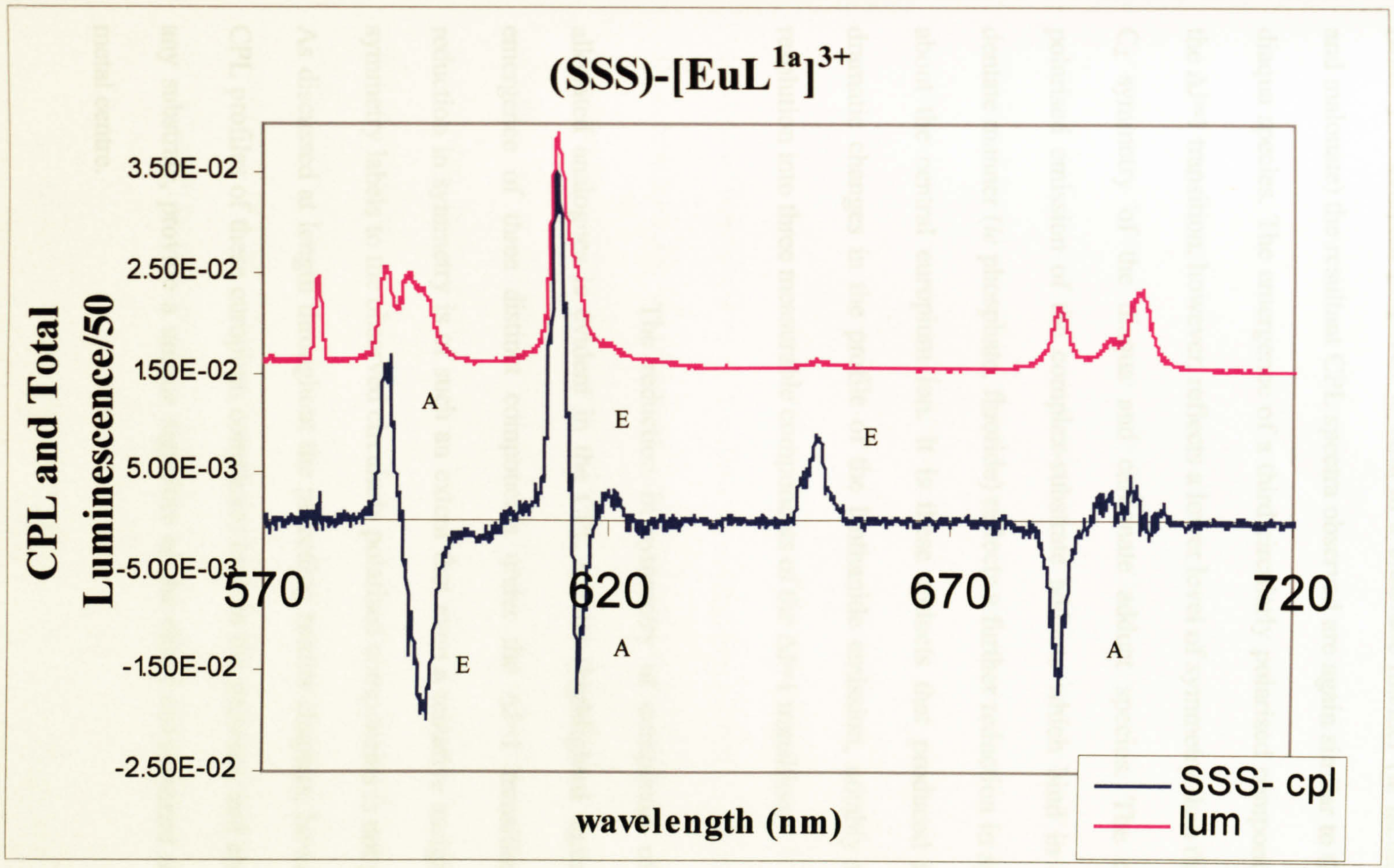

Figure 9.1 *Upper* Total emission of the ΔJ=1,2,3 and 4 transitions of the (SSS)- $[EuL^{1a}]^{3+}$ (2.87mM D_2O solution of complex recorded at 295K and at pD6)*Lower* Circularly polarised emission of the ΔJ=1,2,3 and 4 transitions of the (SSS)-$[EuL^{1a}]^{3+}$ complex under the same conditions with appended symmetry labels of the components.

Of the remaining complex-substrate adducts of the $[EuL^{1a}]^{3+}$ complex proposed to bind in a bidentate manner (ie lactate, citrate and malonate) the resultant CPL spectra observed are again similar to that of the diaqua species. The emergence of a third circularly polarised component under the $\Delta J=1$ transition, however, reflects a lower level of symmetry than the pseudo C_2 symmetry of the diaqua and carbonate adduct species. The circularly polarised emission of the complex-substrate adducts which bind in a mono-dentate manner (*ie* phosphate, fluoride) reflects a further reduction in symmetry about the central europium ion. It is these adducts that produced the most dramatic changes in the profile of the lanthanide emission, notably the clear resolution into three measurable components of the $\Delta J=1$ transition.

The reduction in symmetry of complexes of the N-alkylated analogues is evident in the CPL spectra (highlighted again by the emergence of three distinct components under the $\Delta J=1$ transition.). The reduction in symmetry is of such an extent that even a tentative assignation of symmetry labels to the observed circularly polarised components is not possible. As discussed at length throughout the preceding results chapters, however, the CPL profiles of these europium complexes both in the presence and absence of any substrate, provide a unique signature of the chiral environment about the metal centre.

In conclusion, it can be said that CPL spectroscopy has provided a direct handle on the chiral environment about the central europium ion of these complexes. It has been used to monitor the change in the chiral environment as a selected substrate interacts with the metal centre thus supporting the existing evidence for the proposed structures of the complex-substrate adducts. The most conclusive evidence for the formation of these adducts has come from the crystal structure of the citrate adduct, as shown by **Figures 9.3** and **9.4**. (The crystal structure being determined by Parker and co-workers at the University of Durham).

Although the CPL spectra provide a direct probe of the chirality of these complexes, the absolute configuration of the complexes cannot be determined by the spectra alone (for the reasons as outlined in the introductory section). The spectra obtained, however, provide a raw data set of potential use in the formulation of a theorem to describe the spectra-structure relationship. Most work in this field has been dominated by the study of complexes of axial symmetry. Molecules of this symmetry tend to exclude half of the possible components of the observed transitions. As has been shown, components of both A and E type symmetry are observed in the CPL spectra of the europium complexes of L^{1a}, L^{1b} and L^{1c}.

Considering the titration study of bicarbonate with the europium complexes as described in Chapter 8, it is important to note that two independent measurements were being made. A measurement of the increase in overall luminescence (conventional luminescence studies) as the deactivating

water molecules are displaced, and a measurement of the change in the sense of twist of the helical arrangement of the ligand about the principle axis (CPL studies). Both independent measurements are consistent with each other (as outlined by the similar titration profiles) and signal the binding of bicarbonate.

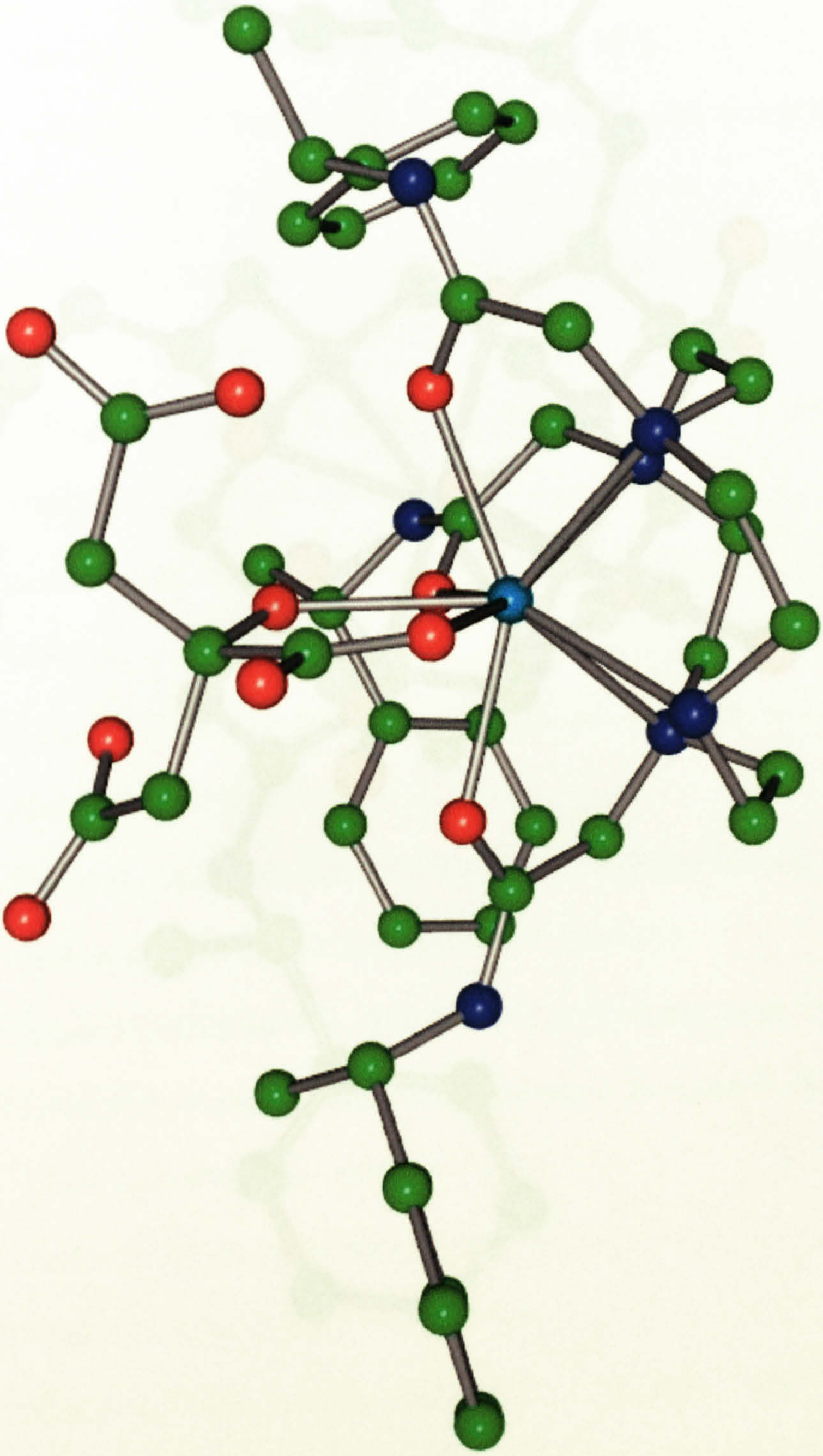

Figure 9.3 . Crystal structure of the complex-citrate adduct (EuL^{1a} complex). (Crystallography carried out by Prof. Parker and co-workers at the University of Durham)

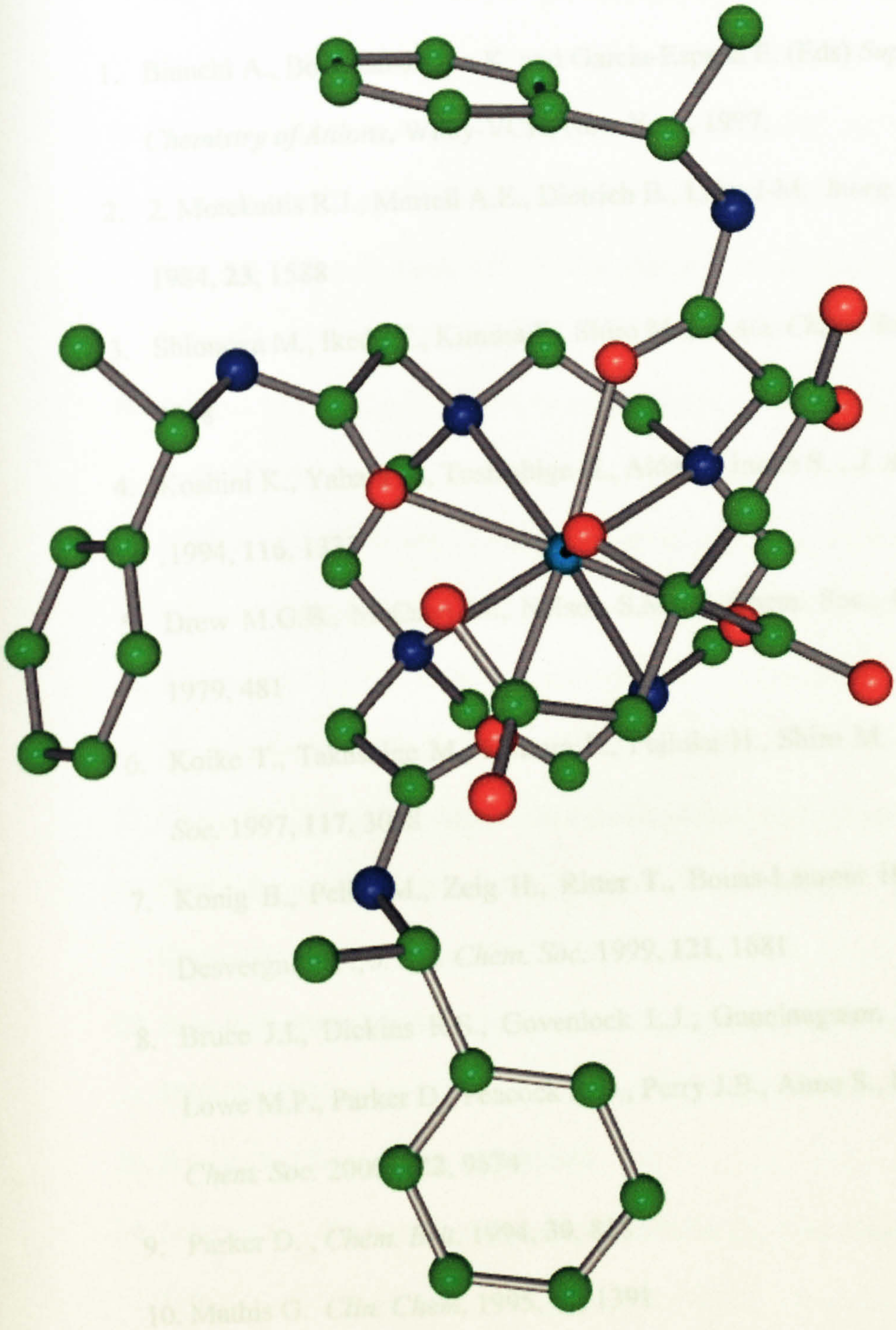

Figure 9.4 . Crystal structure of the complex-citrate adduct (EuL^{1a} complex). (Crystallography carried out by Prof. Parker and co-workers at the University of Durham).

References

1. Bianchi A., Bowman-James K. and Garcia-Espana E. (Eds) *Supramolecular Chemistry of Anions*, Wiley-VCH, New York, 1997.
2. 2. Motekaitis R.J., Martell A.E., Dietrich B., Lehn J-M. *Inorg. Chem.*, 1984, **23**, 1588
3. Shionoya M., Ikeda T., Kimura E., Shiro M. , *J. Am. Chem. Soc.* 1994, **116**, 3848
4. Koshini K., Yahara K., Toshishige H., Aida T., Inoue S. , *J. Am. Chem. Soc.* ,1994, **116**, 1337
5. Drew M.G.B., McCann M., Nelson S.M., J. Chem. Soc., Chem. Comm., 1979, 481
6. Koike T., Takashige M., Kimura E., Fujioka H., Shiro M. , *J. Am. Chem. Soc.* 1997, **117**, 3068
7. Konig B., Pelka M., Zeig H., Ritter T., Bouas-Laurent H., Bonneau R.,. Desvergne J-P., *J. Am. Chem. Soc.* 1999, **121**, 1681
8. Bruce J.I., Dickins R.S., Govenlock L.J., Gunnlaugsson T., Lopinski S., Lowe M.P., Parker D., Peacock R.D., Perry J.B., Aime S., Botta M. , *J. Am. Chem. Soc.* 2000, **122**, 9674
9. Parker D. , *Chem. Brit.* 1994, **30**, 818
10. Mathis G. *Clin. Chem.* 1995, **41**, 1391
11. Coates J., Sammes P.G., Yahioglu G., West R.M. and Garman A.J., *J. Chem. Soc., Chem. Comm.* 1994, 2311
12. Dickins R.S. Howard J.A.K. , Lehman C.W. , Moloney J. , Parker D. , Peacock R.D. *Angew.Chem. Int. Ed,* 1997, **36**, No.5

13. Kataky R. *J. Chem. Soc. Perkin Trans 2,* 1990, 14425

14. Eva F. G. Dickson, Pollack A., Diamandis E.P., *J. Photochem. And Photobiol.,* 1995, **27**, 3.

15. Parker D. and Williams J.A.G., *J. Chem. Soc. Dalton Trans*. 1996, 3613

16. Plenio H. and Burth D., *Organometallics,* 1996, 15, 1151, 4054

17. Beer P.D., Chen Z., Drew M.G.B., Johnson AO.M., Smith D.K., Spencer P., *Inorg. Chem. Acta,* 1996, **246**, 143

18. Tendero M.J.L., Benito A., Martinez-Manez R., and Soto J., *J. Chem. Soc., Dalton Trans,* 1996, 4121

19. Tendero M.J.L., Benito A., Martinez-Manez R., Soto J., Paya J, Edwards A.J. and Raithby P.R., *J. Chem. Soc., Dalton Trans,* 1996, 343

20. Tendero M.J.L., Benito A., Martinez-Manez R., and Soto J., *J. Chem. Soc., Faraday Trans*, 1997, 2175

21. Lloris J.M., Martinez-Manez R., Padilla-Tosta M.E., Pardo T., Soto J., Garcia-Espana E., Ramirez J.A.. Burguete M.I., Luis S.V. and Sinn E., *J. Chem. Soc., Dalton Trans*, 199, 1779

22. Beer P.D., Graydon A.R., Johnson AO.M., Smith D.K., *Inorg. Chem. Acta,* 1997, **36**, 2112

23. Beer P.D., *Chem. Comm.* .1996, 689

24. Lopezm E. , Chypre C., Alpha B. and Mathis G., *Clin. Chem.*, 1993, **39/2**, 196

25. Mathis G., *Clin. Chem.*, 1995, **41/9**, 1391

26. Soini E. and Kojola H. , *Clin. Chem.,* 1983, **29/1**, 65Jaris A., Balzini V., Barigelletti F., Campanga S., Belser P., Von Zelewsky A., *Coord. Chem. Rev.*, 1988, 84, 85

27. Jaris A., Balzini V., Barigelletti F., Campanga S., Belser P., Von Zelewsky A., *Coord. Chem. Rev.*, 1988, 84, 85

28. Meyer T.J., *Acc. Chem. Res.*, 1989, 22, 163

29. Hua X. and Von Zelewsky A., *Inorg. Chem.*, 1995, 34, 5791

30. Demas J.N., De Graff B.A., *Anal. Chem.*, 1991, 63, 829A.

31. DPPZ = dipyrido[3.2-a:2',3'-c]phenazine, bipy=2,2'-bipyridyl

32. Friedman A.E., Chambron J.C., Sauvage J-P., Turro N.J., Barton J.K., *JACS.*, 1990, 112, 4960

33. Barton J.K., *Science,* 1986, 233

34. Baker A.D., Morgan R.J., Strekas T.C., *J. Chem. Soc., Chem. Comm.*, 1992,

35. *Lanthanides and Actinides*, Macmillan Education Ltd., London, 1991, First Ed

36. Kettle S.F.A. *Physical Inorganic Chemistry: A Co-ordination Chemistry Approach*, Spektrum Academic Publishers, Oxford, 1996

37. Forster L.S. , *Chem. Rev.* 1990, **90**, 331

38. de Sa G.F., Malta O.L., de Mello Donega C., Simas A. M., Longo R.L., Santa-Cruz P.A., da Silva Jr E.F., *Coord. Chem Rev.*, 2000, 196, 165

39. Dickens R.S. , Howard J.A.K. , Maupin C.L. , Moloney J. , Parker D. , Peacock R.D. Riehl J.P., Siligardi G., *New J. Chem.* 1998, 891

40. Peacock R.D., *Structure and Bonding,* 1975, 22, 83.

41. Broer L.J.F., C.J. Gorter, J. Hoogschagen, *Physica,* 1945, 11, 231

42. Deutschbein O., *Ann. Phys.*, 1939, 36, 183

43. Judd B.R., *Phys. Rev.*, 1962, 127, 750

44. Ofelt G.S., *Chem. Phys.*, 1962, 37, 511

45. Richardson F.S., *Inorg. Chem.*, 1980, 19, No9

46. Bruce J.I. , Parker D. , Lopinski S. , Peacock R.D. *Chirality*, 2002, **14**, 562-567

47. Faulkner T.R., Richardson F.S., *Mol. Phys.,* 1978, 35, 1141

48. Mason S.F., Peacock R.D., Stewart B. , *Chem. Phys. Lett.,* 1974, 29, 149

49. Mason S.F., Peacock R.D., Stewart B. , *Mol. Phys.,* 1975, 30, 1829

50. .Richardson F.S and Riehl J.P. , *Chem. Rev*. 1986, **86**, 1

51. Mason S.F., *Molecular Optical Activity and Chiral Descriminations*, Cambridge University Press, Cambridge, 1982

52. Barron, L *Molecular Light Scattering and Optical Activity.* Cambridge University Press Cambridge 1982

53. Richardson F.S. and Riehl J.P. *Chem. Rev*. 1977, **77**, 773

54. Emeis C.A. and Oosterhof L.J. ,*J. Chem.Phys. Lett.,* 1967, **1**, 129

55. Schippers, P.H., Dekkers, H.P.J.M., *JACS.*, 1983, **105**, 79

56. Morley, J.P., Saxe, J.D., Richardson F.S. *Mol. Phys.,* 1982, **47**, 379

57. Parker D. and Williams J.A.G., *J. Chem. Soc. Dalton Trans*. 1996, 3613.

58. Kropp J.L. and Windsor M.W., *J. Chem. Phys*. 1963, **39**, 2769

59. Horrocks Jr, W. De W and Snelnick D. R. *J. Am. Chem. Soc*. 19, **101**, 334

60. Horrocks Jr, W De W *Acc.Chem. Rev.* ,19, **14**, 384

61. Hellar A. *J. Am. Chem. Soc*. 1966, **88**, 2058. Haas Y. and Stein G. *Chem. Phys. Lett.* 1971, **11**, 143; *J. Phys. Chem*. 1971, **75**, 3677

62. Spirlet M., Rebizant J., Desreux J.F. and Loncin M.F., *Inorg. Chem*. 1984, **23**, 359

63. Corey E.J. and Bailar J.C., *J. Am. Chem. Soc*. 1959, **81**, 2620

64. Dickson R.S., Gunnlaugsson T. , Parker D. , Peacock R.D. Chem. Commun. 1998, 1643

65. Clarkson I.M. , Dickens R.S., Faulkner S. , Parker D. , Royle L. , de Sousa A.S. , Williams J.A.G. , Geraldes C.F.G.C. *J. Chem. Soc. Perkin 2*, 2001, 1729-37

66. Covington A. K., *R.A.Robinson Memorial Lecture*

67. Looewenthal R.E. and Marais G.R., *Carbonate Chemistry of Aquatic Systems*, Wiley, New York, 1970, chapter 4